NASA-CR-179016

(NASA-CR-179016) SATELLITE ATTITUDE MOTION
MODELS FOR CAPTURE AND RETRIEVAL
INVESTIGATIONS (Auburn Univ.) 87 p CSCL 22B

N87-18599

Unclas
G3/18 43622

SATELLITE ATTITUDE MOTION MODELS

FOR CAPTURE AND RETRIEVAL

INVESTIGATIONS

by

John E. Cochran, Jr. and Brian S. Lahr
Aerospace Engineering Department
Auburn University, Alabama 36849-3501

SATELLITE ATTITUDE MOTION MODELS

FOR CAPTURE AND RETRIEVAL

INVESTIGATIONS

by

John E. Cochran, Jr. and Brian S. Lahr
Aerospace Engineering Department
Auburn University, Alabama 36849-3501

for

NATIONAL AERONAUTICS AND SPACE ADMINISTRATION
George C. Marshall Space flight Center

under

Contract NAS8-36470

Administered through

Engineering Experiment Station
Auburn University, Alabama 36849

October 1986

FOREWORD

TABLE OF CONTENTS

LIST OF TABLES

LIST OF FIGURES

LIST OF SYMBOLS

English Symbols

A, B, C — Principal centroidal moments of inertia about the satellite's x_b-, y_b-, z_b-axes, respectively.

a — $a = H \sin\theta$

b — $b = H \cos\theta$

C — Center of mass of the satellite model; also geometric centroid of right-circular cylinder.

C_R — Center of mass of the rotor.

c_d — "Free molecular flow" accommodation constant, 2.2

$c_{ej3}, \; j=1,2,3$ — Direction cosines between the satellite's body-fixed axes and the earth's polar axis.

$c_{j3}, \; j=1,2,3$ — Direction cosines of the position vector of the satellite's center of mass in the satellite's body-fixed coordinate system.

D — Moment of inertia of the rotor about its symmetry axis

$dS_j, \; j=1,2,3$ — Differential surface elements of the right-circular cylinder used in deriving the aerodynamic torque.

f — True anomaly.

$\underline{f}_1$ — Periodic function of $\underline{x}$ and $\underline{y}$ used to define $\dot{\underline{x}}$.

$\underline{g}_j, \; j=0,1$ — Periodic functions of $\underline{x}$ and $\underline{y}$ used to define $\dot{\underline{y}}$.

H — Magnitude of total rotational angular momentum.

$\underline{H}$ — Total angular momentum vector of the satellite expressed in the satellite's body-fixed coordinate system.

$\underline{H}_H$ — Total angular momentum vector of the satellite expressed in the angular momentum coordinate system.

$\underline{H}_r^{R/C_R}$ — Angular momentum vector of the rotor about the rotor's center of mass expressed in the r-basis.

$\underline{h}$	Internal angular momentum vector of the satellite expressed in the satellite's body-fixed coordinate system.
h_x, h_y, h_z	x_b-, y_b-, and z_b-components, respectively, of $\underline{h}$.
$\underline{\underline{I}}$	Inertia dyadic of the satellite.
I_{R_z}	Moment of inertia of the rotor about the rotor's z-axis.
I_{xx}, I_{yy}, I_{zz}	Moments of inertia about the satellite's x_b-, y_b-, and z_b-axes, respectively, from inertia dyadic $\underline{\underline{I}}$.
I_{xy}, I_{yx}	Products of inertia found in the inertia dyadic $\underline{\underline{I}}$
i	Orbital inclination.
$\underline{\underline{J}}$	Inertia matrix of the rotor about C_R in the b-basis.
J_2	Constant used in the expansion of the gravity-gradient torque expression for the first spherical harmonic.
$\underline{\underline{K}}$	Centroidal inertia matrix of the complete satellite less the contribution by the rotor about its axis of rotation with respect to the satellite.
$\underline{\underline{L}}_{br}$	Transformation matrix from the r-basis to the b-basis.
M	Mean anomaly.
P_α	Angular momentum of the rotor about its axis of rotation with respect to the satellites.
P_ϕ	Momentum conjugate to the angle ϕ.
P_{Ψ_H}	Momentum conjugate to the angle Ψ_H
P_ψ	Momentum conjugate to the angle ψ.
p,q,r	Components of angular velocity about the x_b-, y_b-, z_b-axes.
R	Radius of the satellite's orbit.
$\underline{R}$	Position vector of the satellite's center of mass in the satellite's body-fixed coordinate system.
R_e	Equatorial radius of the earth.

$\underline{r}_j$, j=1,2,3	Position vectors from the centroid of the right-circular cylinder to the surface element dS_j, j=1,2,3, respectively.
S_j, j=1,2,3	Surfaces of the right-circular cylinder.
$\underline{T}$	External torque vector.
$\underline{T}_a$	Aerodynamic torque vector.
$T_{a_x}, T_{a_y}, T_{a_z}$	x_b-, y_b-, and z_b-components, respectively of $\underline{T}_a$.
$\underline{T}_g$	Gravity-gradient torque vector.
$T_{g_x}, T_{g_y}, T_{g_z}$	x_b-, y_b-, and z_b-components, respectively of $\underline{T}_g$.
$\underline{T}_H$	External torque vector expressed in the angular momentum coordinate system.
T_x, T_y, T_z	x_b-, y_b-, and z_b-components, respectively, of the vector $\underline{T}$.
$T_{x_H}, T_{y_H}, T_{z_H}$	x_H-, y_H-, and z_H-components, respectively, of the vector $\underline{T}$.
T_α	Torque on the rotor about its axis of relative rotation.
t	Time
u	Sum of the argument of periapse and true anomaly.
U, V, W	x_b-, y_b-, and z_b-components of $\underline{V}$.
$\underline{u}_j$, j=1,2	Function of $\bar{x}$ and $\bar{y}$ used to make the differential equations for $\bar{x}$ simpler than those for $\underline{x}$.
$\underline{V}$	Total velocity vector of an element on the satellite's surface.
$\underline{V}_C$	Translational velocity vector of the satellite's center of mass in the satellite's body-fixed coordinate system.
$\underline{v}_j$, j=1,2	Function of $\bar{x}$ and $\bar{y}$ used to make the differential equations for $\bar{y}$ simpler than those for $\underline{y}$.

$\underline{x}$	Vector (column matrix) containing the "slow" variables, used in the semi-analytic method.
$\underline{y}$	Vector (column matrix) containing the "fast" variables, used in the semi-analytic method.

Greek Symbols

α	Angle of relative rotation between the satellite, "carrier body," or platform and rotor.
α_a	Aerodynamic angle of attack.
$\underline{\beta}$	Euler parameter vector, $\underline{\beta} = (\beta_1 \ \beta_2 \ \beta_3)^T$.
β_a	Aerodynamic sideslip angle.
$\beta_j, \ j=0,1,2,3$	Euler parameters.
ϵ	Small parameter used in perturbation analysis.
Θ_H	Angle between the orbital plane and the $x_H \ y_H$-plane.
θ	Classical nutation angle.
$\theta_j, \ j=1,2,3$	Roll, pitch, and yaw angles, respectively.
λ	Latitude of satellite center of mass.
$\underline{\lambda}$	Angular velocity of the body-fixed coordinate system with respect to the angular momentum system.
μ_E	Gravitational constant, $\mu_E = (3.986 \times 10^5 \ \frac{km^2}{sec^2})$.
ρ	Atmospheric density.
ϕ	Classical angle of proper rotation.
Ψ_H	Angle used to locate x_H-axis with respect to orbital plane.
ψ	Classical precession angle.
Ω	"Node," the longitude of the ascending node; also spin rate of rotor relative to platform of dual-spin satellite.
$\underline{\frac{\Omega}{r}}$	Angular velocity vector of the rotor in the r-basis.
Ω_o	Initial angular rate of rotor.

ω	Argument of periapse.
$\underline{\omega}$	Angular velocity of the satellite in the satellite's body-fixed coordinate system.
$\underline{\omega}_H$	Angular velocity of the angular momentum coordinate system.
$\underline{\omega}_r$	Angular velocity of the satellite in the r-basis.
$\omega_{x_H}, \omega_{y_H}, \omega_{z_H}$	x_H-, y_H- and z_H-components, respectively, of $\underline{\omega}_H$.
$\omega_{x_o}, \omega_{y_o}, \omega_{z_o}$	x_b-, y_b-, and z_b-components, respectively, of $\underline{\omega}_o$.
$\underline{\omega}_o$	Initial $\underline{\omega}$.

Coordinate Systems

$Cx_by_bz_b$	Satellite body-fixed coordinate system.
$Cx_Hy_Hz_H$	Angular momentum coordinate system.
$Cp x_p y_p z_p$	Dual-spin satellite platform-fixed coordinate system.
$C_R x_R y_R z_R$	Dual-spin satellite rotor-fixed coordinate system.
$Cx_v y_v z_v$	Local vertical coordinate system.
$C_A x_w y_w z_w$	Relative wind coordinate system.
$C\xi\eta\zeta$	Orbiting coordinate system.
EXYZ	Earth-centered inertial coordinate system.
$Ex_o y_o z_o$	Orbital plane coordinate system.

Unit Vectors

$\hat{\underline{a}}_j$, $j=1,2,3$	Angular momentum system unit vector triad.
$\hat{\underline{b}}_j$, $j=1,2,3$	Satellite body-fixed system unit vector triad.
$\hat{\underline{c}}_j$, $j=1,2,3$	Orbital plane coordinate system unit vector triad.
$\hat{\underline{e}}_j$, $j=1,2,3$	Orbiting coordinate system unit vector triad.
$\hat{\underline{I}}, \hat{\underline{J}}, \hat{\underline{K}}$	Inertial coordinate system unit vector triad.
$\hat{\underline{n}}_j$, $j=1,2,3$	Unit vectors normal to the surfaces S_1, S_2, and S_3.

Other Nomenclature

$\dot{(\ )}$ Time rate of change of the elements of ( ).

$\overline{(\ )}$ Averaged value(s) of the elements of ( ).

$\tilde{(\ )}$ Tilde matrix formed from the elements of ( ).

$\overline{\overline{(\ )}}$ Double averaged value(s) of the elements of ( ).

$\overset{\circ}{(\underline{\ })}$ Time rate of change of the components of the <u>vector</u> quantity (_).

Symbols used in the appendices are defined as they are introduced.

I. INTRODUCTION

1.0 Background

To date, successful satellite capture and recovery/repair operations have been executed by Space Shuttle astronauts using the Remote Manipulating Arm and the Manned Maneuvering Unit.[1,2] However, both of these valuable tools are very much range-limited. Furthermore, attempts to capture uncontrolled satellites within the range of the Orbiter can lead to the dangerous exposure of the Space Shuttle crew members and/or the Orbiter to a possibly violently gyrating, uncontrolled satellite. For both of these reasons most future capture and recovery missions will likely be the domain of remotely piloted Orbital Maneuvering Vehicles (OMVs).[3,4]

The potential usefulness of OMVs to affect the capture and retrieval of satellites should be significantly increased by adaptable, yet accurate, simulations of the target satellite's attitude motions. Two primary mathematical models are needed for such simulation capability. First, a long-term model is needed for predicting a satellite's attitude motion as much as six months or more in advance. Second, a "short-term" model adaptable and rigorous enough for use in simulators to train the OMV "pilots" for specific satellite recoveries, is needed.

Although the problem of modeling a spacecraft's motion about its center of mass is one which arose because of space flight, the study of

1

spacecraft attitude dynamics is basically a contemporary application of classical theoretical mechanics. The analytical approach to solving the differential equations of rotational motion of a satellite is typified by Jacobi's classical solution for the free rotational motion of a triaxial rigid body in terms of elliptic integrals and functions. Although analytical solutions have been obtained for only <u>relatively</u> simple models of satellites, the more recent wide availability of digital computers has made it possible to use straightforward numerical integration of differential equations of motion for models composed of rigid and flexible bodies, subjected to various torques and forces.

1.1 The Capture and Retrieval Problem

A time period of several months may elapse between the failure of a satellite (for example, a control system failure, power system failure, maneuvering propellant depletion, or other non-catastrophic type problems which might precipitate the need for capture and retrieval) and the first possible opportunity, or "window," to capture and retrieve it. Hence, an apparently necessary capability is that of accurately predicting the evolution of the attitude motion of a disabled satellite several months into the future, for the purposes of capture feasibility analyses and mission planning. In addition to long-term prediction capability, short-term attitude motion simulation capability is needed to train remote operators. Since all satellites which may be the objects of capture and retrieval missions will most certainly not fit into a single category of satellite or attitude motion, simulation capability must include more than just a single-axis-of-rotation, single-rigid-body model. The satellite model should be rigorous enough

to include the presence of spinning rotors or reaction wheels distributed symmetrically, or asymmetrically. The flexibility of the satellite might also be included.

Another problem involves the quantity and quality of data on the states of the satellite's orbital and attitude motions. These, of course, are functions of the satellite's "mode of failure." There are three general modes, or scenarios, of "failure" which may precipitate a recovery. The first scenario involves a satellite which has not lost its telemetry, but is uncontrollable. In this case, ground controllers would, through the satellite's telemetry data, have at least partial attitude motion information. The second scenario involves a satellite which is both uncontrolled and has lost its telemetry capability. Such a satellite's state was possibly known prior to failure, but additional information can only be obtained through remote observation, if the satellite is observable. The third scenario involves space debris which are, of course, neither controllable nor capable of telemetry. Thus, the debris' rotational states are unknown except for estimates based on any observations which might have been possible. Therefore, in the capture of debris, any of a wide variety of rotational states may be encountered.[5]

1.2 Scope of This Investigation

The primary purpose of this research is to provide mathematical models which may be used in investigation of various aspects of the remote capture and retrieval of uncontrolled satellites. Emphasis has been placed on analytical models; however, to verify analytical solutions, numerical integration must be used. Also, for satellites of

of certain types, numerical integration may be the only practical or perhaps the only possible method of solution. First, to provide a basis for analytical and numerical work, uncontrolled satellites were categorized using criteria based on (1) orbital motions, (2) external angular momenta, (3) internal angular momenta, (4) physical characteristics and (5) the stability of their equilibrium states. Chapter II deals specifically with categorization.

Second, several analytical solutions for the attitude motions of satellite models were compiled, checked, corrected in some minor respects and their short-term prediction capabilities were investigated. These models should be useful in studying the attitude behavior of satellites which have considerable angular momentum, and in "driving" short-term simulation, during which human operators try to capture satellites. Single-rigid-body, dual-spin and multi-rotor configurations are treated. The models are described in Chapter III and Appendices A, B and C of this report. Copies of computer codes for evaluating the solutions are being supplied separately.

Third, as indicated above, to verify the analytical models and to see how the "true" motion of a satellite which is acted upon by environmental torques differs from its corresponding torque-free motion, a numerical simulation code was developed. This code contains a relatively general satellite model and models for gravity-gradient and aerodynamic torques. The spacecraft physical model for the code and the equations of motion are given in Chapter IV. The two environmental torque models are described later in Chapter V and Appendix D.

Fourth, the use of torque-free analytical solutions to represent satellite attitude motion is considered in Chapter VI. Analytical results and numerical results, including gravity-gradient and aerodynamic torque effects for satellites are presented.

Fifth, there are cases in which analytical solutions are not known for the unperturbed attitude motion of a satellite, but available integrals of the motion and extensive numerical results indicate that the motion will in a great many cases be almost periodic. To model the motion in such cases, a semi-analytic method was developed. This method is based on concepts from the Generalized Method of Averaging (GMA), but its application is primarily numerical. The method is described in Chapter VII. It has been used to predict satellite attitude motion over long periods of time. Results obtained using the semi-analytic method and direct numerical integration are presented in Chapter VII.

Finally, Chapter VIII contains conclusions and recommendations.

It should be noted here that this effort did not include an investigation of the effects of internal dissipation of energy on satellite motion. This was considered to be beyond the scope of this effort.

II. CATEGORIZATION OF SATELLITES

2.0 Rationale

Artificial earth satellites can be categorized according to (1) the orbital motion of their centers of mass, (2) their gross (external) rotational motion, (3) their internal motion, (4) their individual physical characteristics and (5) the stability of their equilibrium states.[5] The motion of a satellite's center of mass about the earth is of importance in determining whether the satellite may be reached with the means available. If the satellite is accessible, the orbital characteristics are needed in modeling the effects of environmental torques. The initial rotational motion of the satellite about its center of mass as well as its internal angular momentum determine the satellite's initial rotational kinetic energy and total rotational angular momentum. Using these and satellite physical data, one can predict the general principal characteristics of the uncontrolled attitude motion which may evolve. Examples of this uncontrolled attitude motion include continuous, steady rotation and librating motion.

2.1 Categories

The block diagram shown in Fig. 1 depicts categories of uncontrolled satellites based upon orbital criteria.[5] The first two categories, LEO (Low Earth Orbit) and HEO (High Earth Orbit), are based

6

UNCONTROLLED SATELLITES

CATEGORY I
LEO

CATEGORY IA
NCO

CATEGORY IB
EO

CATEGORY II
HEO

CATEGORY IIA
NCO

CATEGORY IIB
EO

AERODYNAMIC TORQUES SIGNIFICANT

GRAVITY-GRADIENT TORQUES DOMINANT

LEO - LOW EARTH ORBIT
HEO - HIGH EARTH ORBIT
NCO - NEAR CIRCULAR ORBIT
EO - ELLIPTICAL ORBIT
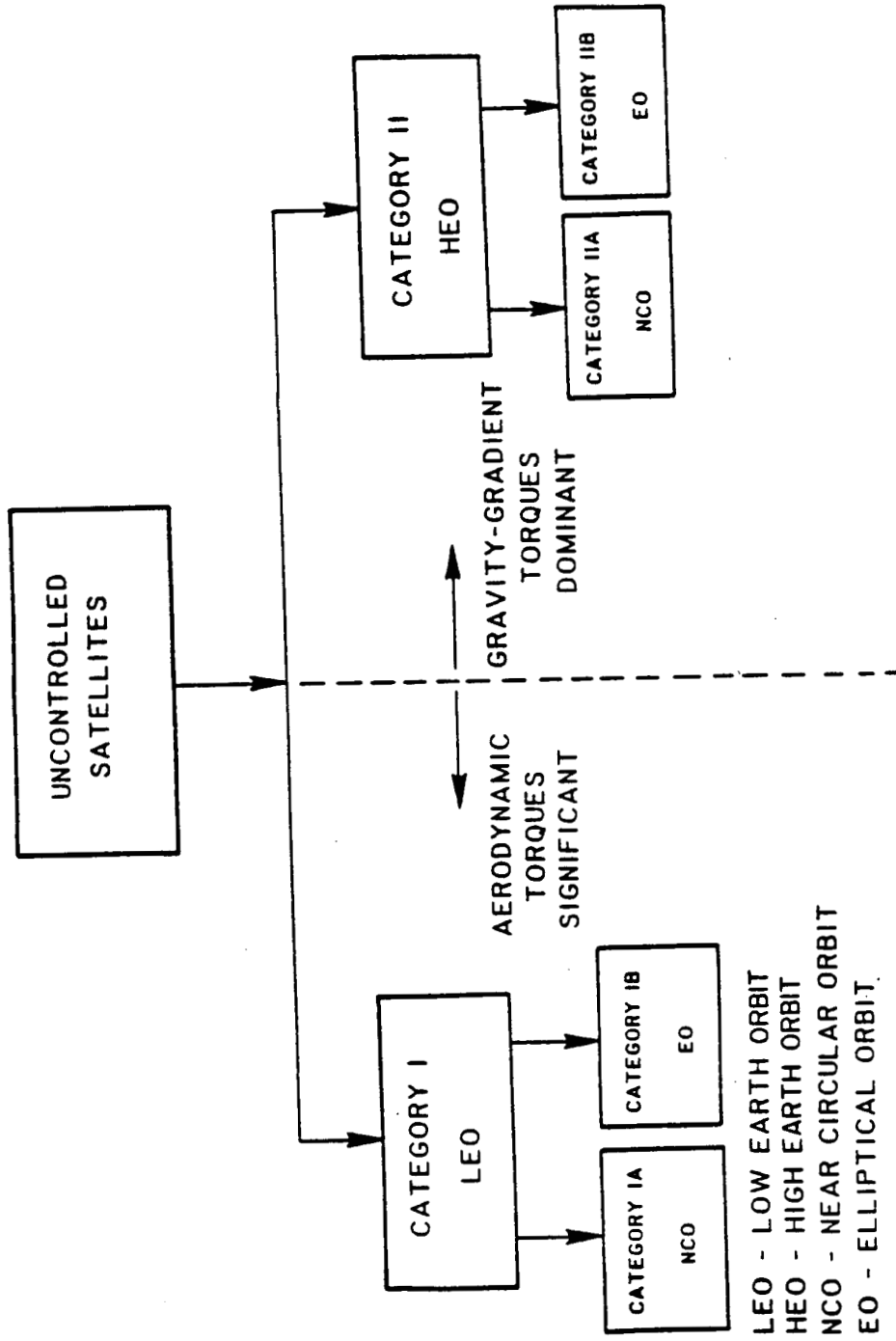
Fig. 1. Block Diagram of Categories of Uncontrolled Satellites.

upon the perigee altitude of the satellite's orbit. A LEO is considered one which has a perigee altitude of less than 600 km. For those periods of time during which the satellite operates in the LEO altitude range, it is subjected to significant aerodynamic torques as well as other environmental torques. For that portion of the satellite's orbit in which it moves in the HEO altitude range, aerodynamic torques become much less significant than gravity-gradient torques.

The next two categories, NCO (Near Circular Orbit) and EO (Elliptic Orbit), determine the satellite's orbital motion with respect to altitude and time. An elliptic orbit of significant eccentricity subjects the satellite to substantial periodic changes in the environmental torques which affect the satellite's attitude motion. On the other hand, for a satellite moving in a circular, or near circular, orbit, the magnitudes of the environmental torques to which it is subjected remain in a narrow range.

Uncontrolled satellites also can be placed into several subcategories based on their rotational motion about their respective centers of mass. These subcategories include High Kinetic Energy (HKE), Low Kinetic Energy (LKE), High Angular Momentum (HAM), and Low Angular Momentum (LAM). The HKE satellites possess rotational kinetic energy which is orders of magnitude larger than the maximum possible potential energy due to gravity-gradient torque acting upon the satellite. This high kinetic energy state could be due to a high "gross" rate of rotation; that is, a high rotational rate of the entire body, and/or due to large amounts of internal angular momentum and internal rotational kinetic energy. Satellites in the HAM subcategory possess rotational

angular momentum, $\underline{H}$, due either to gross or internal relative motion of sufficient magnitude that the ratio of the magnitude of the applied torque to the magnitude of $\underline{H}$ is small. Obviously, the subcategories HAM and HKE are not mutually exclusive. In point of fact, they overlap a great deal.

Other subcategories are defined to deal more specifically with the inertia characteristics of the individual satellites. Two of these subcategories include Asymmetric Inertia (AI) ellipsoid, and Symmetric Inertia (SI) ellipsoid. Still other subcategories may be based upon the initial orientation of the satellite's body-fixed axes with respect to the radius vector between the center of the earth and the satellite's center of mass. This orientation is of central importance in the determination of the torque on the satellite which in turn are modeled in stability analyses. The stability of its initial motion has a direct bearing upon the later motion of a satellites under the effects of aerodynamic and/or gravity-gradient torques. Those subcategories, associated with aerodynamic torques include AS, ANS, AUS (Aerodynamically Stable, Neutrally Stable, and Unstable initial states, respectively). Similarly, for Gravity Gradient stability, we have the subcategories GGS, GGNS, and GGUS.[5] In all these the type of stability considered is static stability rather than dynamic stability.

Finally, satellites can be categorized according to their construction and their components. Such categories relate directly to the choice of the physical model and will approximate a satellite best. Examples are dual-spin satellites and satellites which contain reaction wheels for attitude control.

III. ANALYTICAL MODELS FOR TORQUE-FREE

ROTATIONAL MOTION OF SATELLITES

3.0 Introduction

The kinds of satellites to be considered in this investigation as typical candidates for capture and retrieval include single-rigid-body and dual-spin satellites as well as satellites which contain multiple spinning rotors (reaction wheels). In this Chapter three torque-free analytical models for these three types of satellites are discussed. Such models serve at least three purposes. First, if its rotational angular momentum is not too small, over short time periods such as that required for capture, the actual attitude motion of a satellite is essentially the same as its torque-free motion. Second, to predict satellite motion over longer periods of time, perturbation theories for satellite attitude motion,[6-10] analogous to those for satellite orbital motion may be developed on the basis of analytical solutions for torque-free motion. Third, analytical solutions provide a means for checking the accuracy of numerical integration procedures.

3.1 Single-Rigid-Body Satellite Model

As the name implies, the single-rigid-body model consists of a single, rigid, asymmetric body. Using this single-rigid-body model, and general perturbation methods. Beletski,[9] Crenshaw and Fitzpatrick,[6] Cochran,[7] and Liu and Fitzpatrick,[10] have developed theories to predict

10
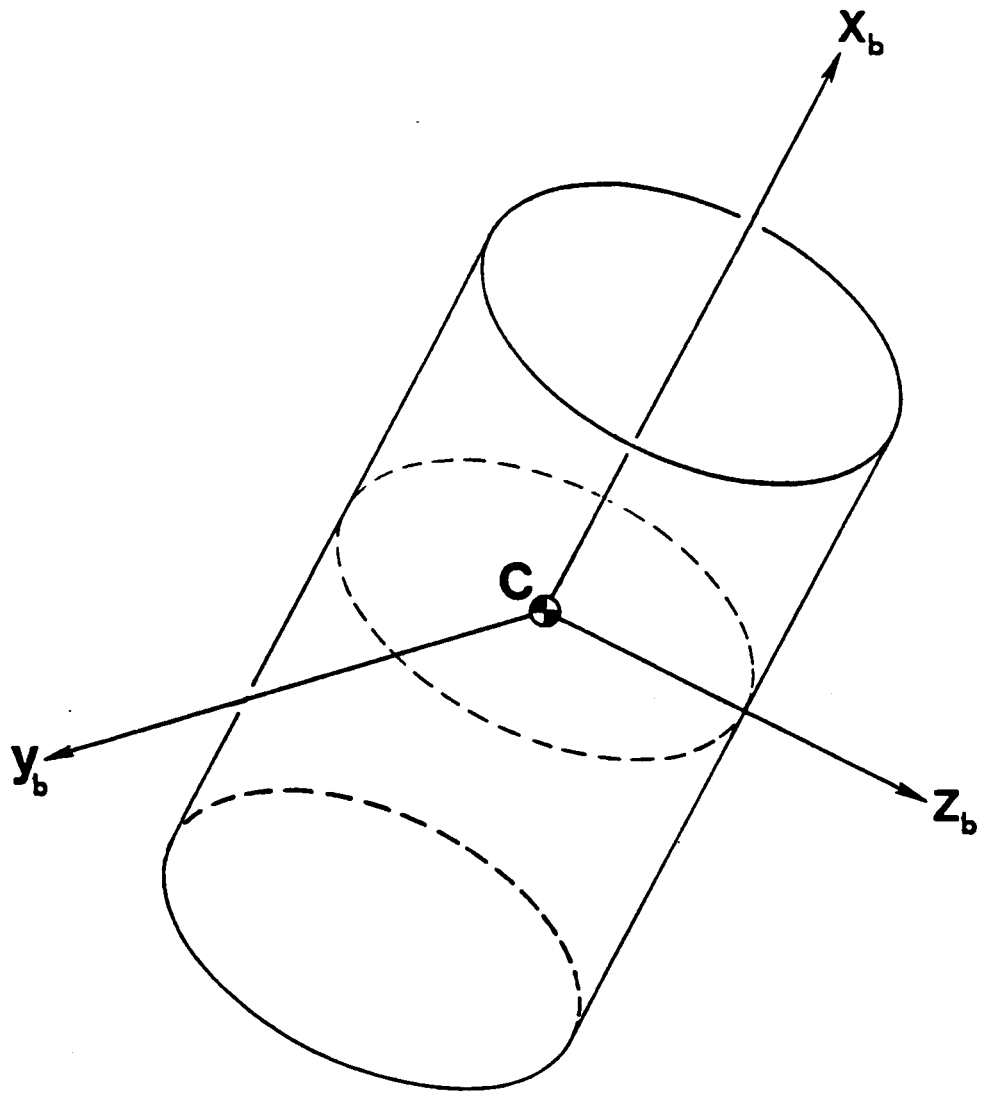
Fig. 2.   Single-Rigid-Body Satellite Model.

the attitude motion in the presence of gravity-gradient torques. If the satellite modeled (see Fig. 2) is rotating rapidly about its center of mass, then its short-term motion is essentially classical "free-Eulerian" motion. This "free-Eulerian" motion may be described by an exact analytical solution which involves elliptic functions and integrals.[11,12] Appendix A contains the details of this mathematical model.

3.2 Dual-Spin Satellite Model

Satellites which contain a single spinning rotor and a nominally despun platform, or "carrier" body, are called "dual-spin" satellites (see Fig. 3). More specifically, the dual-spin satellite can be modeled as a system of two rigid bodies coupled together in such a manner that a rotation about an axis fixed in both bodies is the only relative degree of freedom. A general, exact analytical solution for the torque-free attitude motion of an arbitrary dual-spin satellite does not exist. However, Cochran, Shu and Rew,[13] building on previous work (Ref. 12, page 37) have obtained a complete, exact, analytical solution for the case in which: (1) one body is axisymmetric; (2) the axisymmetric body rotates relative to the other about the former's axis of symmetry; (3) the other body is asymmetric; (4) the axis about which relative rotation occurs is the axis of major, or minor, moment of inertia of the asymmetric body; (5) the relative rotation is either free (no internal torque), or the relative spin rate is constant. A summary of the mathematical model of Ref. 13 is presented in Appendix B for completeness.
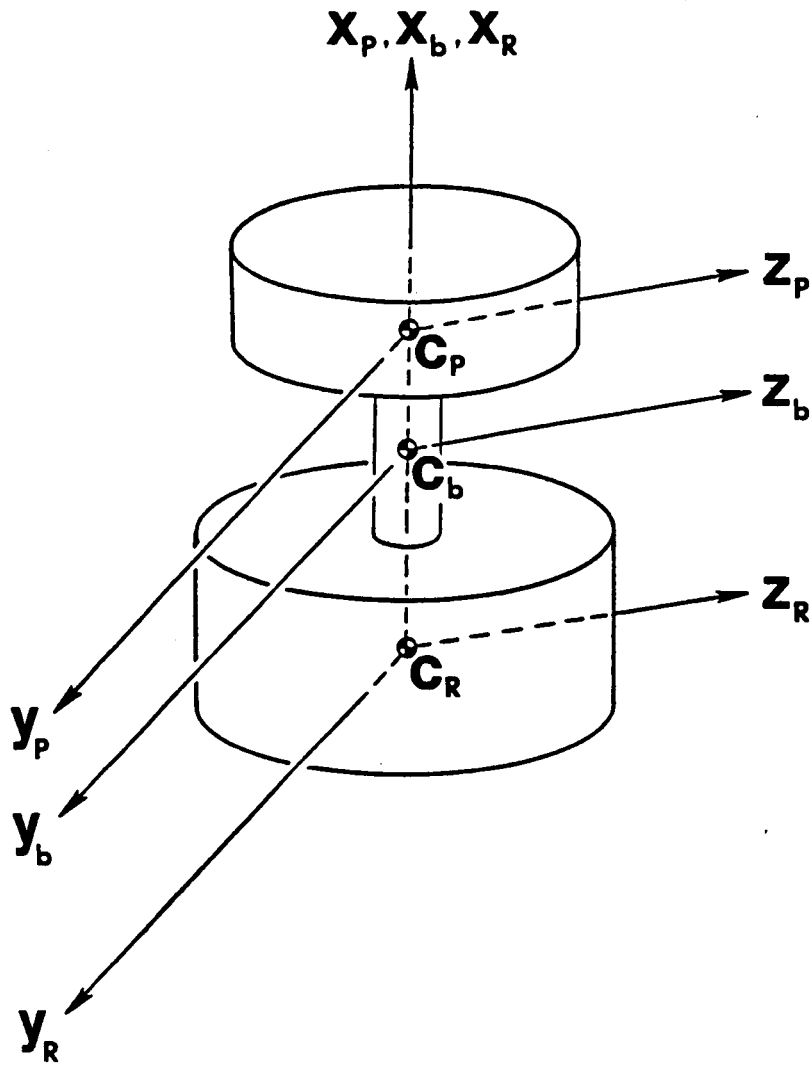
Fig. 3. Dual–Spin Satellite Model.

3.3 Multi-Rotor Satellite Model

An exact analytical solution is also available for the torque-free attitude motion of a particular model of a satellite which contains spinning rotors; i.e., "momentum wheels," or "reaction wheels." In this solution, also due to Cochran and Shu,[14] the satellite physical model (see Fig. 4) is that of a gyrostat, consisting of two axisymmetric, constant-speed rotors, or momentum wheels, and a "carrier" rigid body which has a mass distribution such that the centroidal inertia ellipsoid of the system of rigid bodies is axisymmetric.[14] The model is general enough to represent any axisymmetric satellite that contains an arbitrary number of axisymmetric rotating components which together produce a resultant relative, or "internal," angular momentum vector that is not parallel to a principal axis of the system. As noted, the solution does, however, require constant internal angular momentum and an axisymmetric system. The solution is given in Appendix C.
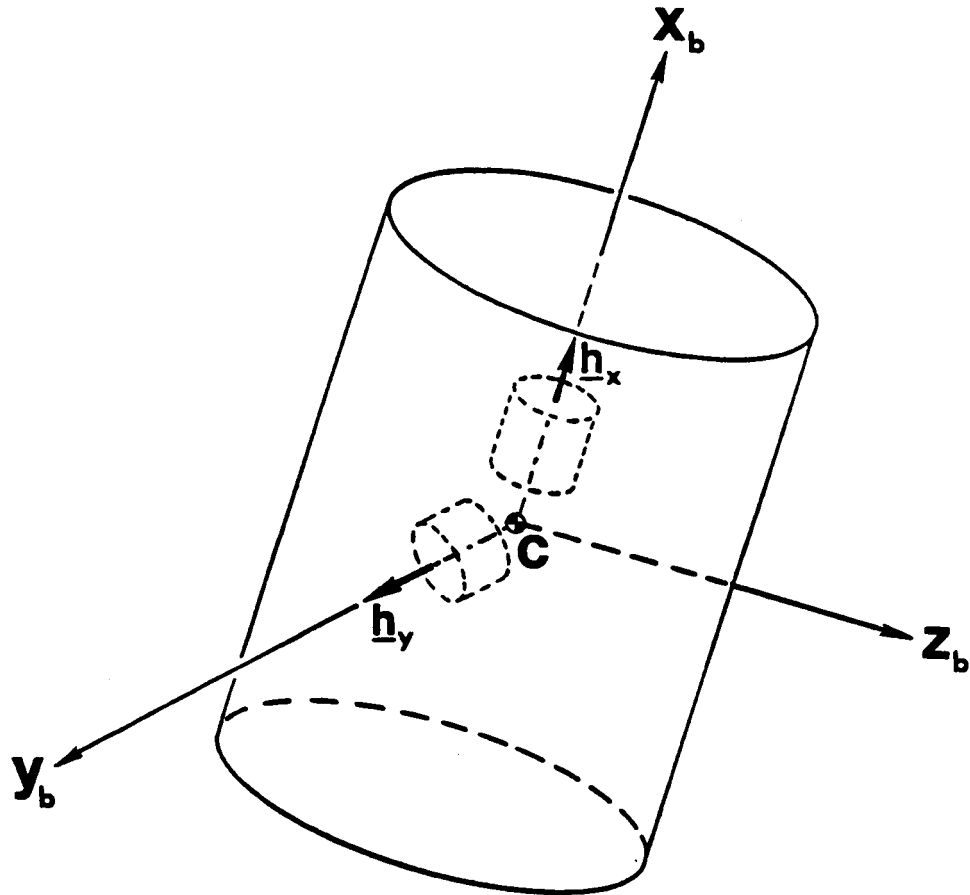
Fig. 4. Multi-Rotor Satellite Model.

IV. SATELLITE MODEL FOR NUMERICAL SIMULATIONS

4.0 Introduction

Many satellites contain variable-speed spinning rotors or other
moving parts. Should an exact analytical solution for the torque-free
attitude motion of such a satellite exist, it will undoubtedly be much
more complicated than the single-rigid-body analytical solution
discussed in Chapter 3 and given in Appendices A, B and C. Thus, for
complex models, a practical alternative is to use numerical integration
techniques to obtain even the torque-free, or "unperturbed" solutions.[15]
Furthermore, to determine the motion of a satellite which is dynamically
complex and/or is exposed to significant perturbing torques (for
example, a LAM satellite in LEO), numerical integration of the equations
of motion is the only approach generally applicable. In this Chapter, a
physical model of a satellite is described. The corresponding
mathematical model presented following the physical model has been
incorporated in a digital simulation code along with models of
gravity-gradient and aerodynamic torques. This code utilizes a
fourth-order, Runge-Kutta, numerical integration algorithm to produce
attitude motion time-histories.

The purposes of the simulation code are: (1) to verify the
correctness of the analytical solutions; (2) to determine the conditions
under which torque-free solutions can be considered reasonably valid;

16

and (3) to produce attitude motion time-histories for cases in which analytical solutions are not known.

4.1 Satellite Physical Model

The "general" satellite model (see Fig. 5) consists of two rigid bodies, each of arbitrary mass distribution, which are coupled together so that the smaller body, or rotor, can be rotated with respect to the main body of the satellite, only about an axis which is fixed in the satellite and the rotor, and passes through the center of mass of the rotor. This physical model can be used to represent single-rigid-body and dual-spin satellites and also satellites which possess internal angular momentum due to constant-speed multiple, spinning components. Since the equations of motion for the general model are to be integrated numerically, environmental torques of some complexity may be included.

Because the description of the attitude motions of satellites requires the use of reference frames and coordinate systems, the coordinate systems in Figs. 6, 7, and 8 are introduced. They are all dextral, orthogonal systems. The nonrotating EXYZ (inertial) coordinate system, depicted in Fig. 6, has its origin at the center of the earth and is considered inertially fixed. The unit vector triad $(\hat{\underline{I}}, \hat{\underline{J}}, \hat{\underline{K}})$ is fixed to the EXYZ system. The coordinate system, $Ex_o y_o z_o$, is called the "orbital plane system" and is defined by requiring that the x_o-axis lie along the line of nodes of the satellite's orbit, directed toward the ascending node, and that the z_o-axis be perpendicular to the orbital plane, collinear with the orbital areal velocity vector. The unit vector triad $(\hat{\underline{c}}_1, \hat{\underline{c}}_2, \hat{\underline{c}}_3)$ is fixed to the
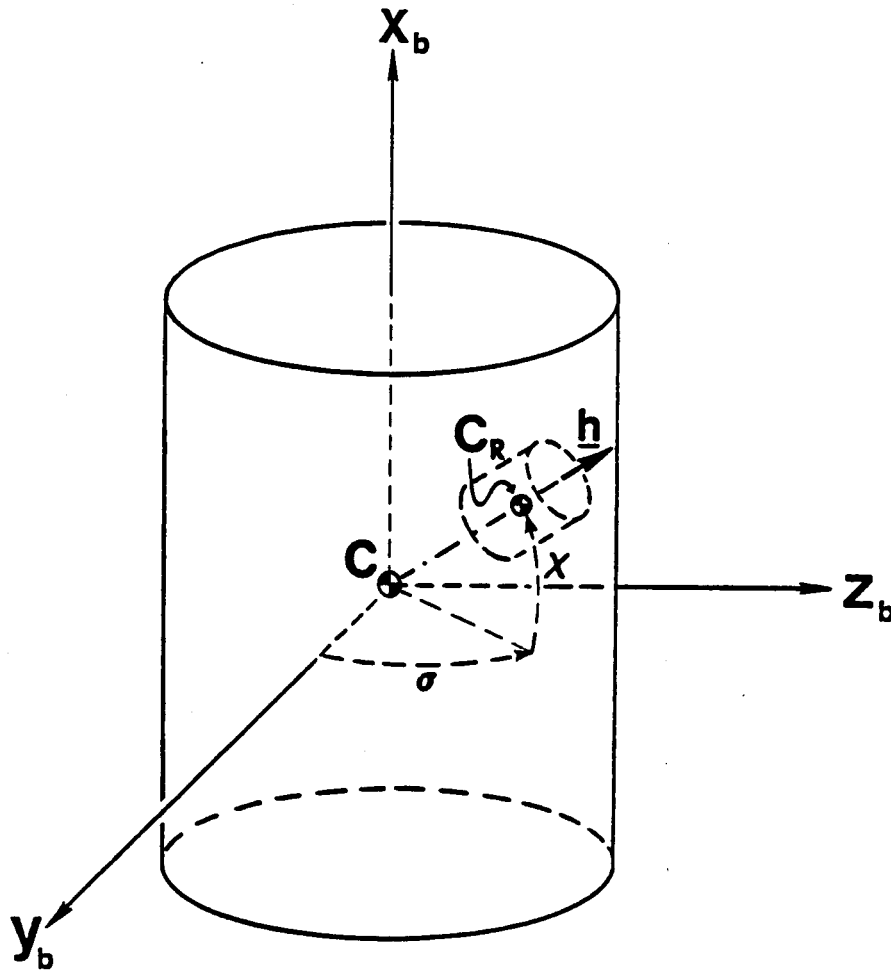
Fig. 5. Generic Satellite Physical Model.
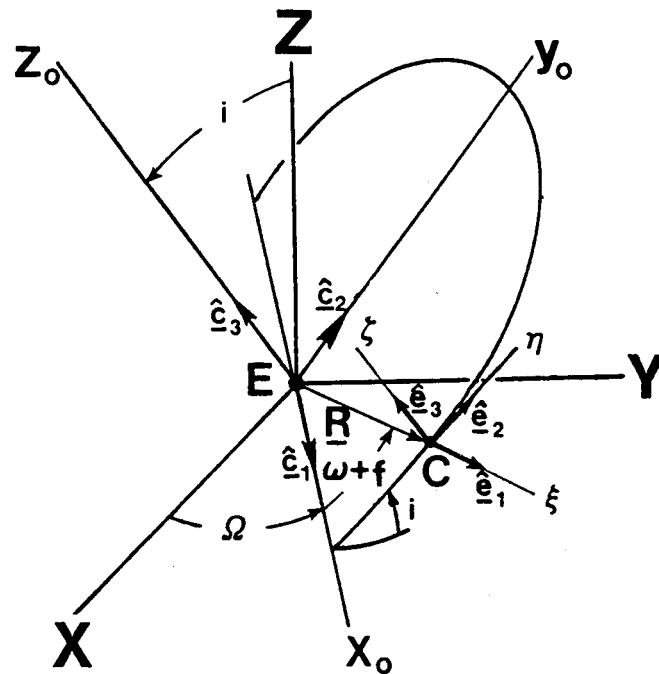
Fig. 6. Inertial, Orbital Plane, and Orbiting Coordinate Systems.
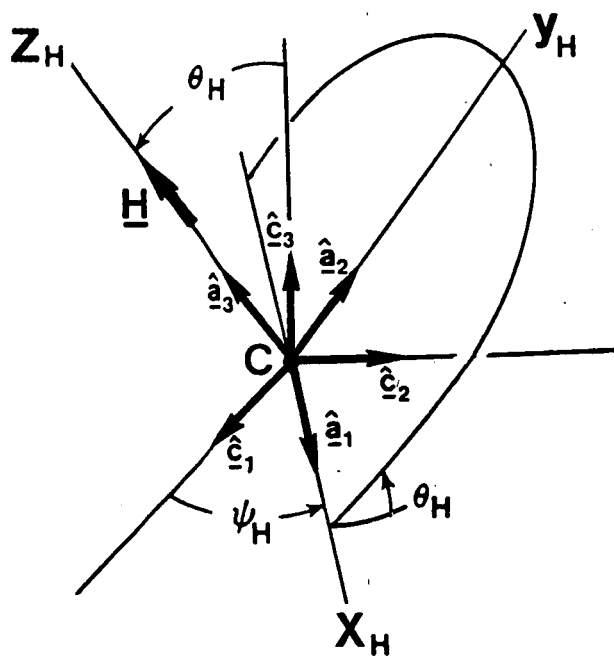
Fig. 7. Orbital Plane and Angular Momentum Coordinate Systems.
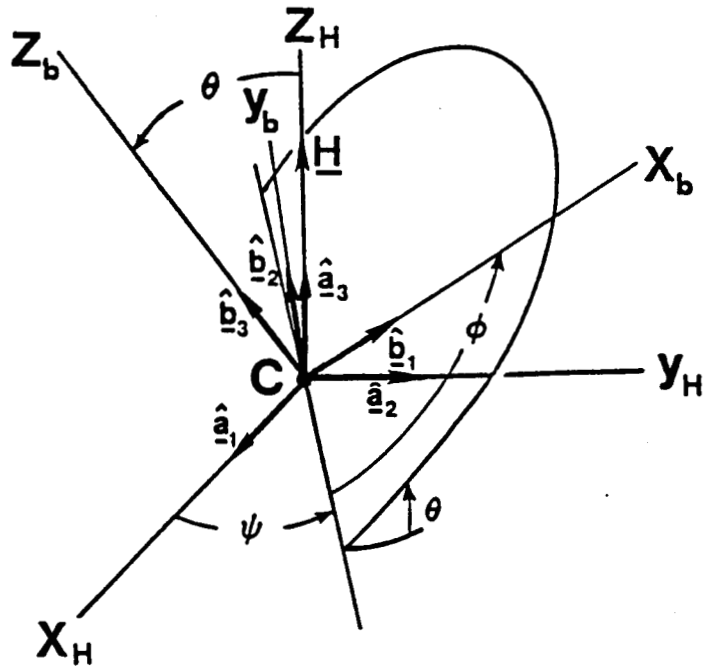
Fig. 8. Angular Momentum and Body-Fixed Coordinate Systems.

$Ex_0y_0z_0$ coordinate system. An "orbiting coordinate system" $C\xi\eta\zeta$ which has its origin at the center of mass of the satellite is also shown in Fig. 6. The ξ-axis of this coordinate system is collinear with $\underline{R}$, the position vector of C. The η-axis lies in the orbital plane and is directed in the sense of increasing true anomaly, f. The unit vector triad $(\hat{\underline{e}}_1,\hat{\underline{e}}_2,\hat{\underline{e}}_3)$ is attached to $C\xi\eta\zeta$. The orientation of the orbiting frame is defined by using the standard angles: Ω, the longitude of the ascending node; i, the inclination; ω, the argument of periapse; and f, the true anomaly. The notation, $u=\omega+f$, is used for convenience.

For cases in which the satellite's rotational angular momentum is large (HAM) compared to the magnitude of the external torque, the orientation of the satellite with respect to the inertial system is specified by first introducing the "angular momentum coordinate system," $Cx_Hy_Hz_H$, which has its z_H-axis collinear with $\underline{H}$, the total angular momentum vector of the satellite due to rotation about its center of mass (see Fig. 7). The angle Ψ_H is used to locate the x_H-axis which lies along the intersection of the orbital plane and the plane which passes through C and is perpendicular to $\underline{H}$. The angle between these two planes is Θ_H. A unit vector triad $(\hat{\underline{a}}_1,\hat{\underline{a}}_2,\hat{\underline{a}}_3)$ is associated with the $Cx_Hy_Hz_H$ system. Finally, the orientation of the satellite-fixed, centroidal, principal system $Cx_by_bz_b$ with respect to $Cx_Hy_Hz_H$ system is defined by using the Euler angles ψ, θ, and ϕ (as shown in Fig. 8) in a 3-1-3 rotation sequence. The angles ψ, θ, and ϕ are identified as the classical angles of precession, nutation, and proper rotation, respectively.[12] The unit vector triad $(\hat{\underline{b}}_1,\hat{\underline{b}}_2,\hat{\underline{b}}_3)$ is attached to $Cx_by_bz_b$.
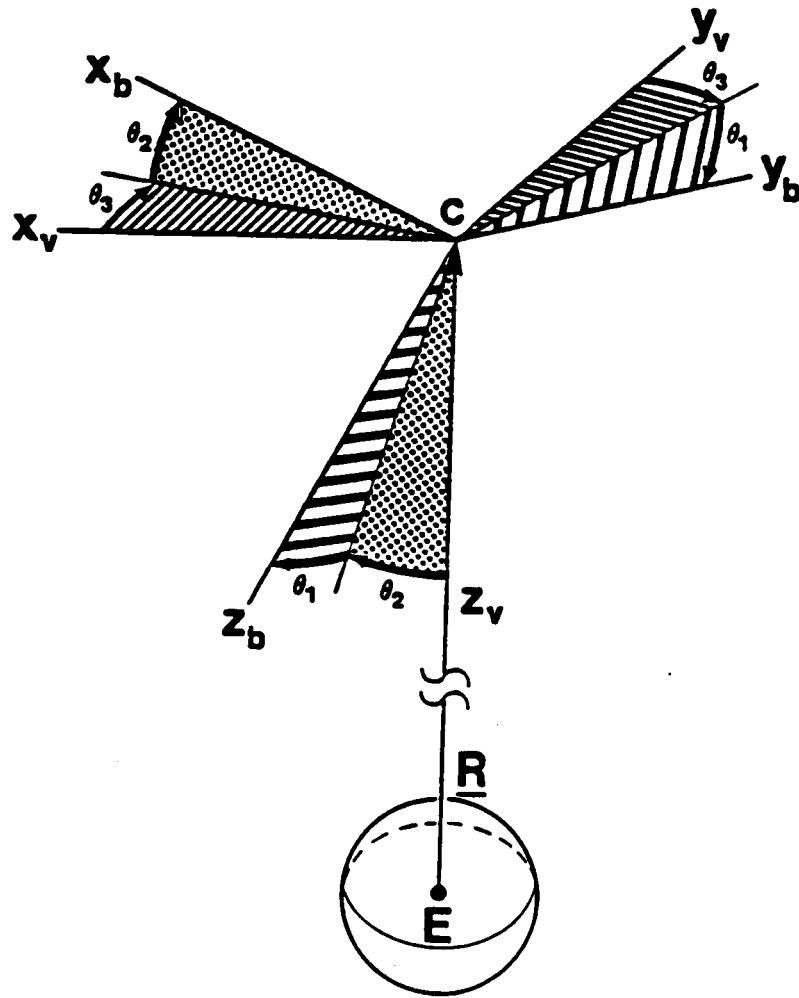
Fig. 9. Local Vertical and Body-Fixed Coordinate Systems.

Alternatively, for the LAM cases in which the satellite's angular momentum vector is small in magnitude compared to that of the external torque, a "local vertical" system $Cx_vy_vz_v$ is used which has its z_v-axis directed parallel to the negative ξ-axis of the $C\xi\eta\zeta$ system and its x_v-axis parallel to the orbital velocity vector. The orientation of the satellite body-fixed system $Cx_by_bz_b$ with respect to the $Cx_vy_vz_v$ system is defined by the angles θ_3, θ_2, and θ_1 (as shown in Fig. 9) in a 3-2-1 rotation sequence. Angles θ_1, θ_2, and θ_3 correspond to roll, pitch, and yaw angles, respectively.

4.2 Equations of Motion

The equations governing the attitude dynamics of the "general" satellite model depicted in Fig. 5, may be derived using $\underline{H}$, the angular momentum of the satellite, expressed in the satellite's body-fixed components; P_α, the angular momentum of the rotor about the axis of rotation of the rotor with respect to the satellite; α, the angle of relative rotation; and four Euler parameters, β_j, j=0,1,2,3.

Let $\underline{\underline{K}}$ denote the centroidal inertia matrix of the complete satellite, less the contribution by the rotor about the axis of rotation of the rotor with respect to the satellite. Then, the total angular momentum can be expressed as

$$\underline{H} = \underline{\underline{K}}\,\underline{\omega} + \underline{h} , \qquad (4.2.1)$$

where $\underline{\omega}$ is the absolute angular velocity of the satellite in the satellite's body-fixed components (b-basis) and where $\underline{h}$, the internal angular momentum vector, is

$$\underline{h} = \underline{\underline{J}} \; \underline{\underline{L}}_a \begin{bmatrix} 0 \\ 0 \\ P_\alpha/D \end{bmatrix} , \qquad\qquad (4.2.2)$$

where $\underline{\underline{J}}$ is the inertia matrix of the rotor about C_R, the center of mass of the rotor, in the b-basis; $\underline{\underline{L}}_{br}$ is the transformation matrix from the r-basis (a coordinate system fixed in the rotor with its 3-axis along the axis of rotation of the rotor with respect to the satellite) to the b-basis; and D is the moment of inertia of the rotor about the rotor axis of rotation.

The differential equation for the matrix, $\underline{\underline{H}}$, is

$$\underline{\dot{H}} = \underline{\underline{\tilde{H}}} \; \underline{\underline{K}}^{-1}(\underline{H}-\underline{h}) + \underline{T} , \qquad\qquad (4.2.3)$$

where

$$\underline{\underline{\tilde{H}}} = \begin{bmatrix} 0 & -H_z & H_y \\ H_z & 0 & -H_x \\ -H_y & H_x & 0 \end{bmatrix} \qquad\qquad (4.2.4)$$

and $\underline{T}$ is the external torque expressed in the satellite's body-fixed components. The momentum P_α varies according to

$$\dot{P}_\alpha = (0 \quad 0 \quad 1)[\underline{H}_{R/C_R}({}_r\underline{\omega}_r + {}_r\underline{\Omega}_r)] + T_\alpha \qquad\qquad (4.2.5)$$

where ${}_r\underline{H}_{R/C_R}$ is the angular momentum vector of the rotor about its own center of mass, expressed in the r-basis; ${}_r\underline{\omega}$ and ${}_r\underline{\Omega}$ are the angular velocities of the satellite and the rotor, respectively, also expressed in the r-basis; and T_α is the torque on the rotor about the axis of relative rotation.

The Euler parameters β_j, $j=0,1,2,3$, vary with time according to

$$\dot{\beta}_0 = -\frac{1}{2}\,\underline{\omega}^T\,\underline{\beta} \qquad\qquad (4.2.6)$$

and

$$\dot{\underline{\beta}} = -\frac{1}{2}\,\tilde{\underline{\omega}}\,\underline{\beta} + \frac{1}{2}\,\beta_0\,\underline{\omega}\;, \qquad\qquad (4.2.7)$$

where $\underline{\beta} = (\beta_1\ \ \beta_2\ \ \beta_3)^T$. (see, for example, Ref. 17, pp. 17-18 and 26). The direction cosine matrix, $\underline{\underline{L}}_{bI}$, which defines the orientation of the $Cx_b y_b z_b$ system with respect to the inertial coordinate system EXYZ may be expressed in terms of β_j, $j=1,2,3$, as follows:

$$\underline{\underline{L}}_{bI} = \begin{bmatrix} 1 - 2(\beta_2^2 + \beta_3^2) & 2(\beta_1\beta_2 + \beta_3\beta_o) & 2(\beta_1\beta_3 - \beta_2\beta_o) \\ 2(\beta_1\beta_2 - \beta_3\beta_o) & 1 - 2(\beta_1^2 + \beta_3^2) & 2(\beta_2\beta_3 + \beta_1\beta_o) \\ 2(\beta_1\beta_3 + \beta_2\beta_o) & 2(\beta_2\beta_3 - \beta_1\beta_o) & 1 - 2(\beta_1^2 + \beta_2^2) \end{bmatrix}\;. \qquad (4.2.8)$$

V. TORQUES

5.0 Introduction

The environmental torques which act on artificial satellites are
very small compared to, for example, the aerodynamic torques which act
on aircraft. However, when even small torques act over significant
periods of time, large changes in attitude motion can occur. As
discussed in the chapter on "Categorization," if the time period of
concern is relatively short, and if the magnitude of the satellite's
rotational kinetic energy is relatively large compared to the work done
on the satellite by its environment, the change in a satellite's
attitude will occur very slowly. A very important factor governing the
effects of environmental torques on the attitude motion of satellites is
the ratio of $|\underline{T}|$, the magnitude of the perturbing torque to $|\underline{H}|$, the
magnitude of the satellite's total angular momentum. When the ratio
$|\underline{T}|/|\underline{H}|$ is very small, say $\mathcal{O}(10^{-4})$, as it would be for a HAM satellite,
the short-term effects may be considered "minute." However, over long
periods of time they can significantly perturb a HAM satellite's
attitude motion. When $|\underline{T}|/|\underline{H}|$ is much larger, say $\mathcal{O}(1)$, as it might be
for a LAM satellite in LEO, the satellite's attitude motion will be very
strongly perturbed, even in the short term. In some cases, tumbling
motion which exhibits no well-defined pattern may occur. Under other
circumstances a LAM satellite will tend to oscillate "about a position
of relative equilibrium."[6,9]

27

Generally, environmental torques fall into two main categories. The first category consists of environmental torques which are derivable from a potential function. The most studied member of this category is the gravity-gradient torque; however portions of the "aerodynamic" torque (due to interactions of the atmosphere and a satellite) may also be derivable from a potential function. These torques are therefore "conservative." However, when the motion of the center of mass of the satellite is specified, there is generally no integral of the motion corresponding to conservation of energy, but in the special case of a circular orbit, a Jacobi-type integral does exist if only "conservative" torques are present. The other category of torques is that of "dissipative," or "damping," torques. These nonconservative torques cause secular changes in the rotational kinetic energy of the satellite and its attitude motion. The more significant of these are: the dissipative parts of the aerodynamic torques; the torques due to the solar radiation pressure--direct from the sun, as well as reflected by the earth and its atmosphere; and torques resulting from the interaction of conducting parts of satellites with the earth's magnetic field. The most dominant in orbits of altitude up to 300 km are the aerodynamic torques.[6,9,16]

Many of the perturbation techniques employed in the treatment of satellite orbital motion can be employed analogously to study satellite attitude motion in the presence of perturbing environmental torques. Any further discussion, or reference, to environmental torques in this report will center on the two most dominant, gravity-gradient and aerodynamic.

5.1 Gravity-Gradient Torques

According to Beletskii,[9] the primary effect of gravity-gradient torques "amounts to secular precession of the angular momentum vector around the normal to the orbital plane." He goes on to say that "periodic nutations of the angular momentum vector (with a period comparable to the satellite's orbital period) are superimposed on this secular precession."[9]

Gravity-gradient torques are due to the fact that the earth's gravitational field is not uniform. This non-uniformity in both the magnitude and direction of the field over distances even as small as the dimensions of an orbiting artificial satellite result in a "gravity-gradient" potential over the satellite body. This gravity-gradient potential over the satellite results in a gravity-gradient torque about the satellite's center of mass. This gravity-gradient torque was first considered in the context of celestial mechanics in 1749 by d'Alembert and Euler, and later in 1780 by Lagrange.[17,18]

A number of factors are involved in determining the perturbation effect of gravity-gradient torque upon the satellite's attitude motion. If one assumes that the satellite is a single-rigid-body orbiting a spherical primary in a circular orbit, the problem is greatly simplified. With these assumptions, the gravity-gradient torque becomes a function of the distance from the center of mass of the satellite to the center of the earth; the values of the principal moments of inertia; and the orientation of the satellite's body-fixed axes with respect to the radius vector between the center of the earth and the satellite's center of mass. Using the above assumptions, the gravity-gradient

torques on an asymmetric satellite in a Newtonian gravitational field can be expressed in the form[9,16,17,19]

$$
\underline{T}_g = \frac{3\mu_E}{R^3} \begin{bmatrix} (C-B) \ c_{23}c_{33} \\ (A-C) \ c_{33}c_{13} \\ (B-A) \ c_{13}c_{23} \end{bmatrix} ,
$$

(5.1.1)

where R is the magnitude of $\underline{R}$, the position vector from the center of the earth to the satellite's center of mass; A, B, and C are the principal centroidal moments of inertia; and the c_{j3}, j=1,2,3, are the direction cosines of $\underline{R}$ in the satellite's body-fixed coordinate system. If the above simplifying assumptions are not made the expression for the gravity-gradient torque is much more complex. For example, if one assumes an "oblate earth," the expression for the x_b-component of the gravity-gradient torque has the form[17]

$$
T_{g_x} = \frac{3\mu_E}{R^3} (C-B) \ c_{23}c_{33} + \frac{3\mu_E J_2 R_e^2}{2R^5} (C-B)[5(1-7 \ \sin^2\lambda)c_{23}c_{33}
$$

$$
-10 \ \sin \lambda(c_{23}c_{e33} + c_{33}c_{e23})-2c_{e23}c_{e33}]
$$

(5.1.2)

where $J_2 = 1.083 \times 10^{-3}$, λ is the latitude of the center of mass of the satellite, R_e is the equatorial radius of the earth, and c_{ej3}, j=1,2,3, are the direction cosines between the body-fixed axis and the earth's polar axis. Note that the additional gravity-gradient torque terms in Eq. (5.1.2) diminish at a rate of R^{-5} while the terms in Eq. (5.1.1) diminish at a rate of R^{-3}. For small satellites, the additional terms due to the asphericity of the primary can be neglected as they normally

result in less than a 1% difference, even for satellites in "low earth orbits."[17] However, if one were to consider a larger satellite, such as the proposed Space Station, then the higher order terms would take on greater significance.[17]

Another concern is that of more than one celestial body. In the earth, moon and sun system one must consider the gravity-gradient effects of the other celestial bodies in much the same manner that one considers their perturbing effects upon orbital trajectories. For near earth orbits, one may assume that the satellite is within the "sphere of influence" of the earth, and include only the perturbing effects of the earth. To illustrate this point, consider that for a geosynchronous orbit the gravity-gradient torque due to the moon is less than 0.0023% of that due to the earth, and the gravity-gradient torque at geosynchronous altitudes due to the sun is less than 0.0011% of that due to the earth.[17]

To summarize, for the purposes of the simulations used in this investigation, the following assumptions were found to give a sufficiently accurate representation of gravity-gradient torques on the satellites modeled: (1) the satellite mass distribution is that of a single, tri-inertial (or asymmetric), rigid body; (2) its center of mass is moving in a two-body orbit about a spherical primary; (3) the greatest dimension of the satellite is much smaller than the radius of the orbit of its center of mass; and (4) the orbital plane may be rotating in a prescribed manner.

5.2 Aerodynamic Torques

As noted in the introduction to this chapter on environmental torques, there are a number of dissipative torques. The most dominant of these in the LEO altitude range are the aerodynamic torques. Although well outside the domain of "atmospheric vehicles," artificial earth satellites are by no means free of the effects of the atmosphere. This is demonstrated by the constant attention which those who track satellites pay combating the problem of orbital decay due to atmospheric drag. The treatment of aerodynamics at orbital altitudes as opposed to lower altitudes is different. At orbital altitudes the "mean free paths" between molecules are on the order of a kilometer or more, much larger than the dimensions of LEO satellites. This means that one need not consider collisions between molecules approaching the satellite's surface with those leaving the surface. Thus, one can use a "free-molecular flow model" to approximate the "aerodynamics" of satellites. This treatment greatly simplifies the determination of the aerodynamic torques acting upon a satellite.[9,17]

There are four primary aerodynamic effects on satellites moving in the free-molecular flow regime. The first effect is similar to the "Weather Cock" effect which occurs in the lower portions of the atmosphere. This effect is due to the fact that the center of pressure and the center of mass of the satellite do not coincide. As a result of this, there is a restoring torque which tends to stabilize the satellite in the direction of the resultant of the orbital velocity of the satellite and the local velocity of the atmosphere due to the earth's rotation. The second effect is due to the angular velocity of the

satellite about its own center of mass. The torques developed due to this effect are known as the "spin damping dissipative torques."[6,9] Since even for high rates of satellite rotation the linear velocity due to rotation is much smaller than the satellite's orbital velocity, these torques can be considered to vary linearly with angular velocity. The last two effects are small by comparison and are usually ignored. These are pressure gradient and the molecular thermal velocity effects. The pressure gradient effect is due to the density differential which exists over the satellite surface (being higher on the portion of the satellite facing the earth). The contribution of molecular thermal velocity is generally neglected because it is much smaller than the orbital velocity of the satellite.[9]

For the purposes of this research effort, only the first two aerodynamic effects were considered to be significant. The model chosen to simulate the satellite in a free-molecular flow regime is a right-circular cylinder, a shape which is common among satellites. The coordinate axes chosen, as seen in Fig. 9, are very similar to those used by Etkin[20] to describe the motion of atmospheric vehicles. Note that the axis of symmetry has been designated the x_A-axis in a $Cx_Ay_Az_A$ system. For the purposes of this work, it is assumed that the axes of $C_Ax_Ay_Az_A$ are <u>aligned</u> with the axes of $Cx_by_bz_b$, but that C and C_A do not coincide. The $C_Ax_wy_wz_w$, "relative wind" system, has its x_w-axis along the orbital velocity vector and its z_w-axis lies in the orbit plane and points (nominally) toward the center of the earth. The angles, α_a and β_a, between the relative wind system and the body-fixed system are the angle of attack and the sideslip angle, respectively, of the satellite (see Fig. 10). For the purpose of
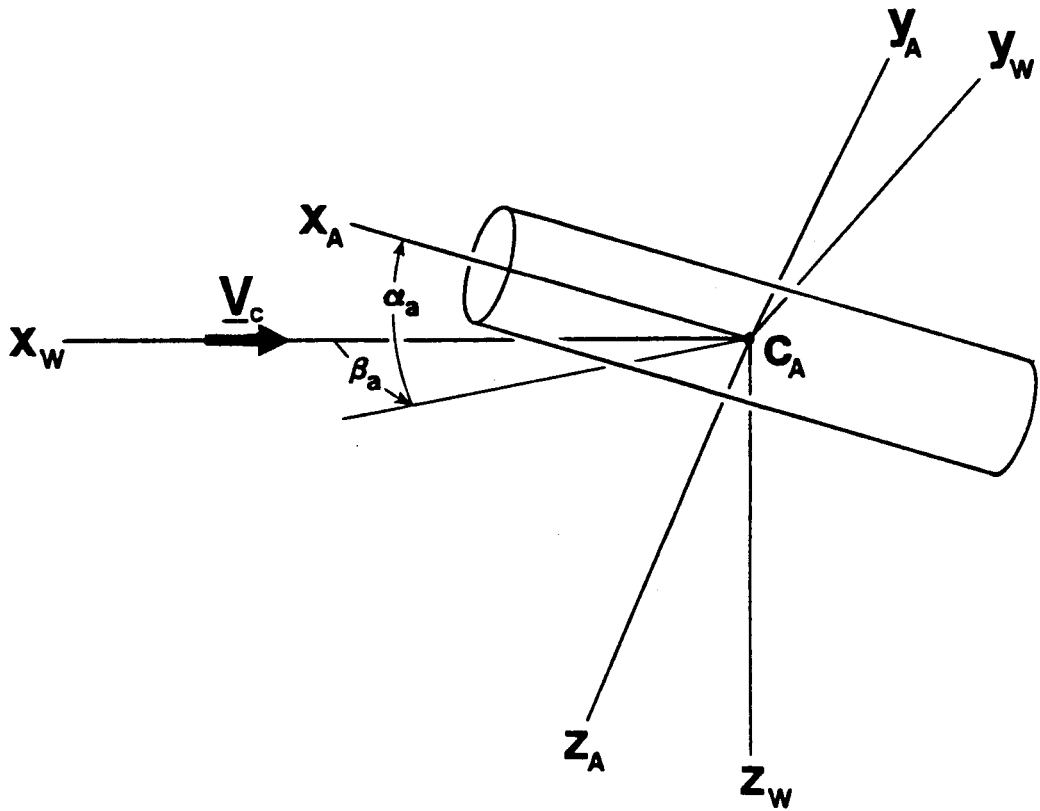
Fig. 10. Angle of Attack and Sideslip Angles.
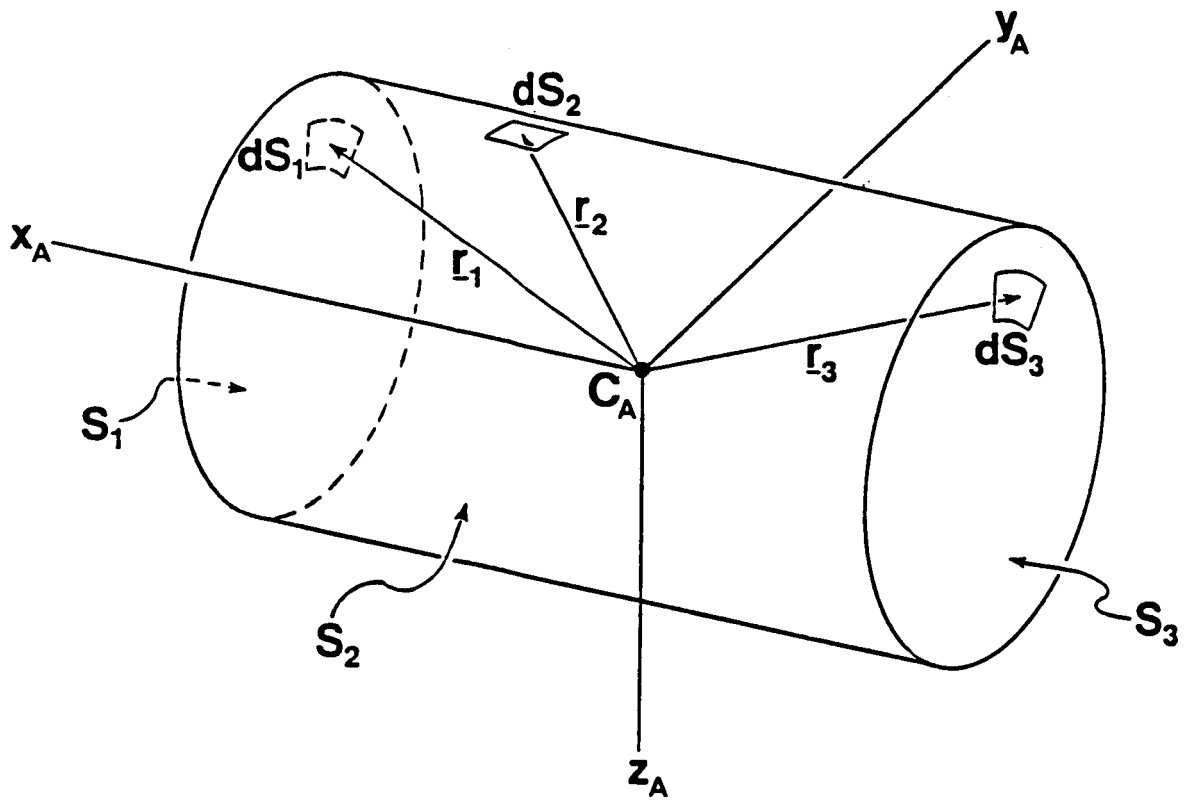
Fig. 11. Diagram of Aerodynamic Cylinder Model.

integrating the force per unit area, the cylinder is divided into three

surfaces, S_1, S_2 and S_3 (see Fig. 11). Position vectors, $\underline{r}_1$, $\underline{r}_2$, and

$\underline{r}_3$ from the centroid of the cylinder to the surface elements dS_1, dS_2,

and dS_3, respectively, are used in deriving an expression for the torque

about C_A. The aerodynamic torque on the cylinder may be written as

follows:

$$\underline{T}_a = - \; 1/2 \; \rho \; c_d [\int_{S_1} \underline{r}_1 \; x \; (\hat{\underline{n}}_1 \cdot \underline{V})\underline{V} \; dS_1 + \int_{S_2} \underline{r}_2 x(\hat{\underline{n}}_2 \cdot \underline{V})\underline{V} \; dS_2$$

$$+ \int_{S_3} \underline{r}_3 x \; (\hat{\underline{n}}_3 \cdot \underline{V})\underline{V} \; dS_3] \; , \tag{5.2.1}$$

where ρ is atmospheric density, c_d is an accommodation constant,

$\hat{\underline{n}}_1$, $\hat{\underline{n}}_2$, and $\hat{\underline{n}}_3$ are the normal unit vectors normal to each respective

surface, $\underline{V} = \underline{V}_C + \underline{\omega} \; x \; \underline{r}_j$, $j=1,2$, or 3, where $\underline{V}_C$ is the translational

velocity of the satellite's center of mass,* and $\underline{\omega} = (p \; q \; r)^T$. The

results of the derivation of the aerodynamic torques on the right

circular cylinder are given in Appendix D.

It must be realized that any model of the aerodynamic torque on a

satellite in orbital space is an approximation. Two factors which limit

the accuracy of the modeling are variations in atmospheric density, and

"shadowing," or "blanketing," of portions of the body by its other

portions, for example, solar panels.[17],[21] Since the purpose of the

simulations contained in this thesis is to determine <u>qualitatively</u> the

---

*Note that strictly speaking the velocity $\underline{V}_{C_A}$ should be used.

However, this would only modify the results by changing the $\underline{r}_j$,

$j=1,2,3$, slightly.

effects of environmental torques, a rather simple exponential
atmospheric density model was adopted. Obviously, this model does not
take into account such sources of variations in density as the diurnal
cycles, orbital inclination (latitude variations at equal altitudes),
and solar activity. Also, although a right-circular cylinder is a good
approximation to the shape of many satellites, for satellites which have
complex geometries (such as those with large sun seeking solar arrays)
shadowing is a major problem. Such arrays can, at certain satellite
attitudes, blanket large portions of the satellite surface resulting in
torques greatly different from those on an unshadowed body.[21] However,
the modeling of these complex satellite arrays for all possible aspects
is extremely difficult and is beyond the scope of this effort.

VI. SHORT-TERM APPLICABILITY OF TORQUE-FREE

ANALYTICAL MODEL

6.0 Introduction

When a closed-form analytical solution exists for the torque-free

motion of a particular satellite, it is generally the more efficient

solution for short-term attitude motion simulations. Numerical

solutions, although generally available, tend to require much more

computer time than torque-free analytical solutions, especially in the

case of satellites with high rates of rotation which necessitate the use

of small integration step-sizes. However, when one attempts to

incorporate the perturbing effects of environmental torques into the

analytical approach, the complexity of the analytical solution increases

significantly. In some cases, specifically, those in which the

magnitude of the total angular momentum is much larger than the

magnitude of the environmental torques acting upon the satellite, the

torque-free analytical solutions are very accurate over short time

periods. In other cases, for example, those in which the magnitude of

the environmental torque is greater than the magnitude of the total

angular momentum of the satellite, a numerical approach incorporating

environmental torques is usually necessary.

The purposes of this chapter are to investigate the fidelity and

applicability of the analytical solutions discussed in Section 3.3 and

to present some results of numerical simulations of LAM satellite atti-

tude motion. First, to verify their fidelity, the analytical solutions

are compared with results from the numerical simulation code. Second, to determine the <u>applicability</u> of the torque-free analytical solutions, they are compared with numerical simulation results obtained using the same initial conditions, but including gravity-gradient torques. This comparison illustrates how, at lower angular momentum levels (as compared to the magnitude of the environmental torque), the fidelity of the torque-free analytical solutions degenerates rapidly, indicating the need to use either an analytical or a numerical solution which incorporates environmental torques. Third, to show that there are cases for which the analytical solutions cannot be expected to provide accurate results, some examples of simulated attitude time-histories of actual satellites in the LAM category are presented.

6.1 Applicability of Analytical Solutions

To verify the analytical solutions, the numerical simulation code was run with the data shown in Table 1. The data used in the analytical solutions is given in Table 2. Note that the moments of inertia in Table 1 differ slightly from those in Table 2. This is due to the fact that the numerical code uses a <u>single</u> <u>movable</u> <u>rotor</u> to simulate the two rotors of the analytical model. In each, the <u>system</u> is axisymmetric. As verification of the analytical solution, the results for the four cases are shown in Figs. 12, 13, 14, and 15. The variable "TAU" is a "no-dimensional" time, defined as TAU = Ht/A. The numerical results are shown as triangles superimposed on the corresponding analytical time-histories (continuous curves) of the precession, nutation, and proper rotation angles, respectively. The first three cases (shown in Figures 12, 13, and 14) are for an oblate satellite with various initial angular velocities. The fourth case (Fig. 15) is for a rapidly spinning

Table 1 Data for Numerical Verification of Torque-Free Analytical Simulation of Attitude Motion of Satellites with Asymmetric Internal Angular Momentum.

	Case I	Case II	Case III	Case IV
Moments of Inertia ($kg\text{-}m^2$):				
Main Body I_{xx}	400.	398.42	398.42	185.
I_{yy}	280.	285.77	285.77	399.2
I_{xx}	300.	300.	300.	400.
$I_{xy} = I_{yx}$	0.	-4.743	-4.743	-1.98
Rotor I_{R_z}	20.	15.81	15.81	15.13
Initial Angular Rates (rad/sec):				
ω_{x_o}	3.2	2.0	0.1	3.5
ω_{y_o}	0.4	0.1	0.05	0.1
ω_{z_o}	0.001	0.001	0.001	0.001
Rotor Rate Ω_o	10.	10.	10.	10.
Orientation of Rotor Spin Axis	Along y-axis	In x-y plane 71.56° from x-axis	Same as Case II	In x-y plane 7.6° from x-axis

Table 2 Data for Torque-Free Analytical Simulation of Attitude Motion of Satellites with Asymmetric Internal Angular Momentum.

		Case I	Case II	Case III	Case IV
Moments of Inertia (kg-m^2):					
	A	400.	400.	400.	200.
Main Body	B	300.	300.	300.	400.
	C	300.	300.	300.	400.
Initial Angular Rates (rad/sec):					
ω_{x_o}		3.2	2.	0.1	3.5
ω_{y_o}		0.4	0.1	0.05	0.1
ω_{z_o}		0.001	0.001	0.001	0.001
Internal Angular Momenta (kg-m^2/sec):					
h_x		0.0001	50.	50.	50.
h_y		200.	150.	150.	150.
h_z		0.	0.	0.	0.

41

Fig. 12 a. Multi-Rotor Numerical Verification Case I, Precession
            Angle Time-History.

Fig. 12 b.   Multi-Rotor Numerical Verification Case I, Nutation Angle
             Time-History.

Fig. 12 c. Multi-Rotor Numerical Verification Case I, Angle of Proper
Rotation Time-History.

Fig. 13 a.   Multi-Rotor Numerical Verification Case II, Precession
             Angle Time-History.
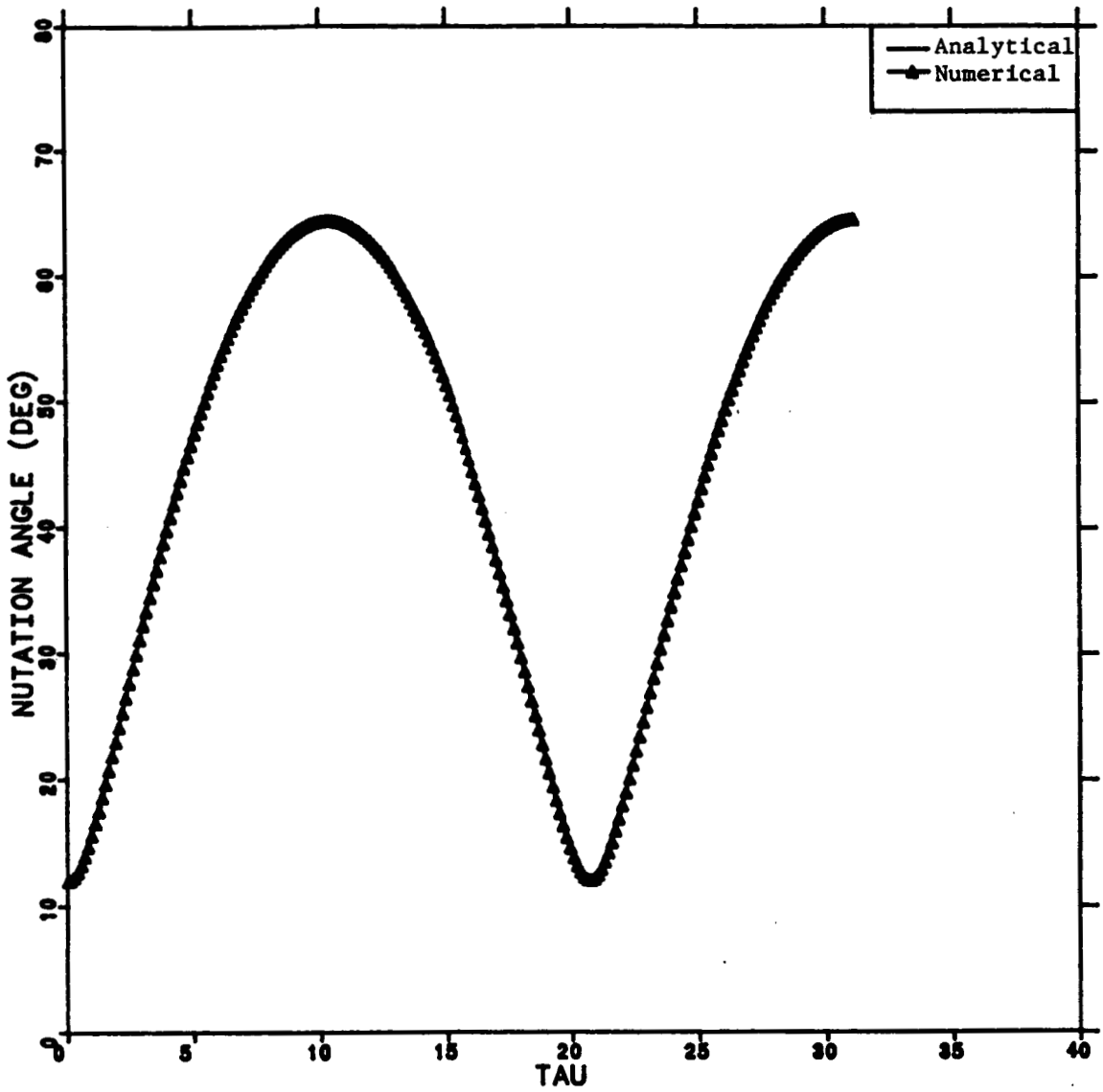
Fig. 13 b. Multi-Rotor Numerical Verification Case II, Nutation Angle
Time-History.
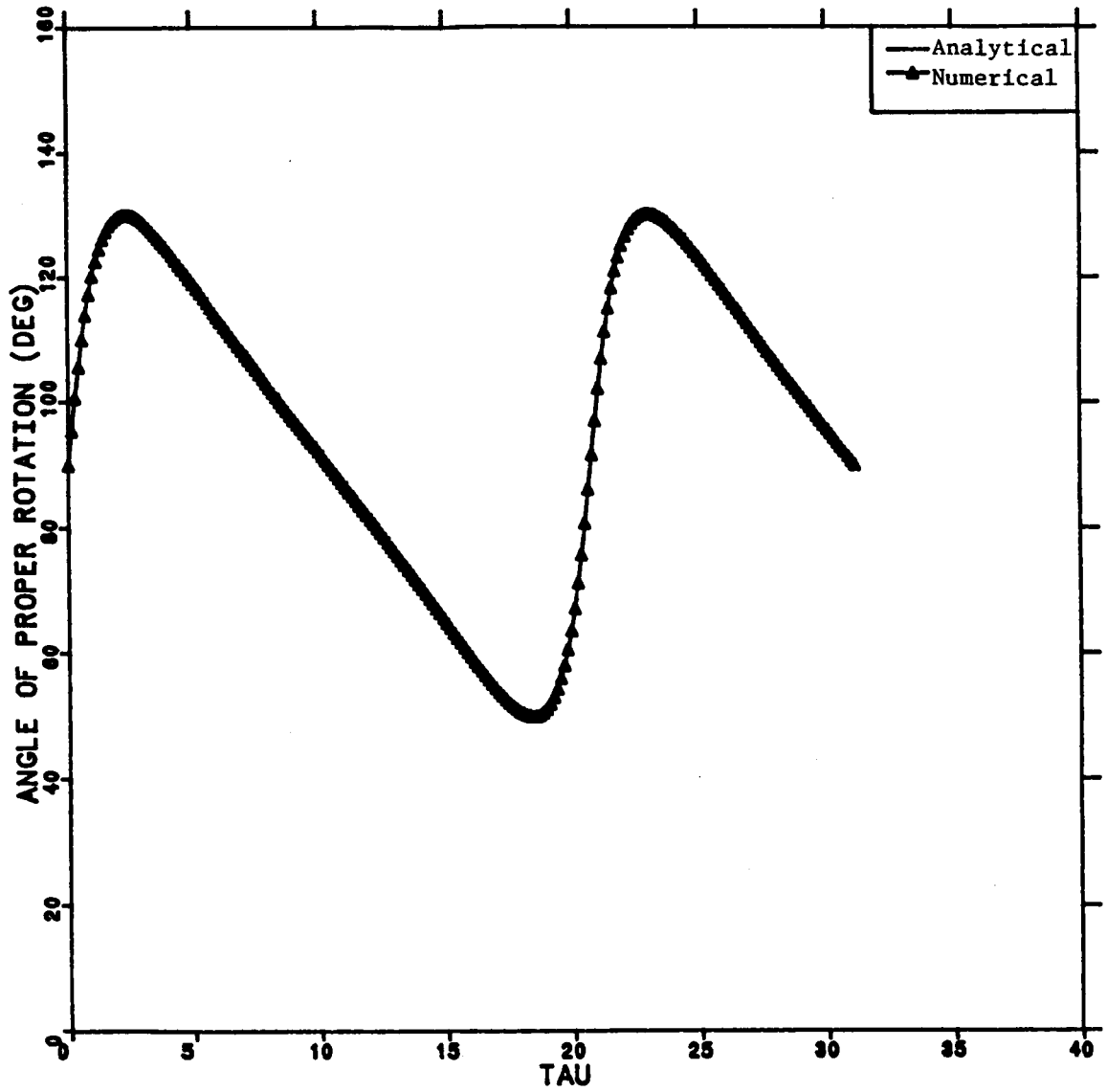
Fig. 13 c. Multi-Rotor Numerical Verification Case II, Angle of Proper
            Rotation Time-History.
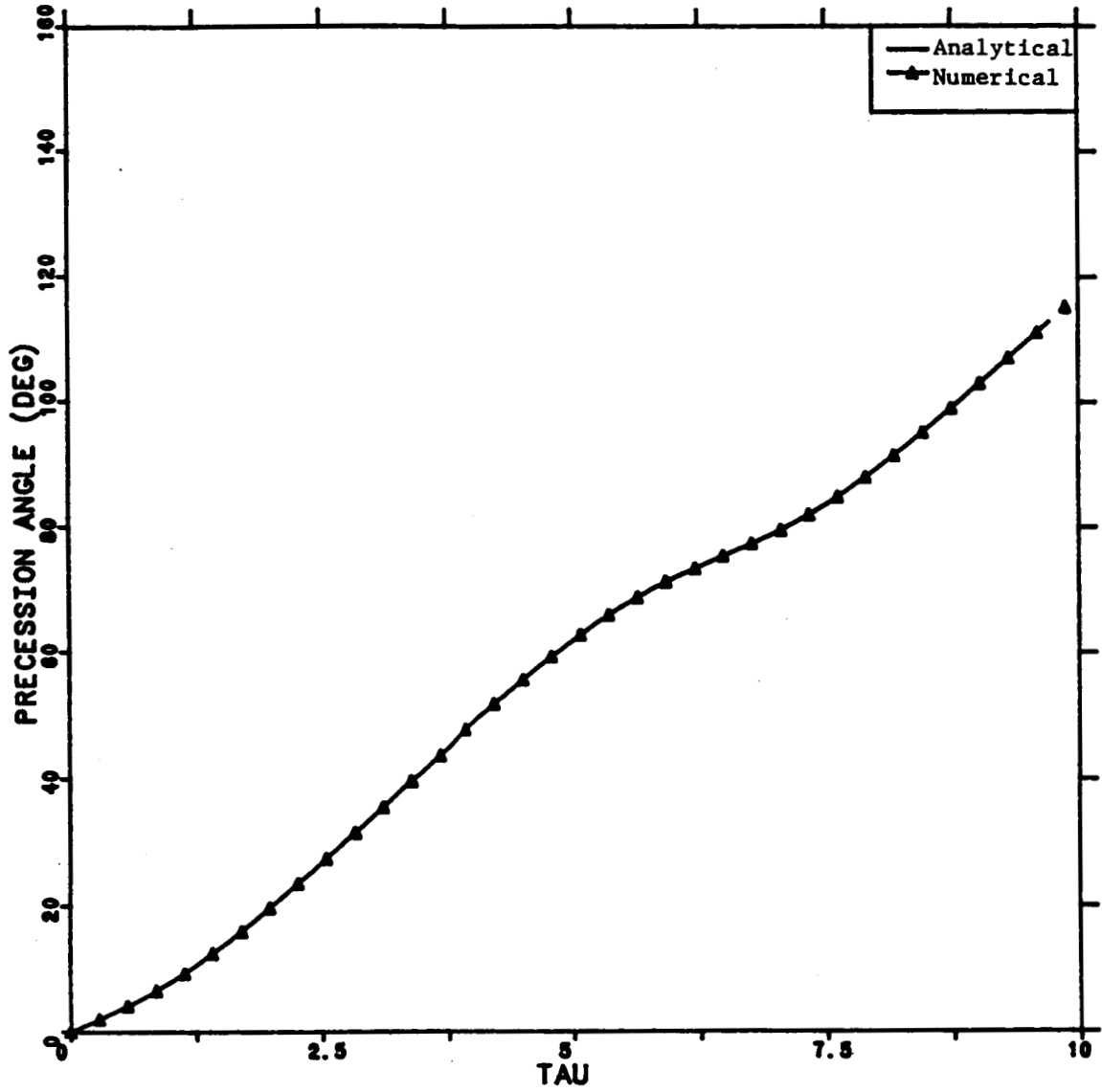
Fig. 14 a.   Multi-Rotor Numerical Verification Case III, Precession
Angle Time-History.
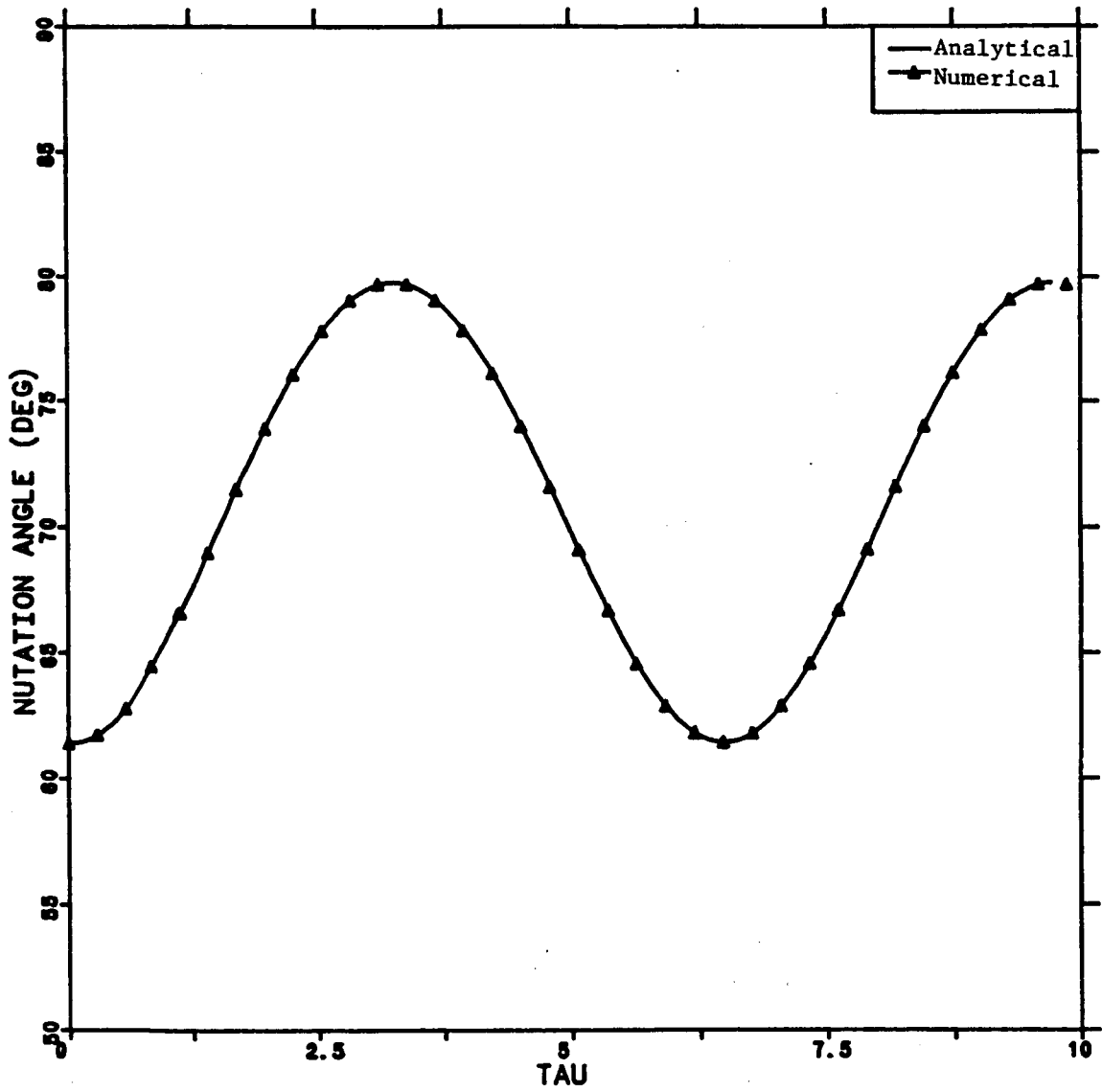
Fig. 14 b. Multi-Rotor Numerical Verification Case III, Nutation Angle
           Time-History.
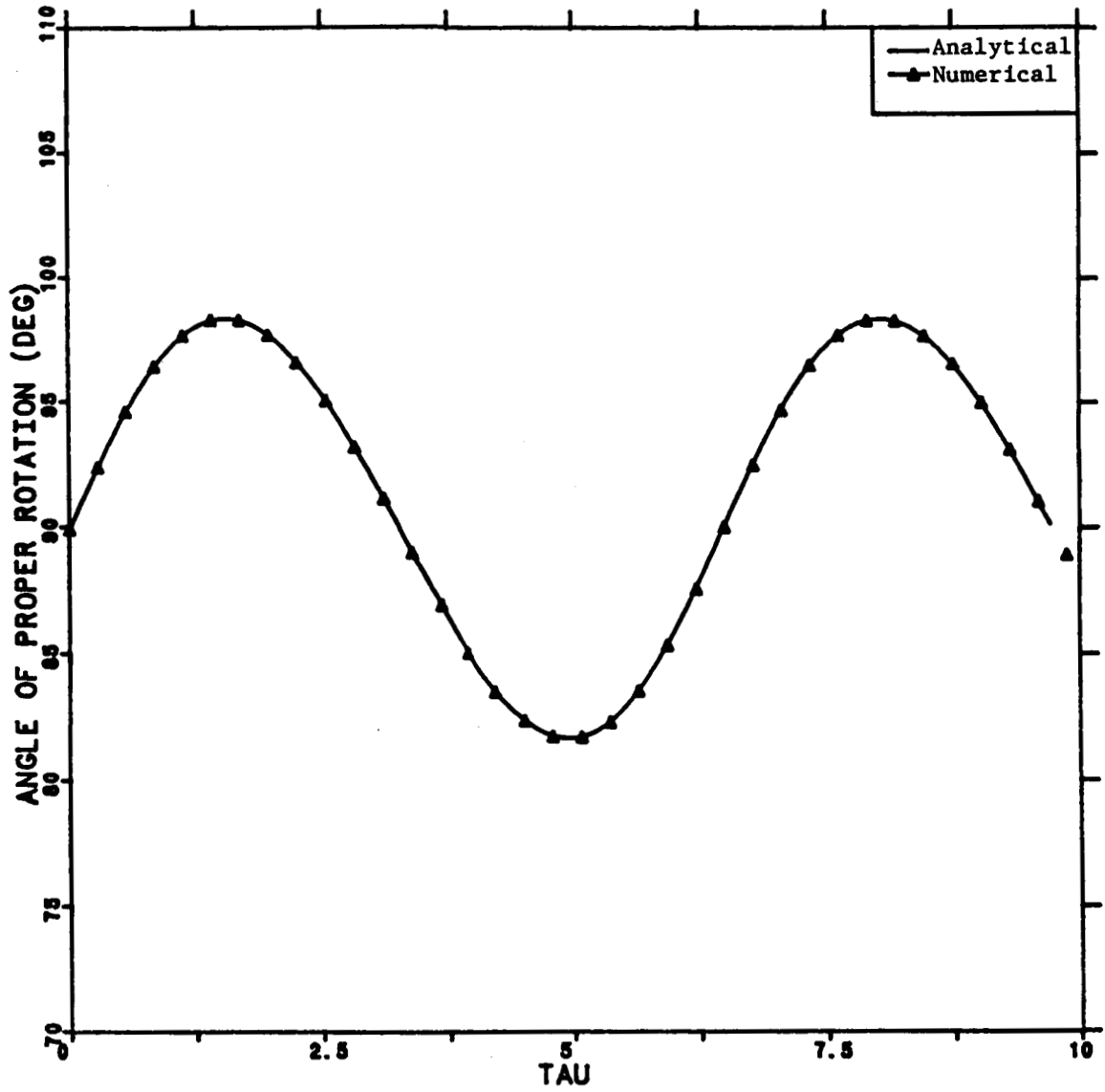
Fig. 14 c. Multi-Rotor Numerical Verification Case III, Angle of Proper
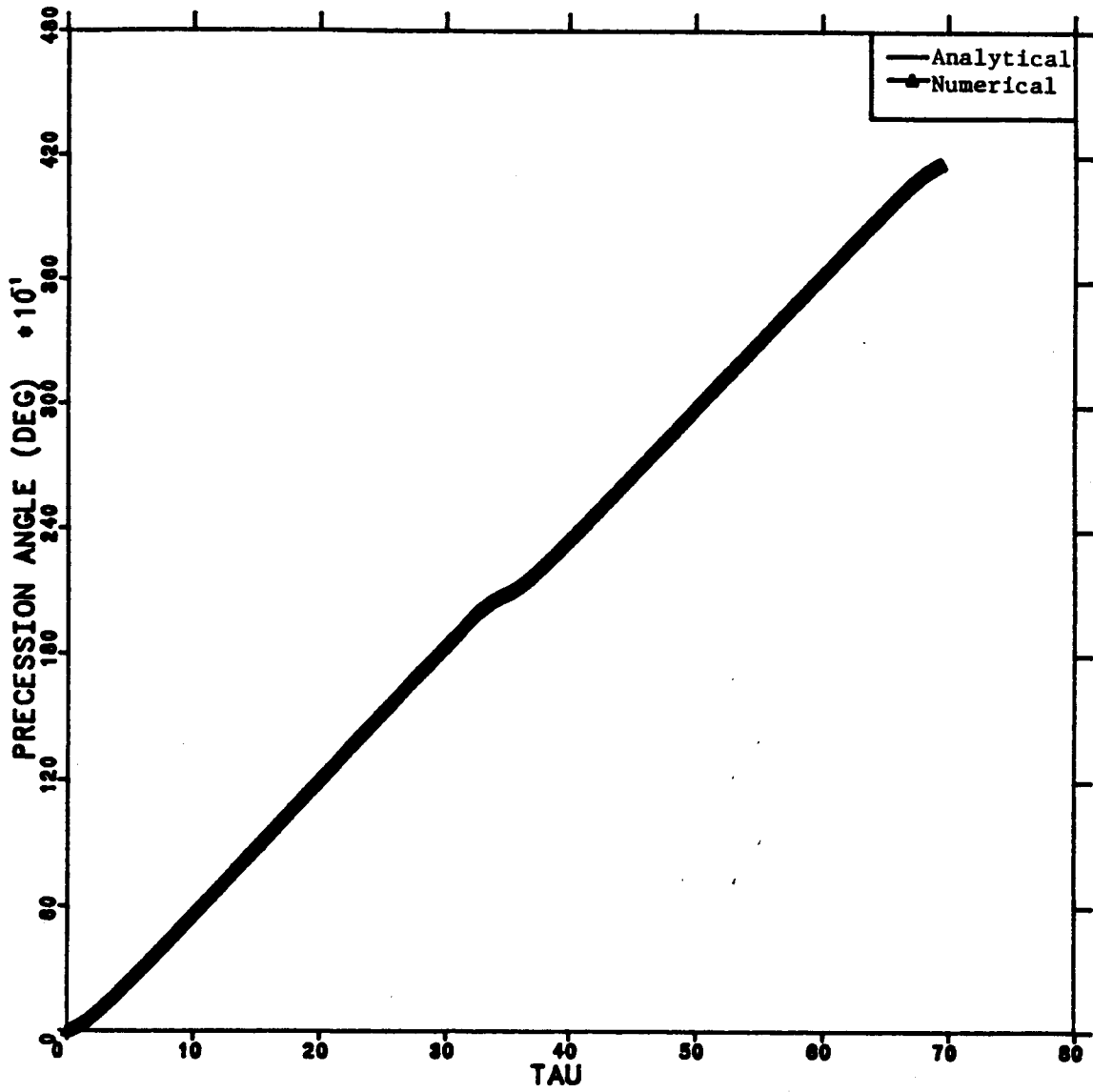Rotation Time-History.
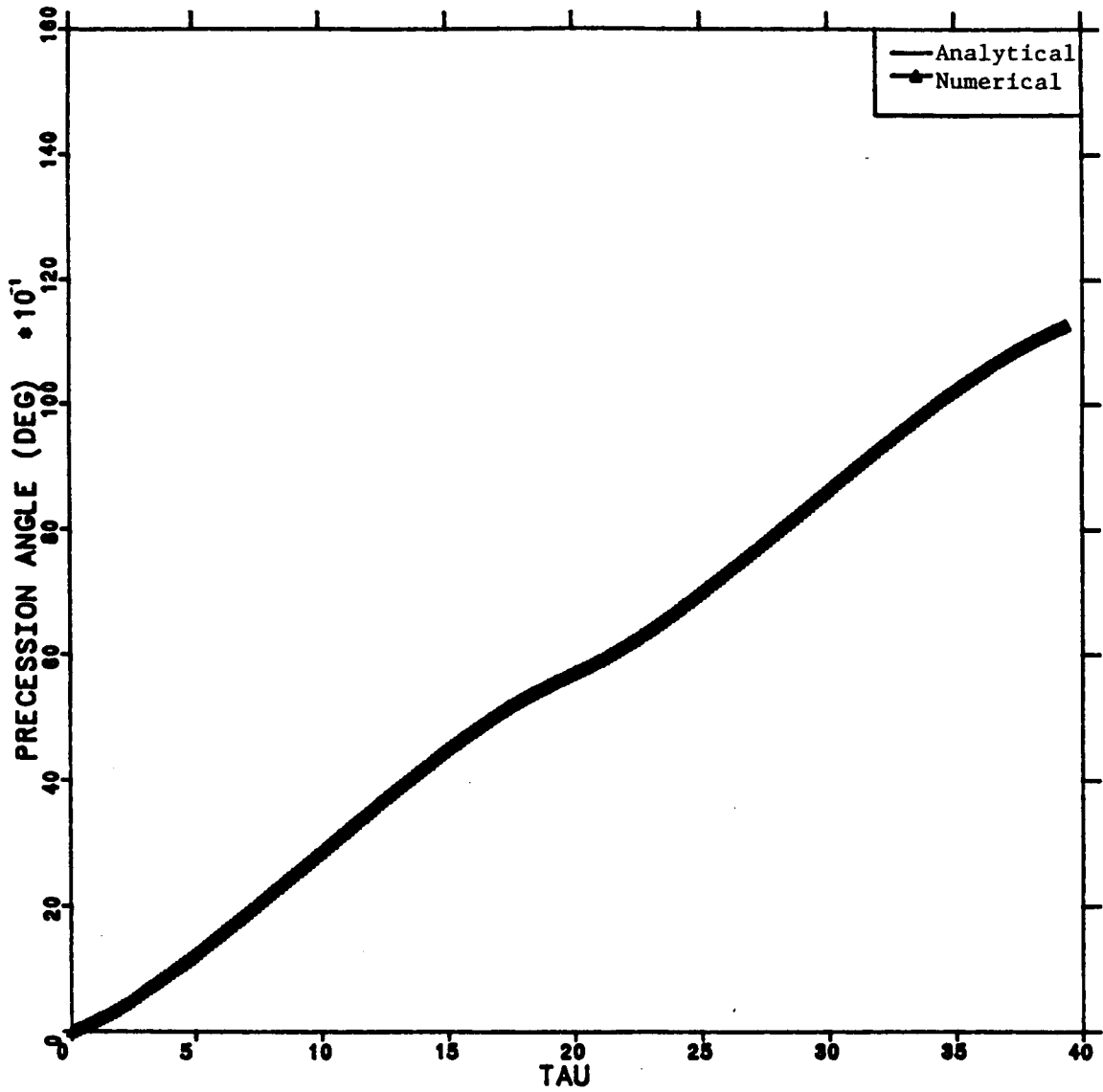
Fig. 15 a. Multi-Rotor Numerical Verification Case IV, Precession Angle
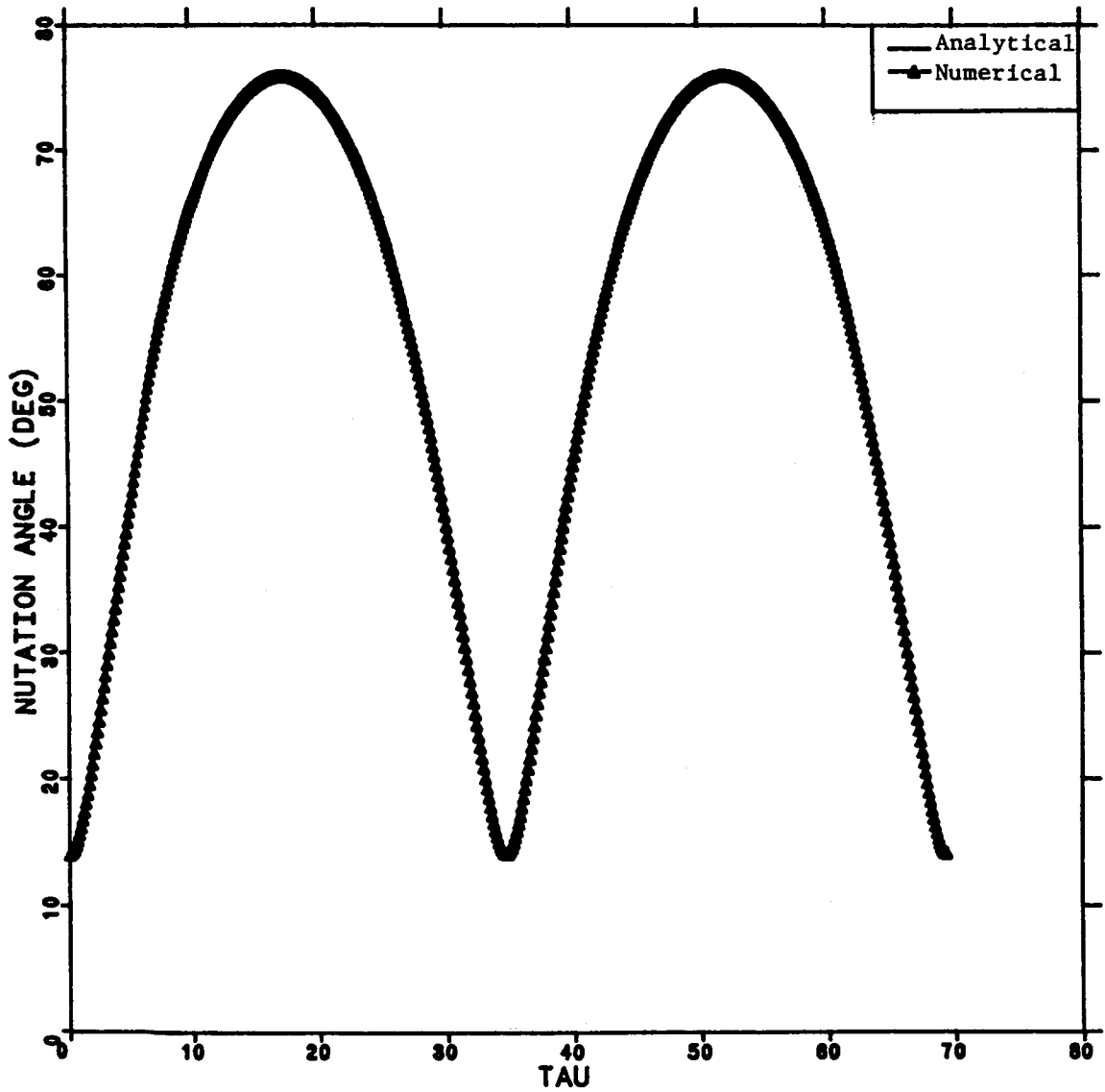Time-History.
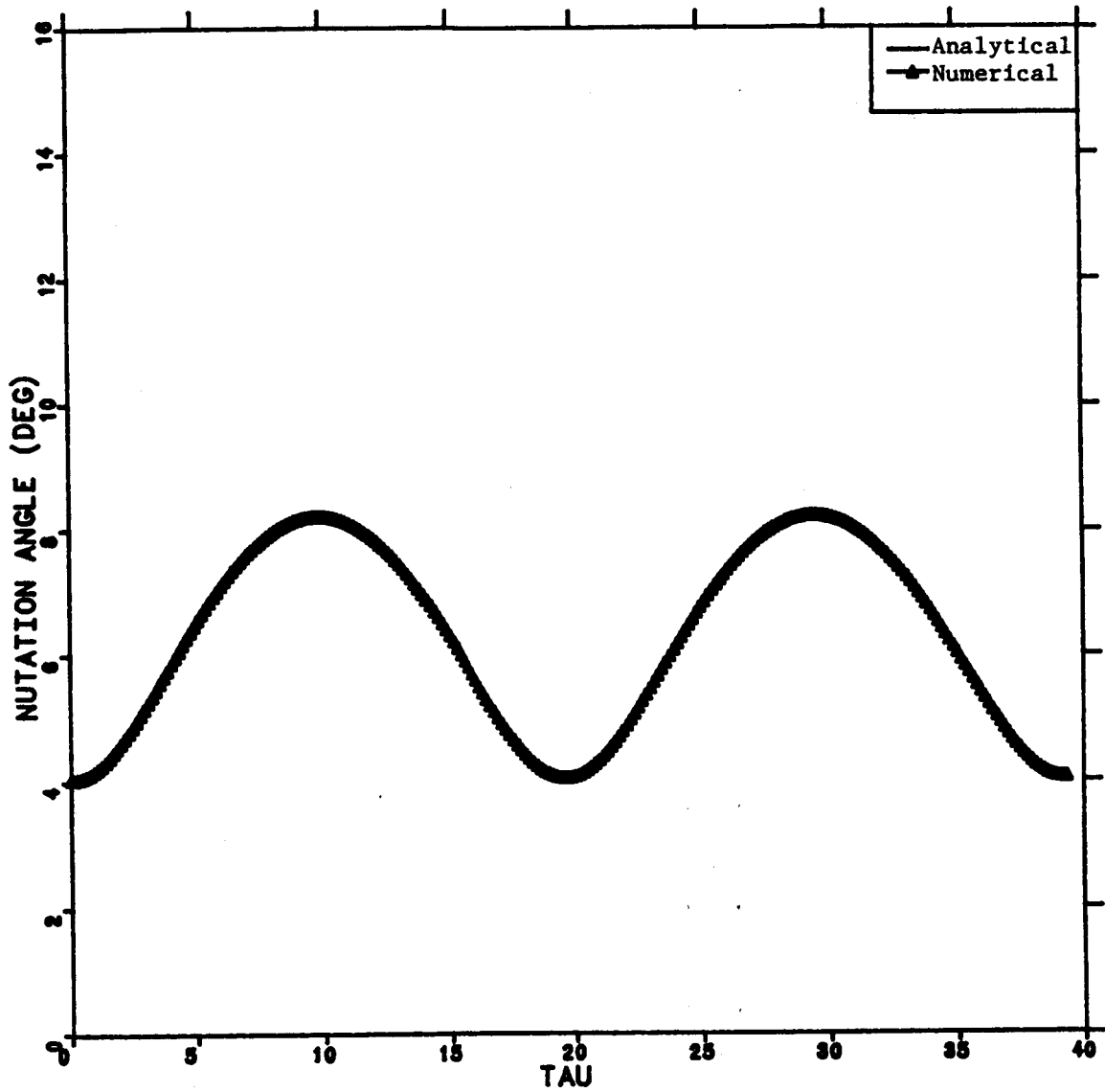
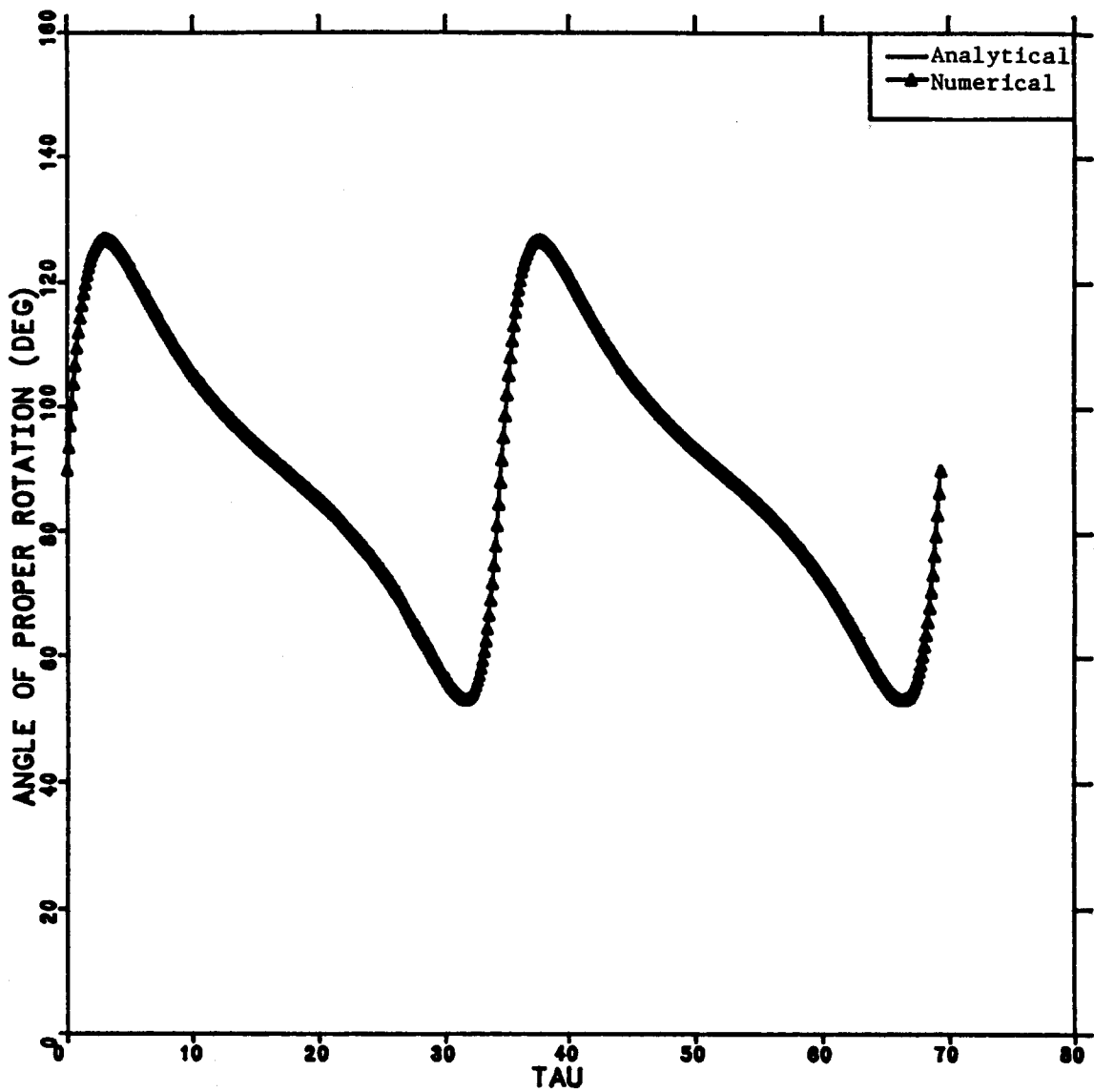Fig. 15 b. Multi-Rotor Numerical Verification Case IV, Nutation Angle
            Time-History.
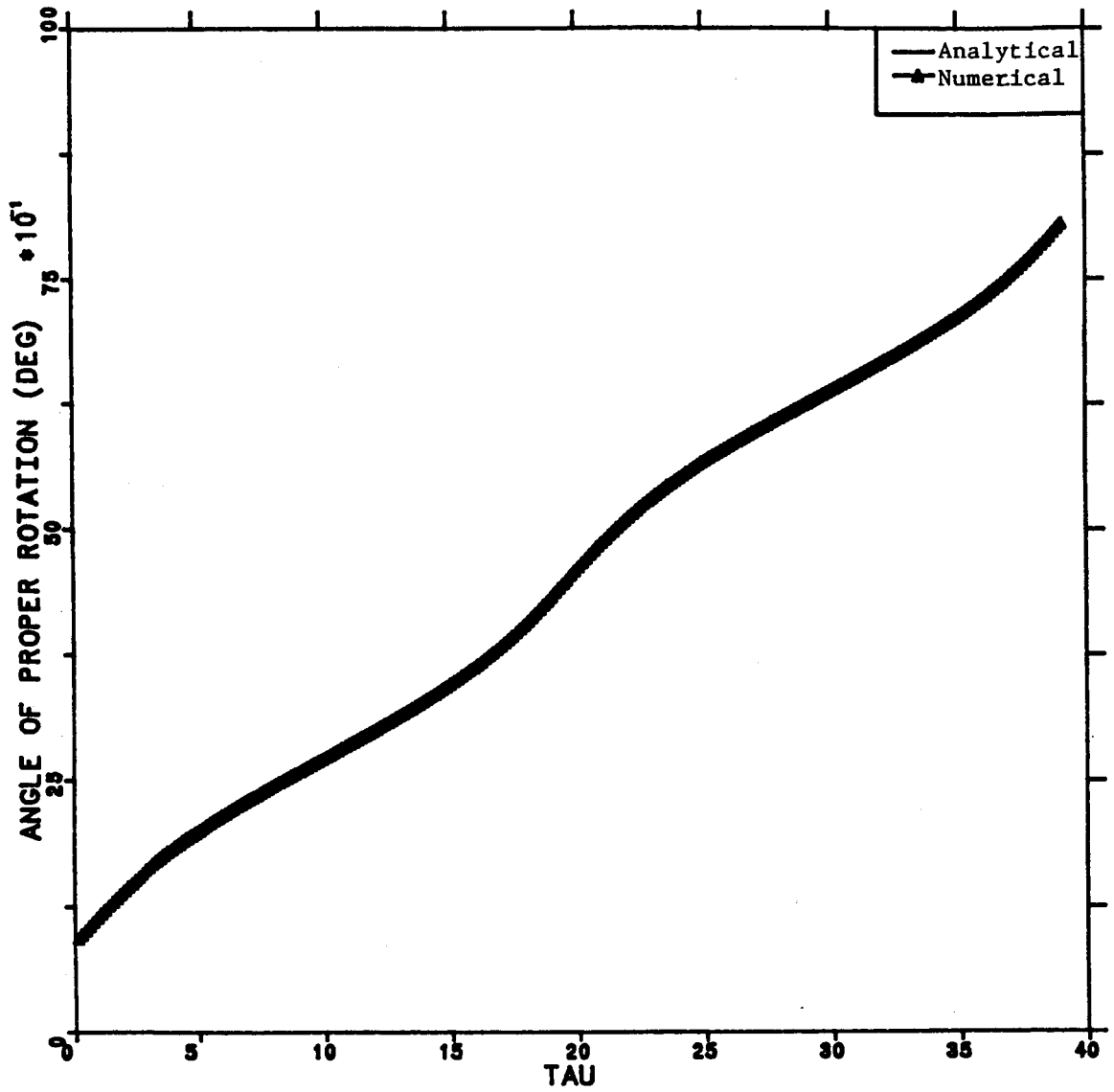
Fig. 15 c. Multi-Rotor Numerical Verification Case IV, Angle of Proper
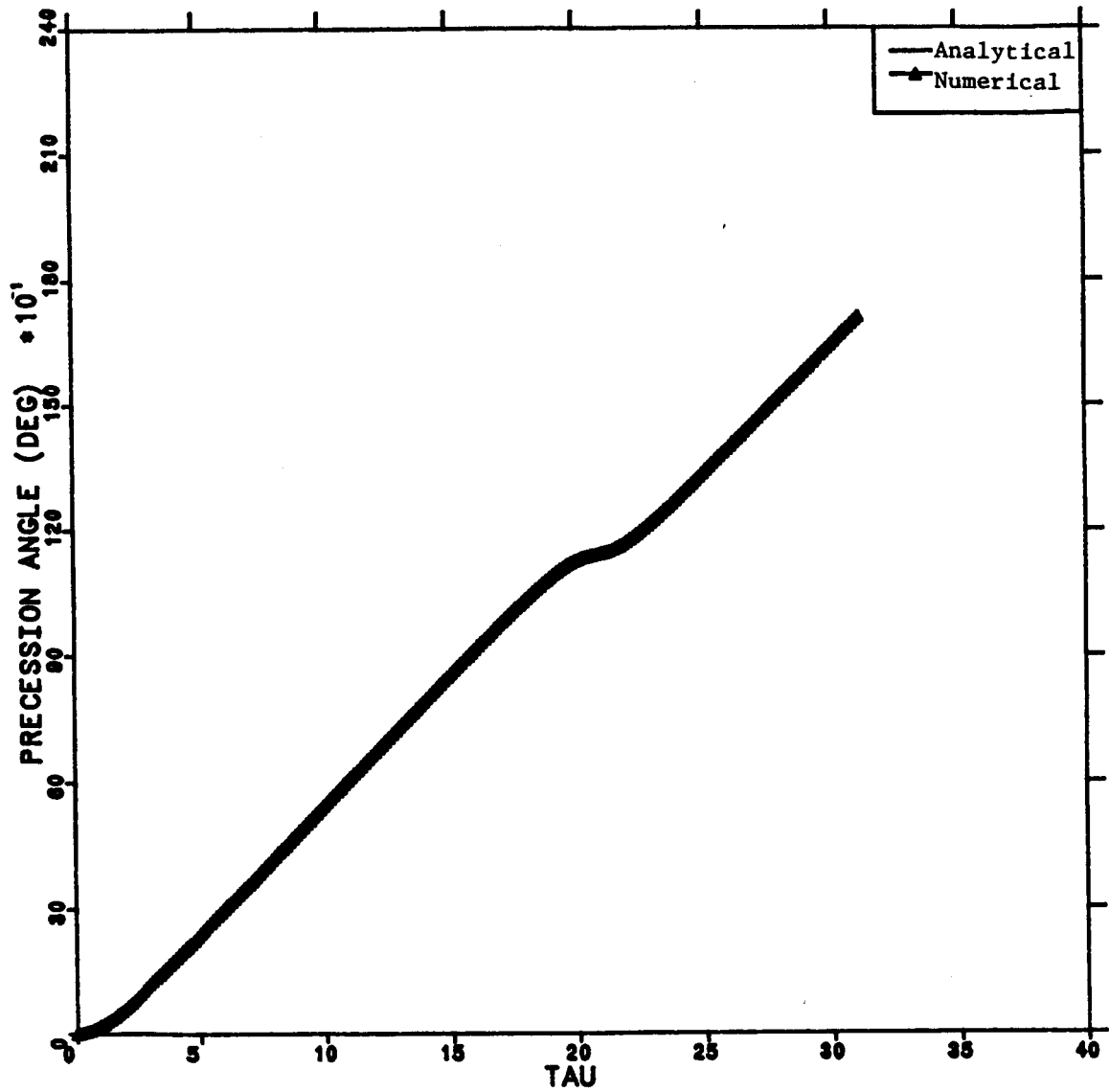Rotation Time-History.

prolate, dual-spin satellite with a misaligned rotor. As can be seen,
the numerical and analytical results are, within the numerical
precession of the calculations, the same.

The numerical simulation code was modified to demonstrate the
fidelity of the analytical solution for HAM cases in the presence of
environmental torques. The modifications to the code included the
incorporation of gravity-gradient torques, and a routine which would
allow the sampling of the time-histories of the three attitude angles at
a time many nutation periods in the future. The computer program was
used to integrate the equations of motion over the intervening period,
but output to data files for plotting was limited to the desired sample.
The case which was run used the data from Case III in Table 1. The
attitude motion of the satellite as perturbed by gravity-gradient torque
was simulated for a time equal to a quarter of an orbit (1342.6 sec for
an orbital altitude of 250 km). As can be seen in Fig. 16, the torque-
free analytical time histories and the projected numerical solutions
agree in amplitude very well. There is a "phase shift" which is prob-
ably due to to the fact that the nutation period was not exactly equal
to the number used to determine the beginning of the second sample time.

To determine the magnitude of rotational angular momentum for which
there would be significant disagreement between the two solutions, the
initial angular momentum was successively reduced. To obtain the
results shown in Fig. 17, the initial angular velocity and internal
angular momentum components were each divided by 120. The results were
chosen for illustrative purposes because they show a large difference in
the amplitudes of the solutions, but the attitude motion structure has
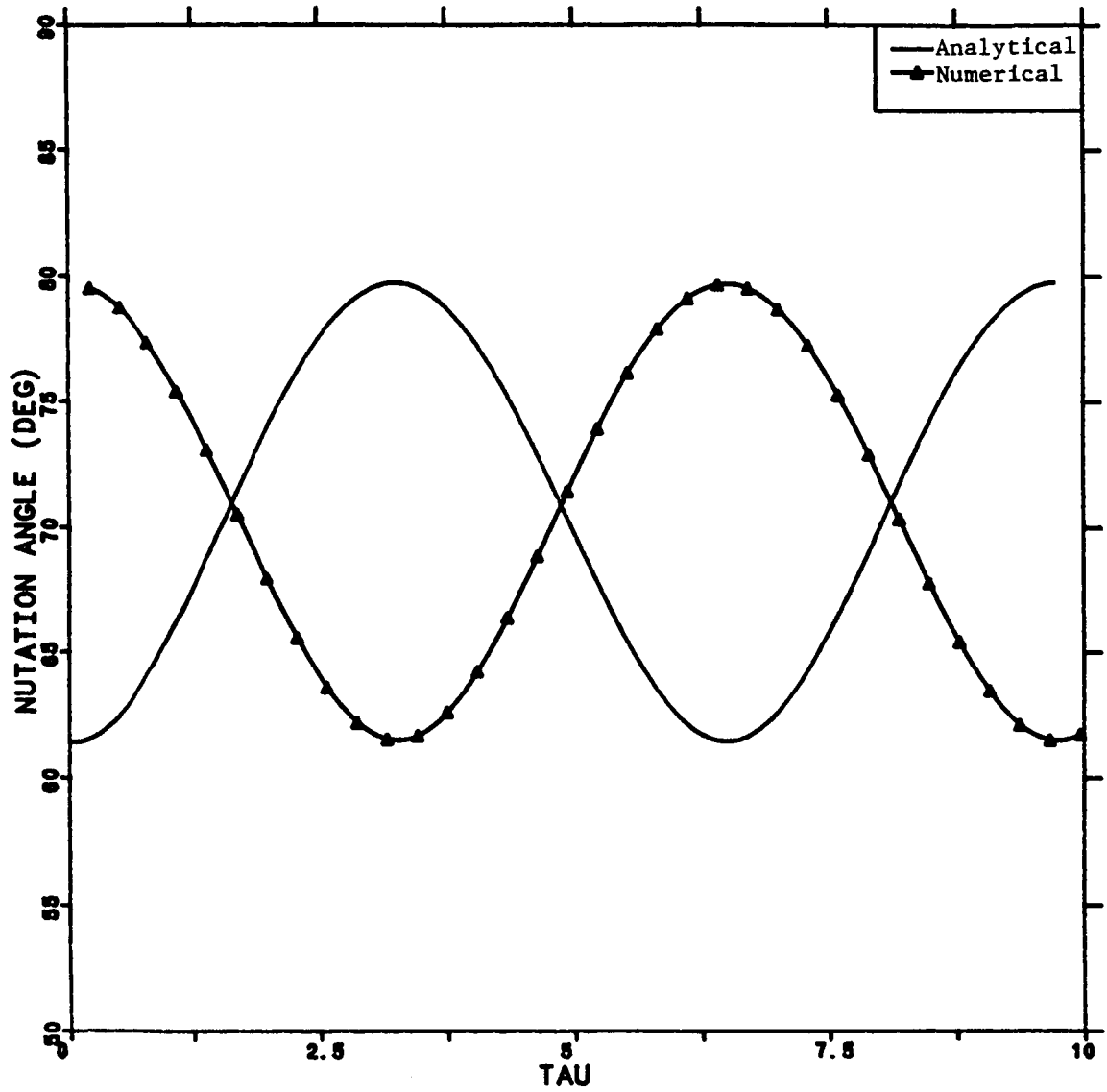
Fig. 16 a. Fidelity of Multi-Rotor Results in the Presence of
Gravity-Gradient Torque, HAM Case, Nutation Angle
Time-History.

56
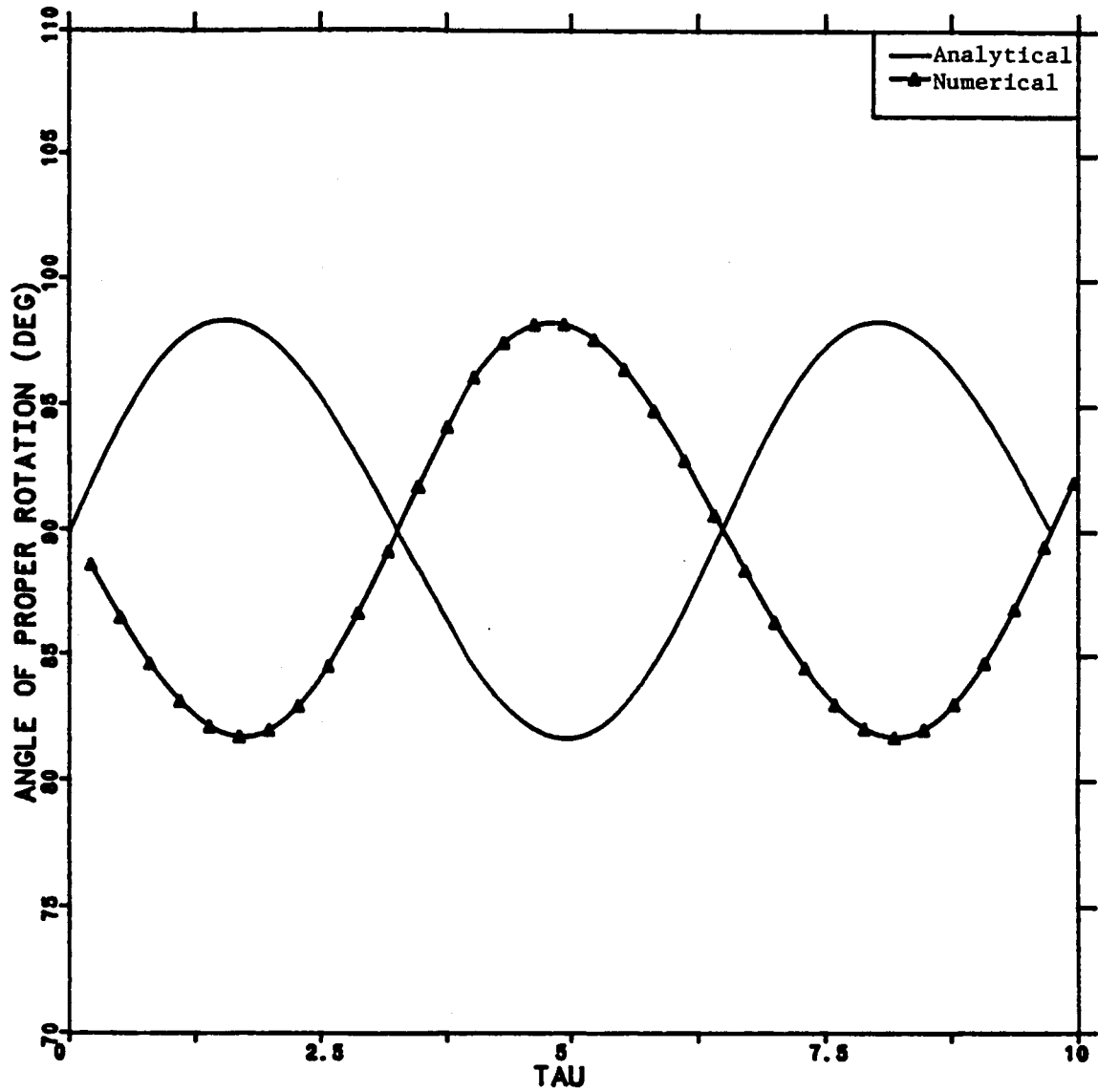
Fig. 16 b. Fidelity of Multi-Rotor Results in the Presence of
            Gravity-Gradient Torque, HAM Case, Angle of Proper
            Rotation Time History.
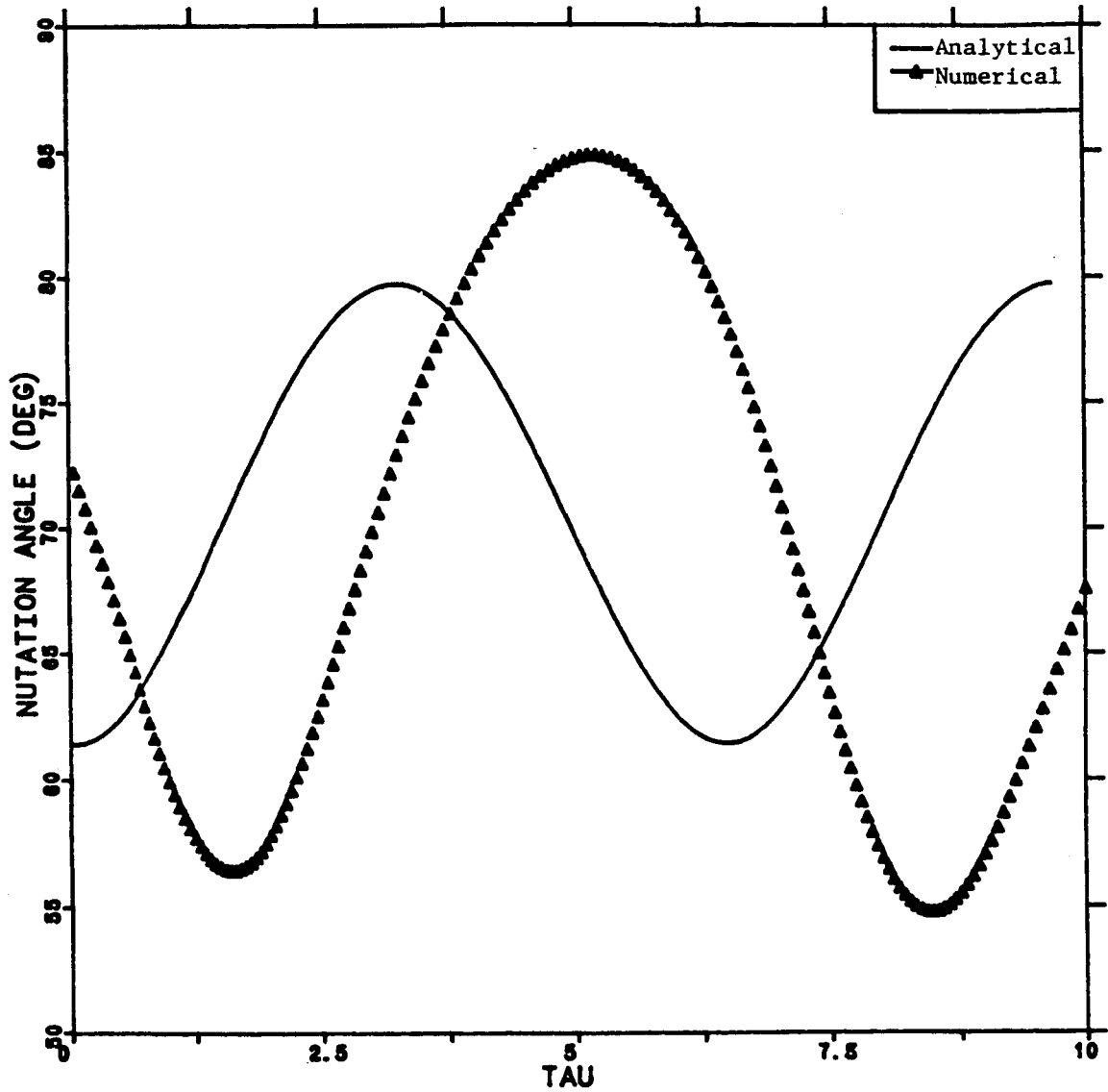
Fig. 17 a. Fidelity of Multi-Rotor Results in the Presence of
Gravity-Gradient Torque, LAM Case, Nutation Angle
Time-History.
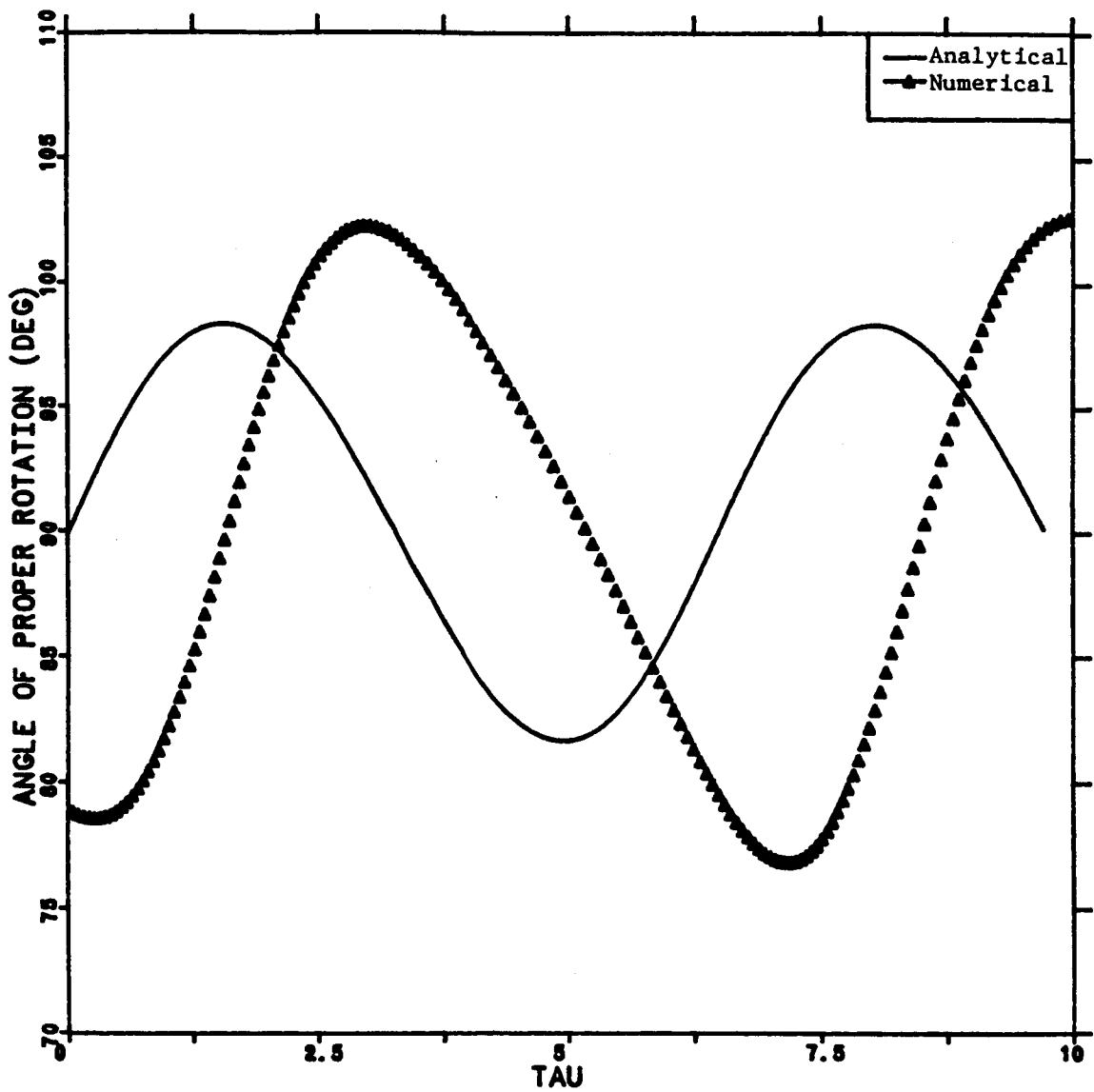
Fig. 17 b. Fidelity of Multi-Rotor Results in the Presence of
Gravity-Gradient Torque, LAM Case, Angle of Proper
Rotation Time-History.

not yet broken down. That is, the three angles of precession, nutation,

and proper rotation are still appropriate for describing the motion of

the satellite. As was noted previously in Section 4.1, at low angular

momentum levels, roll, pitch, and yaw angles are more appropriate for

describing the satellite's attitude motion because then ψ, θ, and ϕ are

not well defined. The amplitudes of the LAM (torqued) numerical results

are significantly greater than the HAM torque-free analytical results.

One could infer from these that the torque-free analytical solutions

would be appropriate for short-term HAM satellite attitude motion

simulations, and that the (torqued) numerical simulations more

appropriate for short-term LAM satellite attitude motion simulations.

6.2 Low Angular Momentum Examples

The capability of the numerical simulation code when applied to low

angular momentum (LAM) satellite simulations, was demonstrated by making

eight simulation runs using data for three actual satellites. Four

simulation runs were made using data for the Hubble Space Telescope

(HST). Then, using the data from the Earth Resources Satellite

(LANDSAT) and the Advanced X-Ray Astrophysics Facility (AXAF), two

computer runs were made for each of the two satellites. The satellite

physical data for the HST satellite simulations can be found in Table 3.

The corresponding orbital data can be found in Table 4. The data used

for the LANDSAT and AXAF simulation runs found in Tables 5 and 6 is

presented in the same manner.

All of the results from the simulations are in the form of

time-histories of selected parameters over five orbital periods.

These parameters are: (1) the Euler parameters, β_0, β_1, β_2, and β_3;

Table 3. Hubble Space Telescope (HST) Numerical Simulation, Satellite Physical Data.

		Case I	Case II	Case III	Case IV
Moments of Inertia (kg-m^2):					
Main Body	I_{xx}	3.19×10^4	3.19×10^4	3.19×10^4	3.19×10^4
	I_{yy}	7.69×10^4	7.69×10^4	7.69×10^4	7.69×10^4
	I_{zz}	7.71×10^4	7.71×10^4	7.71×10^4	7.71×10^4
Rotor	I_{R_z}	0.84	0.84	0.84	0.84
Initial Angular Rates (rad/sec):					
	ω_{x_o}	0.	0.	0.	0.
	ω_{y_o}	-1.17×10^{-3}	-1.038×10^{-3}	-1.17×10^{-3}	-1.17×10^{-3}
	ω_{z_o}	0.	0.	0.	0.
Rotor Rate	Ω_o	20.	20.	20.	20.
Orientation of Rotor Spin Axis:		Along x_b-axis	Along x_b-axis	Along x_b-axis	Along x_b-axis

Table 4 Hubble Space Telescope (HST) Numerical Simulation Data.

	Case I	Case II	Case III	Case IV
Gravity-Gradient Torques:	Yes	Yes	Yes	No
Semi-Major Axis (km):	6628.27	7178.27	6628.27	6628.27
Eccentricity:	0.	0.	0.01	0.01
Inclination (deg):	28.5	28.5	28.5	28.5
Period (sec):	5370.46	6052.58	5370.46	5370.46
Aerodynamic Torques:	Yes	Yes	Yes	No
Right-Circular Cylinder Dimensions (m):				
Length	12.924	12.924	12.924	12.924
Diameter	4.572	4.572	4.572	4.572
Initial Orientation (deg):				
Roll	0.	0.	0.	0.
Pitch	45.	45.	45.	45.
Yaw	0.	0.	0.	0.

Table 5 LANDSAT and AXAF Numerical Simulation, Satellite Physical Data.

		LANDSAT CASE I	LANDSAT CASE II	AXAF CASE I	AXAF CASE II
Moments of Inertia (kg-m^2):					
Main Body	I_{xx}	9.8052×10^2	9.8052×10^2	6.37043×10^4	6.37043×10^4
	I_{yy}	3.10479×10^3	3.10497×10^3	1.97348×10^5	1.97348×10^5
	I_{zz}	3.10497×10^3	3.10497×10^3	1.93959×10^5	1.93959×10^5
Rotor	I_{R_z}	None	None	None	None
Initial Angular Rates (rad/sec):					
	ω_{x_o}	1.126×10^{-3}	1.043×10^{-3}	1.0×10^{-3}	1.0×10^{-3}
	ω_{y_o}	$0.$	$0.$	1.0×10^{-4}	1.0×10^{-4}
	ω_{z_o}	1.986×10^{-4}	1.839×10^{-4}	$0.$	$0.$

Table 6 LANDSAT and AXAF Numerical Simulation Data.

	LANDSAT CASE I	LANDSAT CASE II	AXAF CASE I	AXAF CASE II
Gravity-Gradient Torques:	Yes	Yes	Yes	No
Semi-Major Axis (km):	5730.27	7083.27	6778.27	6778.27
Eccentricity:	0.	0.	0.	0.
Inclination (deg):	98.2	98.2	28.5	28.5
Period (sec):	5494.9	5932.8	5553.8	5553.8
Aerodynamic Torques:	No	No	Yes	No
Right-Circular Cylinder Dimensions (m):				
Length	4.298	4.298	13.015	13.015
Diameter	2.195	2.195	4.267	4.267
Initial Orientation (deg):				
Roll	0.	0.	0.	0.
Pitch	10.	10.	45.	45.
Yaw	-80.	-80.	-45.	-45.

(2) orientation of the satellite with respect to its local vertical coordinate system in terms of roll, pitch, and yaw angles; (3) the body-fixed components of the satellite's total angular momentum vector; (4) where applicable, the body-fixed components of the aerodynamic torque, and (5) again, where applicable, the components of the gravity-gradient torque, also with respect to the satellite's body-fixed axes.

The four HST cases run include circular LEO, circular HEO, and elliptic LEO cases, all with environmental torques, and an elliptic LEO case without environmental torques. The results for the HST are shown in Figures 18, 19, 20, and 21. The LANDSAT cases are a circular LEO case and a circular HEO case. Both include only gravity-gradient torques. The two AXAF cases run are both circular LEO, one with environmental torques and one without. The results of the LANDSAT simulations are found in Figures 22 and 23. The results of the AXAF simulations are found in Figures 24 and 25. A more detailed analysis of the simulation results is made in the following paragraphs.

6.2.1 HST Simulations

In the first HST case, as with other HST cases, the satellite is initially "pitching down," or rotating, about its negative y_b-axis at orbital rate. The satellite also has some internal angular momentum due to a reaction wheel spinning about its x_b-axis. All of the HST cases begin with a 45° pitch angle with respect to the local horizontal.

HST Case I

The first figure for the HST (see Fig. 18 a) shows the time-histories of the Euler parameters, henceforth referred to as the "Beta plots." The individual Euler parameters oscillate in two modes; a

"low" frequency mode with a comparatively large amplitude and a "high" frequency mode with a much smaller amplitude. The time-histories of the roll, pitch, and yaw angles are presented in Fig. 18 b. Note that the pitch angle begins at 45° and oscillates at a relatively high frequency at progressively lower amplitude due to aerodynamic damping. After five orbits, the amplitude of the oscillation is approximately half its initial value. The roll angle shows relatively steady oscillations at low frequency, approximately equal to the orbital frequency and a smaller amplitude high-frequency mode. The yaw angle shows the same high frequency oscillation with fairly regular pulse-like changes in amplitude.

The third figure (see Fig. 18 c) shows plots of the angular momentum components in which the damping of the component about the y_b-axis is commensurate with the damping in pitch. The angular momentum component about the x_b-axis remains nearly constant, and is due to the internal angular momentum and the lack of environmental torques about that axis. The x_b-component is similar to the yaw oscillations in that it has relatively small amplitude pulses.

The variations in the components of aerodynamic torque, shown in Fig. 18 d, are proportional to the corresponding angular momentum plots in all three components. In order to give the satellite model a margin of static stability, the center of gravity was placed 1/10 of the length of the satellite forward along the x_b-axis from center of pressure (the centroid of the right-circular cylinder model). This was also done for the AXAF satellite.

Fig. 18 a. Time-Histories of Euler-Parameters for HST,
Case I (250 km. Orbital Altitude).

Fig. 18 b. Time-Histories of Roll, Pitch, and Yaw Angles for HST,
Case I (250 km. Orbital Altitude).

Fig. 18 c. Time-Histories of Angular Momentum Components for HST,
Case I (250 km. Orbital Altitude).

Fig. 18 d. Time-Histories of Aerodynamic Torque Components for HST,
Case I (250 km. Altitude).

Fig. 18 e.   Time-Histories of Gravity-Gradient Torque Components for
HST, Case I (250 km. Orbital Altitude).

The fifth, and last, set of plots for this case is given in Fig. 18 e. These are the time-histories of the components of the gravity-gradient torque. Here again the variations in the three components are proportional to those of the corresponding components of the vectors shown in the previous three figures. Notice, however, that the maximum amplitude of the oscillations in the gravity-gradient torque components is two orders of magnitude smaller than that for the aerodynamic torque.

HST Case II

Results for the second HST case were obtained using all of the same initial conditions as the first case except of orbital altitude. The first HST case was a circular orbit with an altitude of 250 km. In the second case, the orbit model was a circular orbit with an altitude of 800 km. The Beta plots for this case (see Fig. 19 a) show somewhat similar low frequency/high amplitude oscillations of the parameter, but the high frequency/low amplitude oscillations have disappeared. The attitude angles (see Fig. 19 c) are very different from that for the first case. The pitch angle shows oscillations of similar amplitude initially, but does not exhibit the same aerodynamic damping. Also, the frequency of the oscillation in pitch is much lower for this case. The roll and yaw angles both oscillate at lower frequencies but at greater amplitudes than in the previous case. Also, note that roll angle oscillation is changing secularly in the negative direction. The angular momentum plot (see Fig. 19 c) shows that the x_b-component remains constant. Note that the maximum amplitude the oscillations is an order of magnitude less than the first case. This is due to the
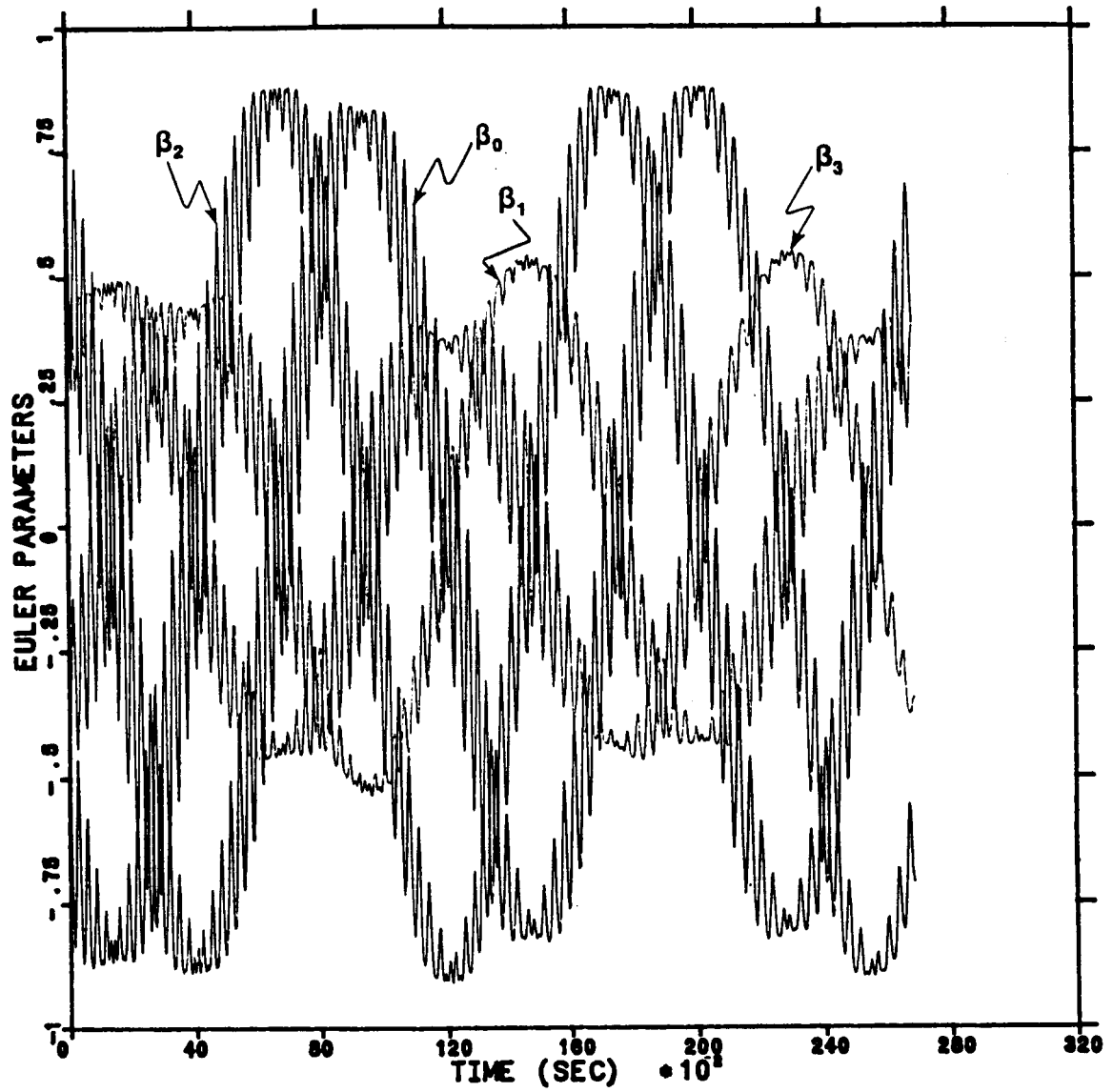
Fig. 19 a. Time-Histories of Euler-Parameters for HST,
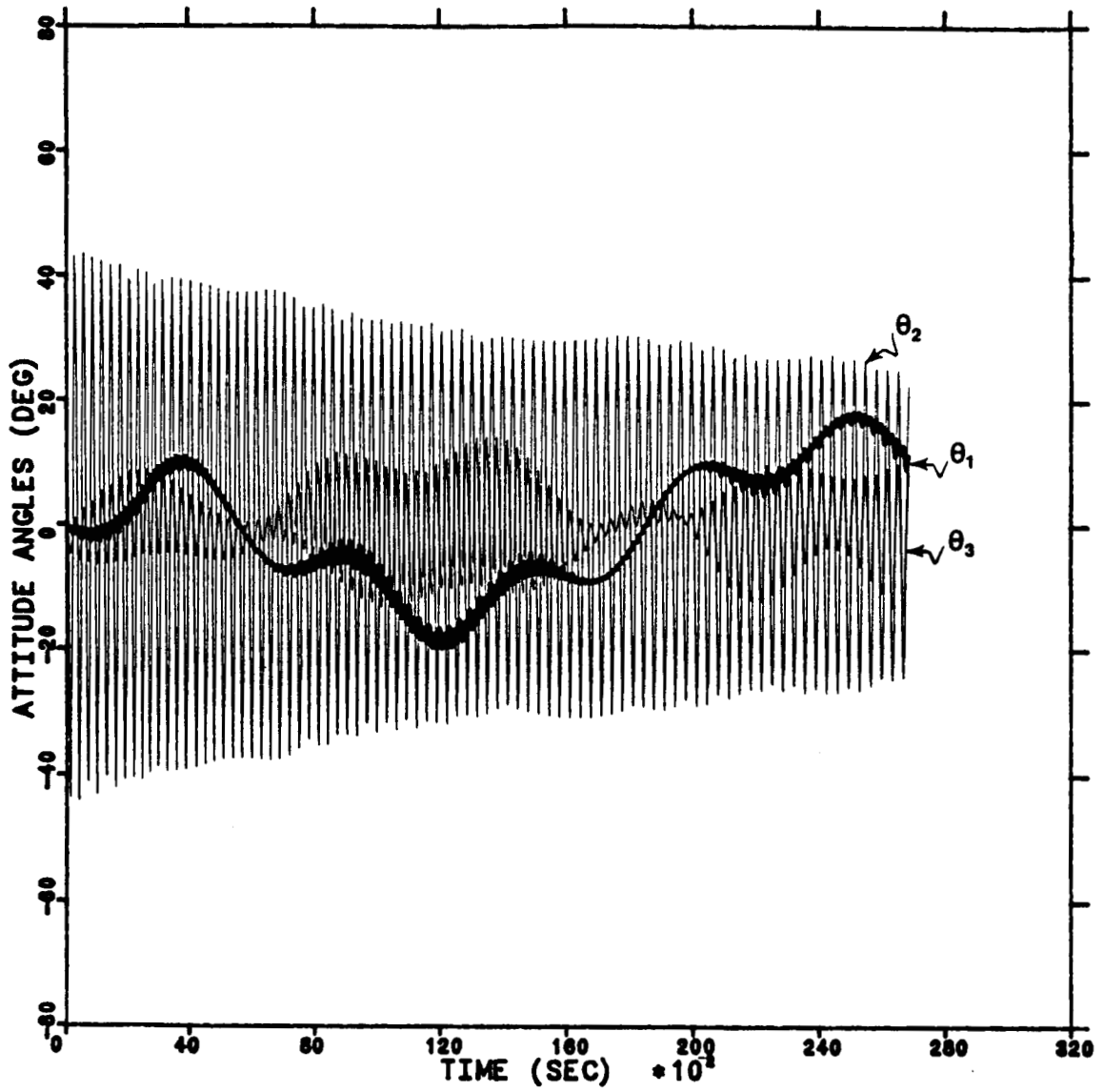CASE II (800 km. Orbital Altitude).

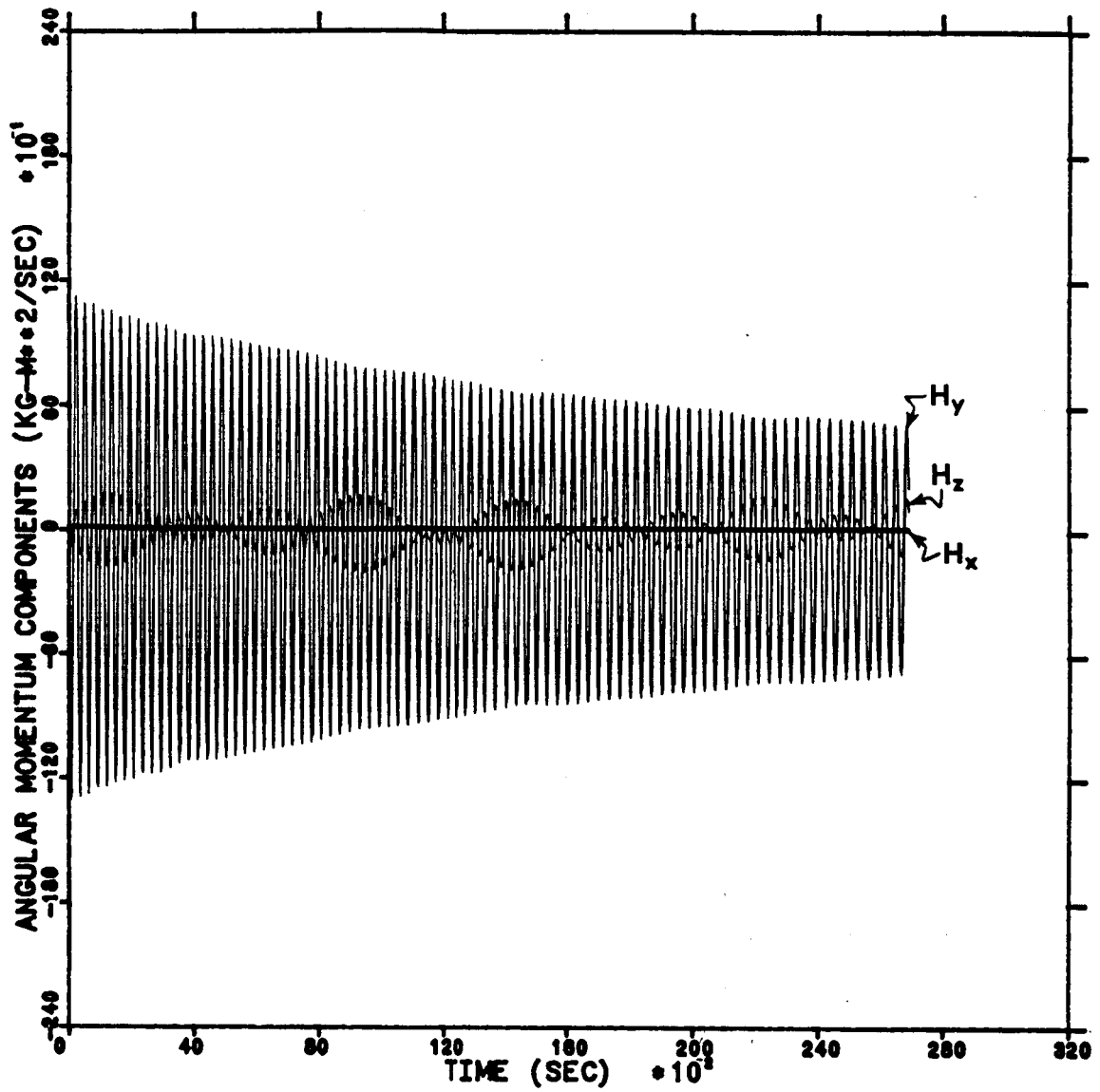Fig. 19 b. Time-Histories of Roll, Pitch, and Yaw Angles for HST, Case II (800 km. Orbital Altitude).

Fig. 19 c. Time-Histories of Angular Momentum Components for HST, Case II (800 km. Orbital Altitude).
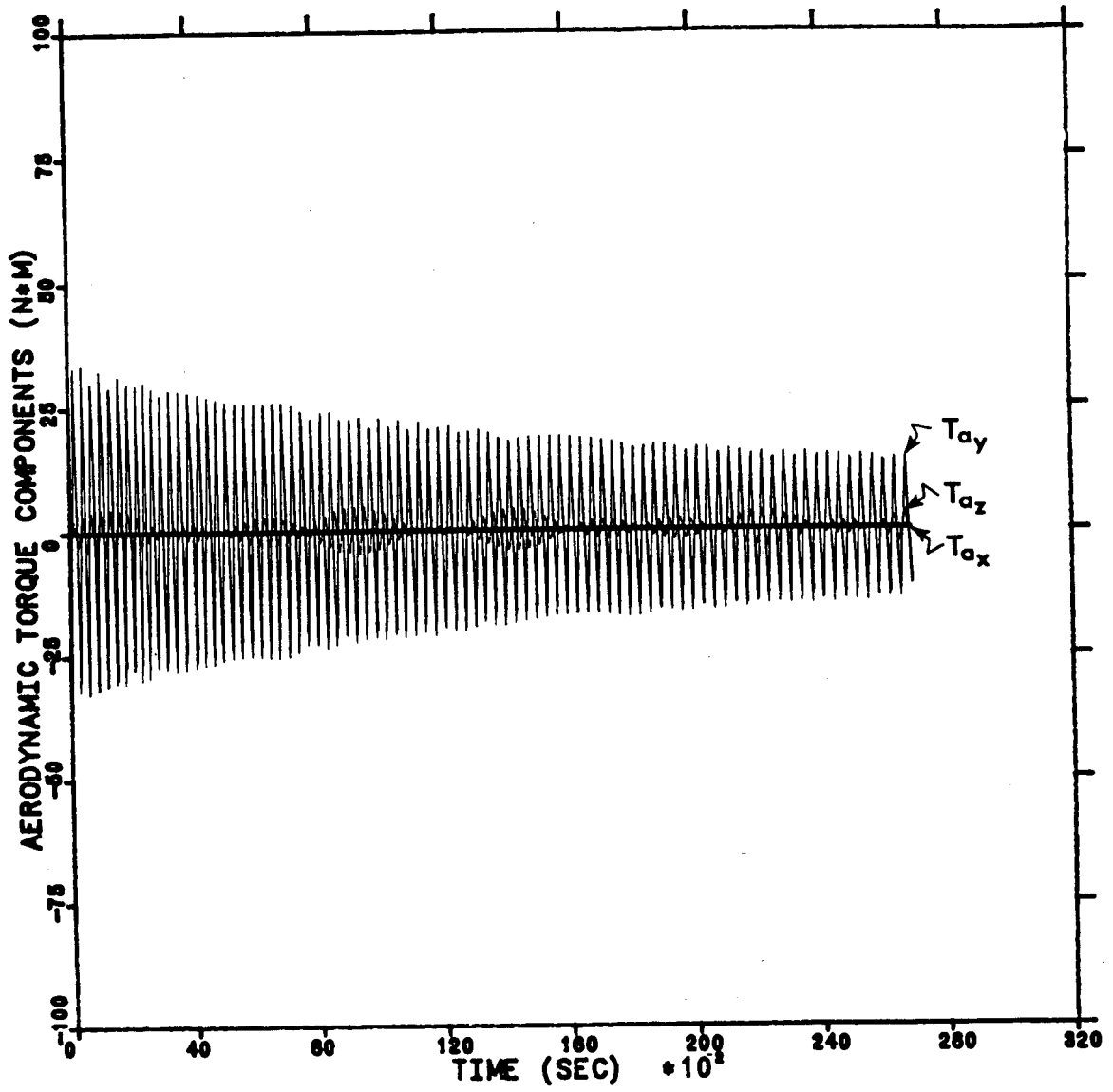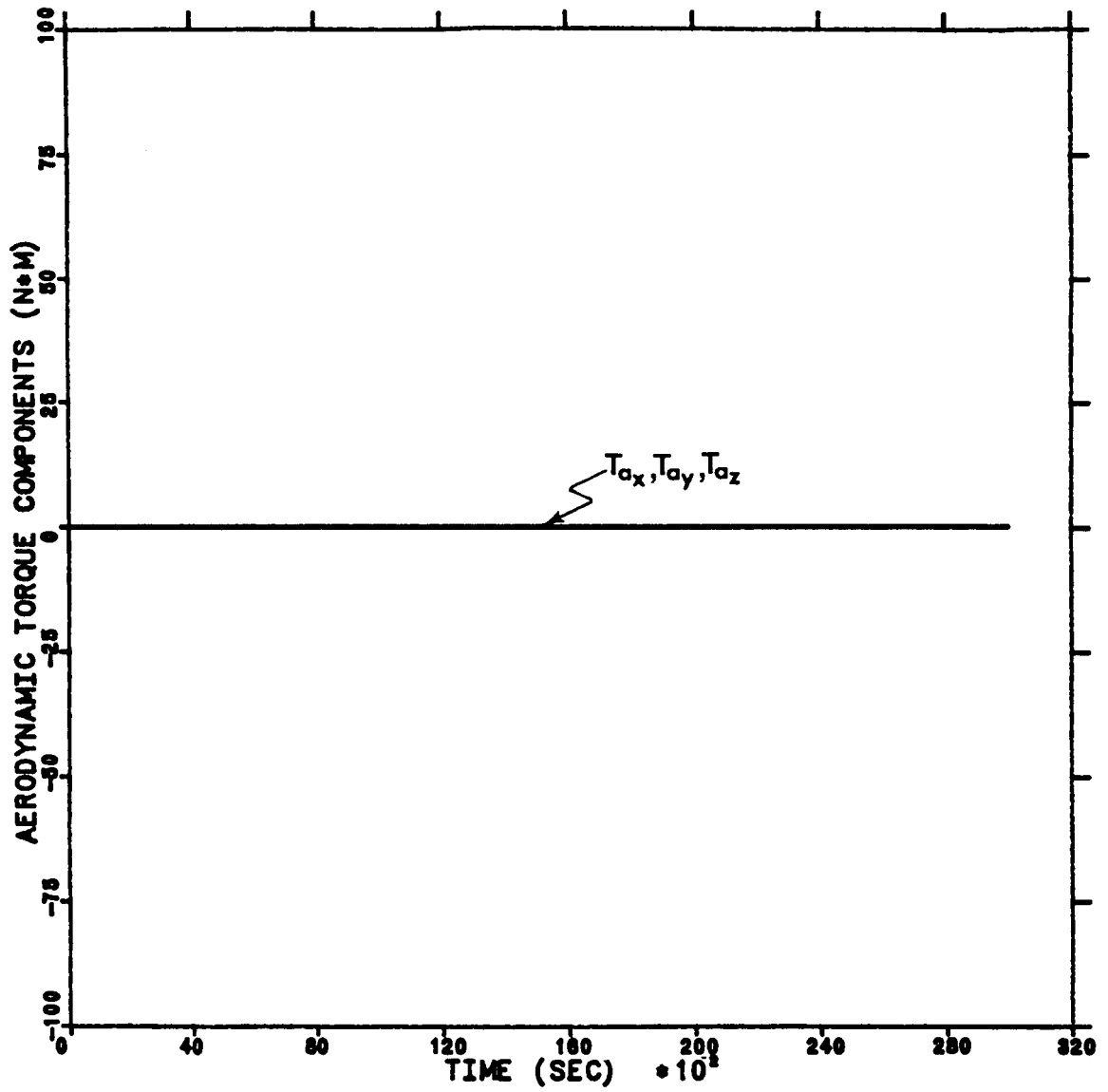
Fig. 19 d. Time-Histories of Angular Momentum Components for HST,
Case II (800 km. Orbital Altitude).
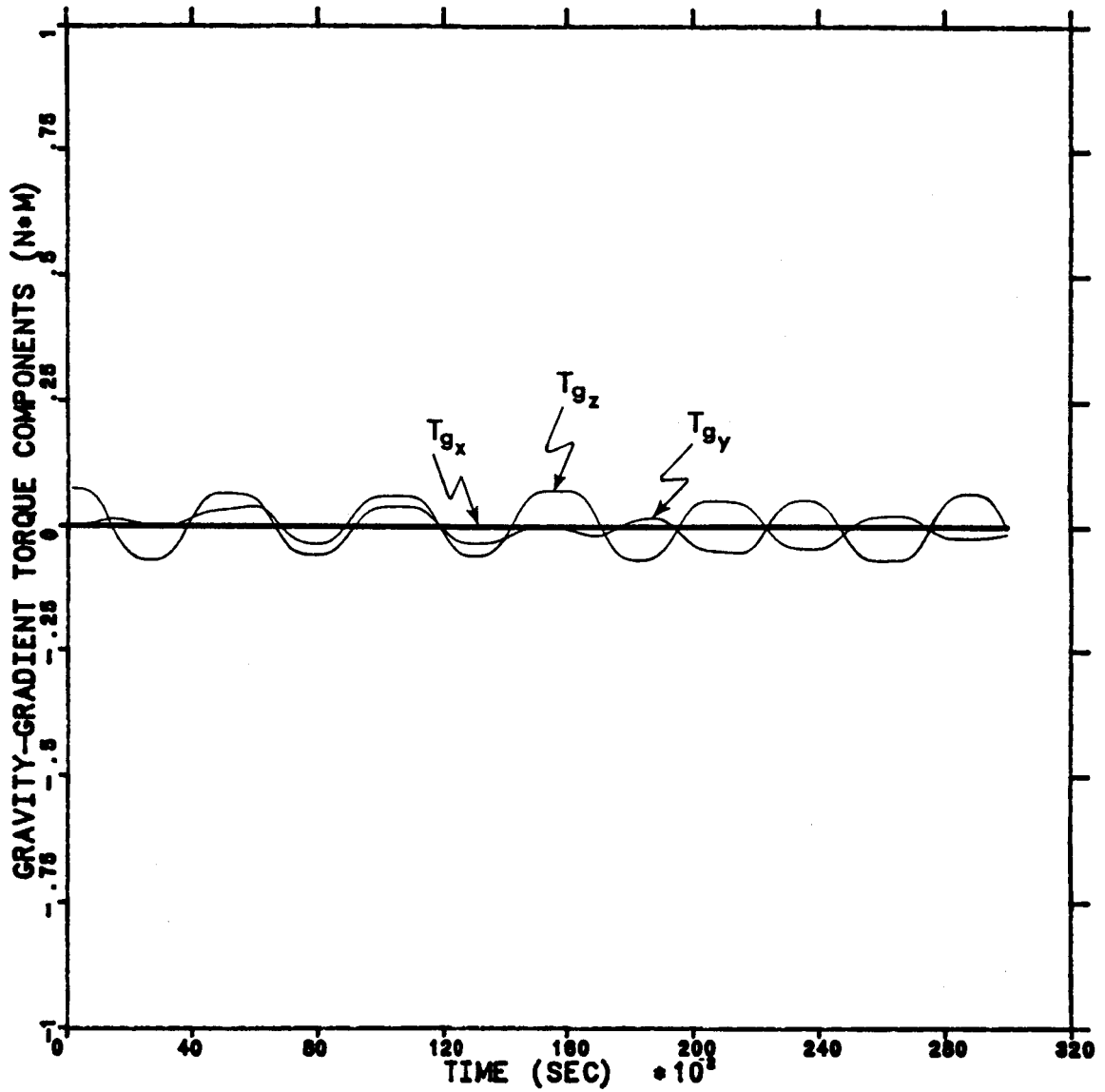
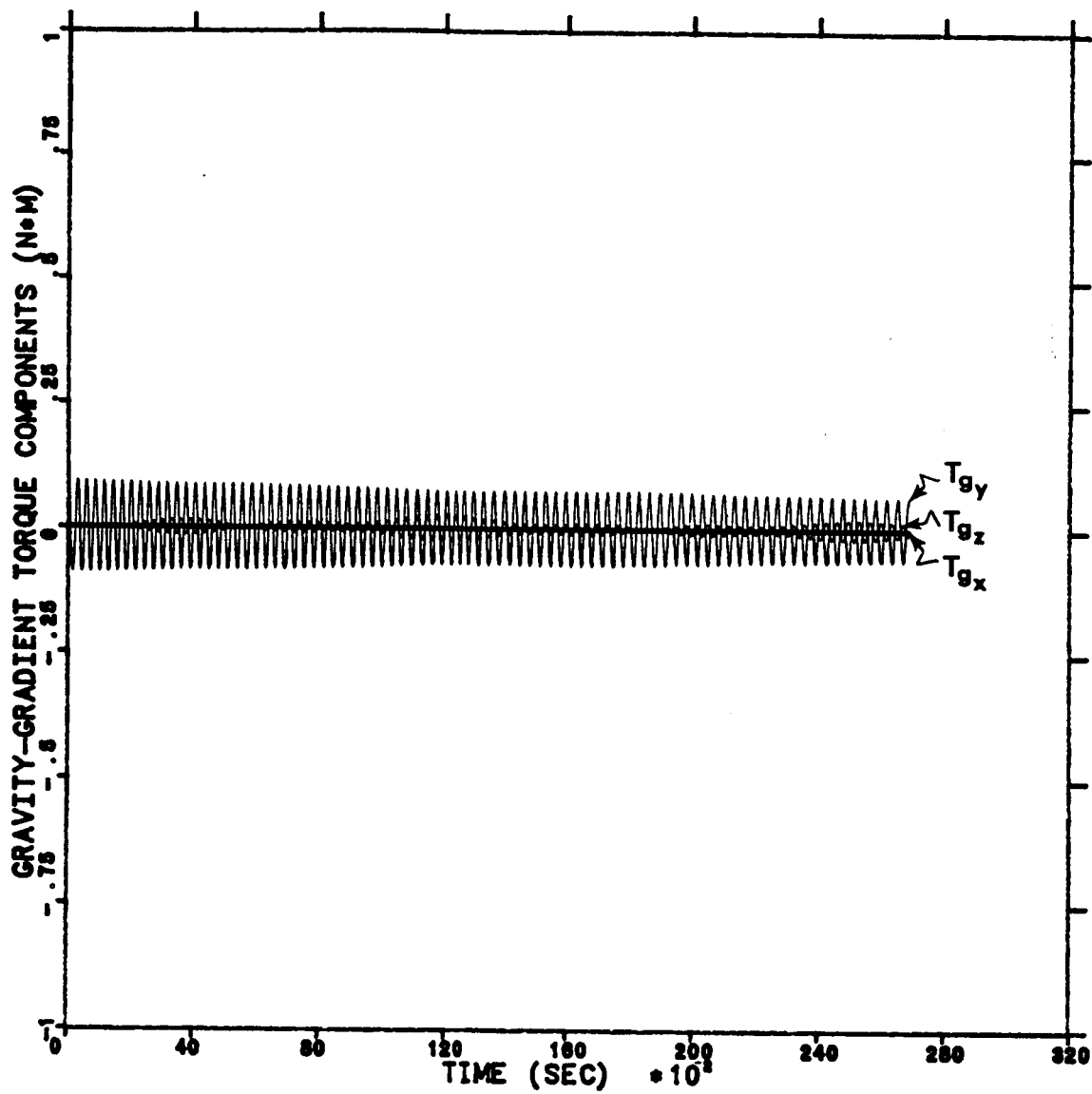Fig. 19 e. Time-Histories of Gravity-Gradient Torque Components for
HST, Case II (800 km. Orbital Altitude).

lower orbital rate and low level of excitation by aerodynamic torque. The y_b-component is varying secularly in the positive sense while oscillating slowly with amplitude which decreases and then increases. The z_b-component exhibits what appear to be long-period variations. While changing in this manner, the z_b-component is also oscillating much like the y_b-component. The aerodynamic torque components (see Fig. 19 d) are several orders of magnitude smaller than they were in the first case; in fact, they are smaller than the gravity-gradient torque components (see Fig. 19 e). This is due to the fact that the model of the density of the atmosphere decreases exponentially with altitude, whereas the gravity-gradient torque is proportional to the inverse cube of orbital radius.

HST Case III

The third HST case is a low, slightly elliptic orbit (e = .01). As a result of the ellipticity, the orbital altitude ranges from a perigee altitude of 184 km to an apogee altitude of 316 km. The Beta plots in Fig. 20 a exhibit two frequency modes seen in Case I. But the amplitudes of the lower frequency/high amplitude modes show some parameters with growing amplitudes and others with diminishing amplitudes. The attitude plot for this case (see Fig. 20 b) shows that the roll angle oscillates in two frequency modes as in the first case, but it is also changing secularly in a negative sense. The pitch angle time history contains a high frequency oscillation (as in the first case) and is decreasing in amplitude as time progresses, but there are amplitude pulses which initially coincide with apogee passage. These pulses most likely result from the lower level of pitch damping due to
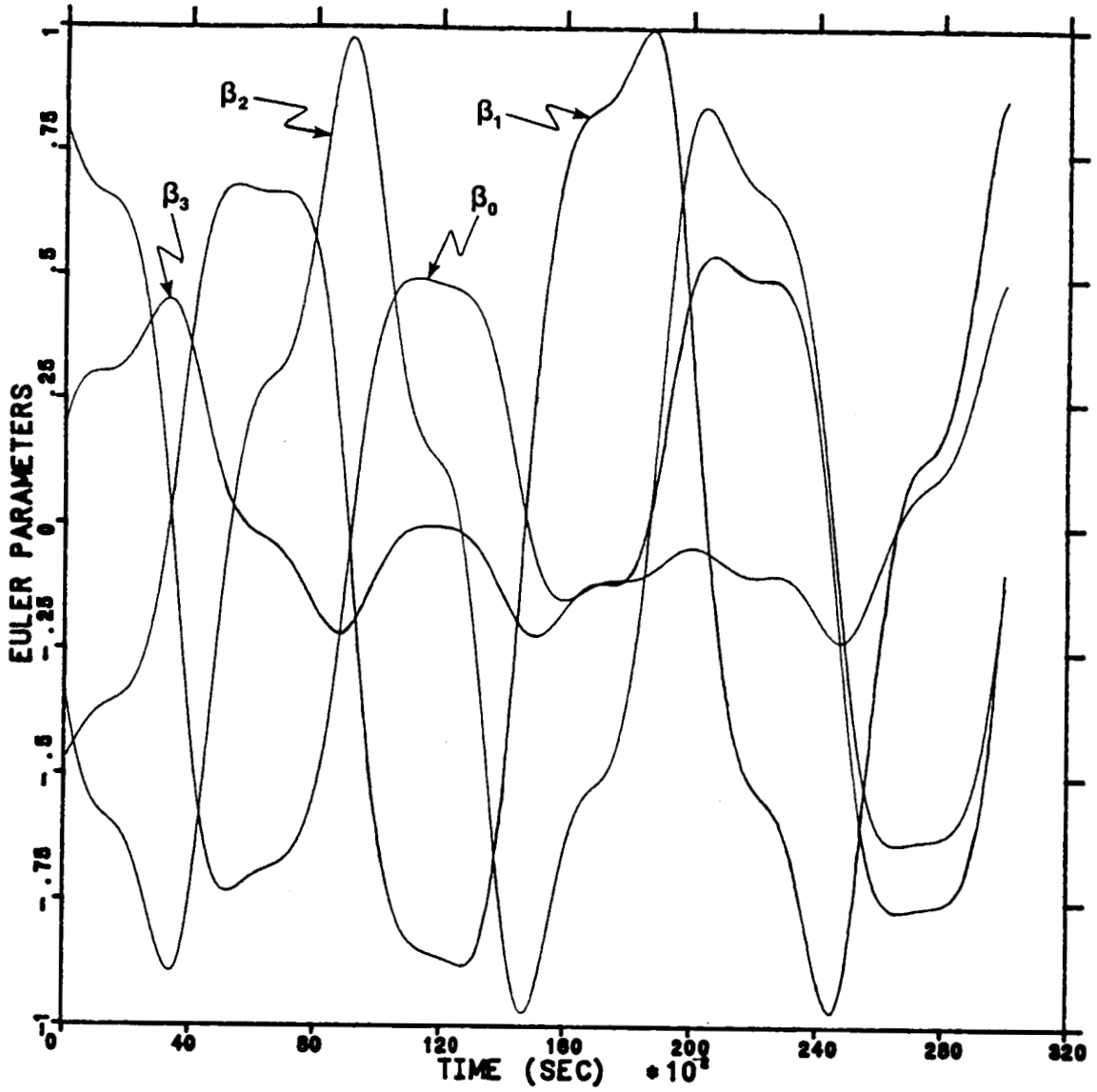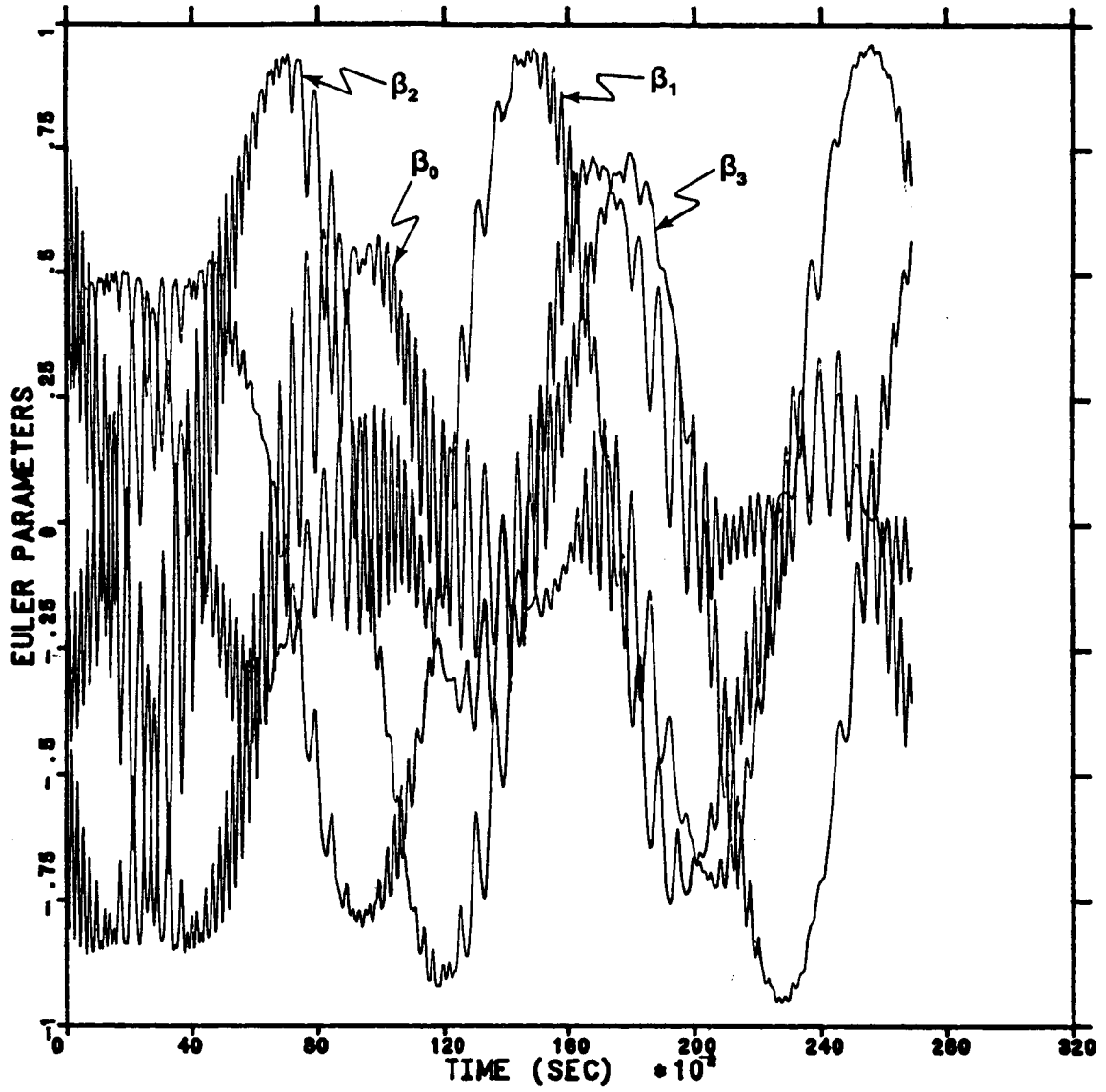
Fig. 20 a.   Time-Histories of Euler-Parameters for HST,
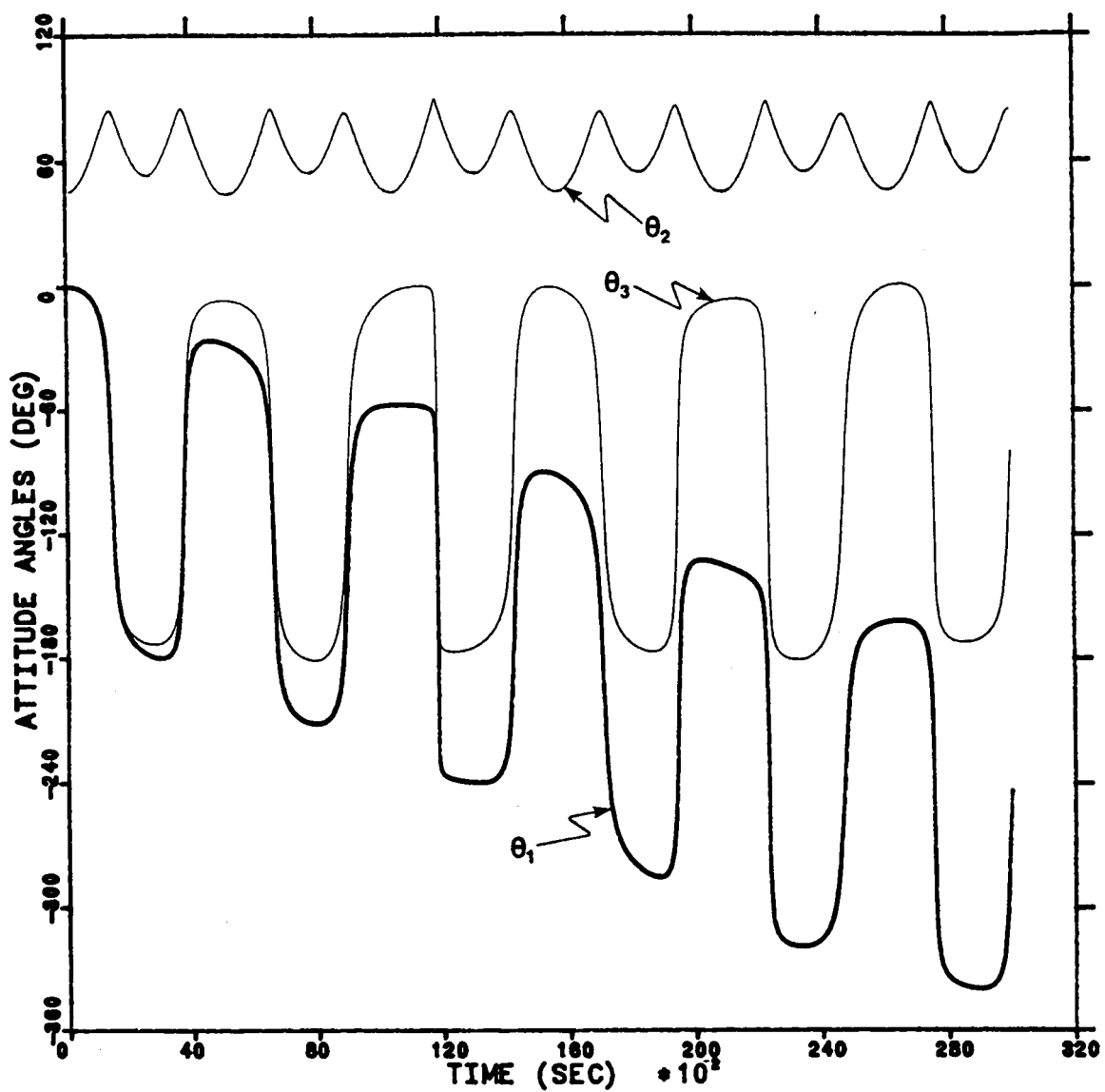   Case III (184 km. x 316 km. Orbital Altitude).
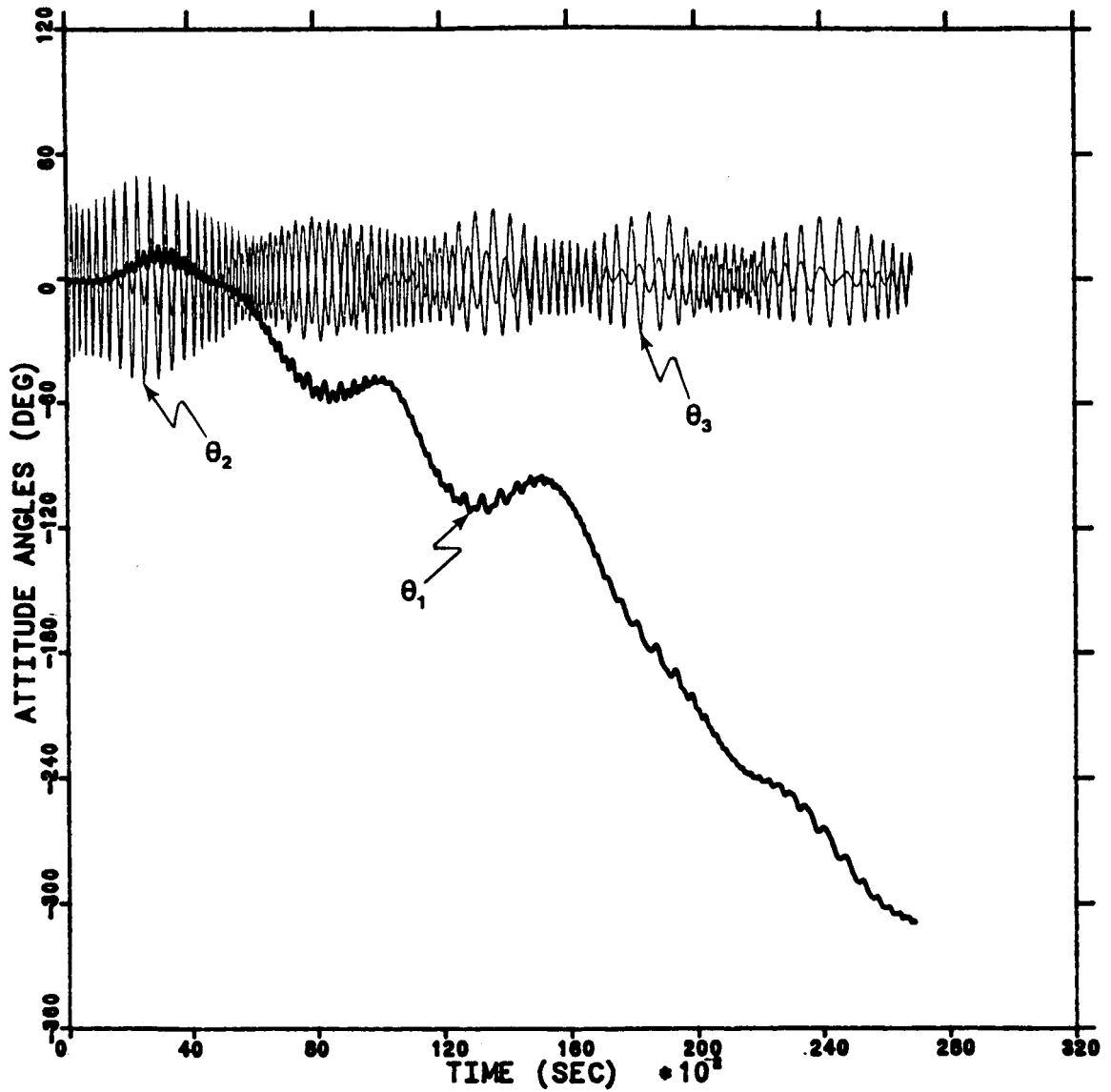
Fig. 20 b. Time-Histories of Roll, Pitch, and Yaw Angles for HST,
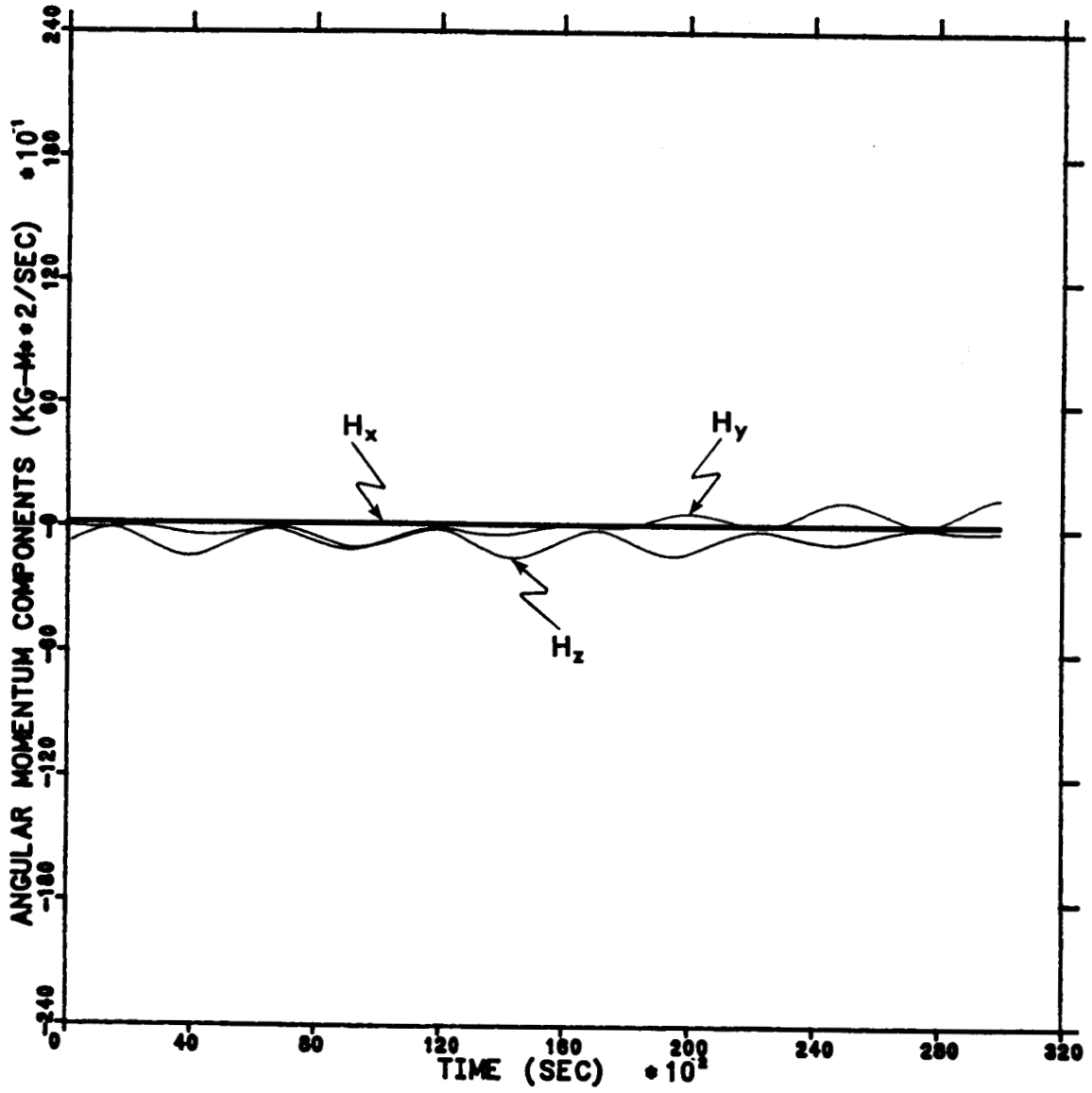Case III (184 km. x 316 km. Orbital Altitude).
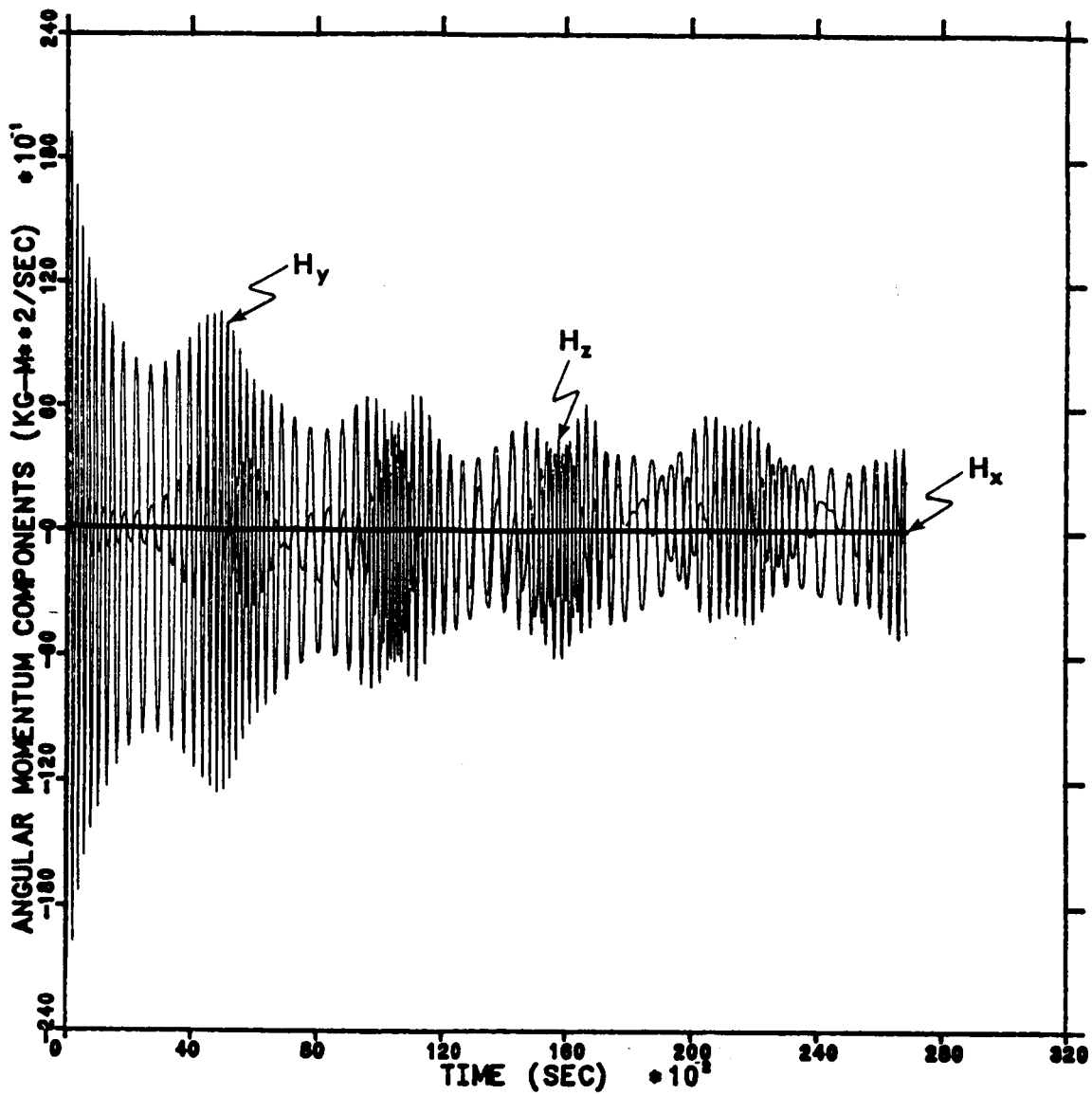
Fig. 20 c. Time-Histories of Angular Momentum Components for HST, Case III (184 km. x 316 km. Orbital Altitude).

C·2
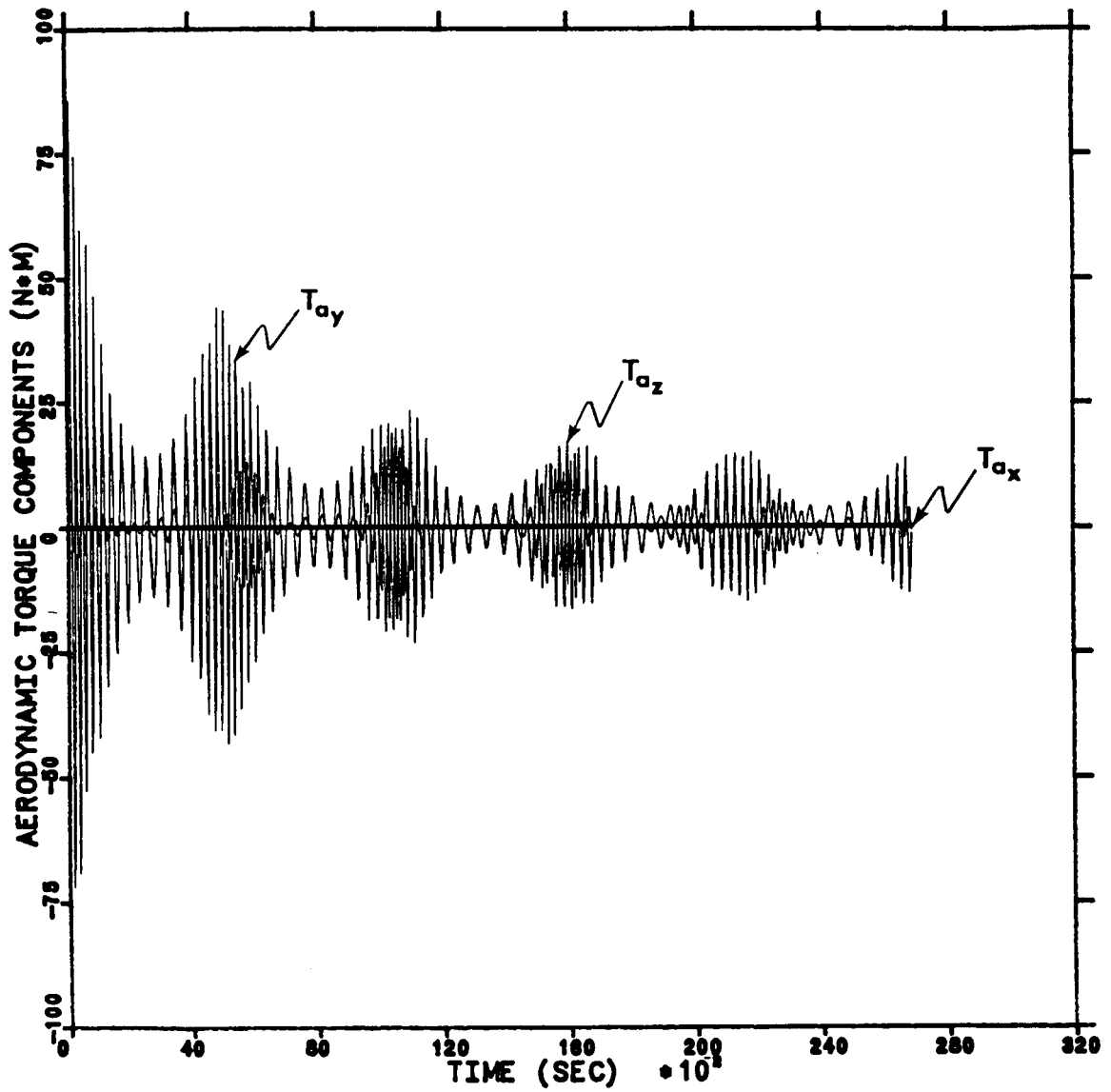
Fig. 20 d. Time-Histories of Aerodynamic Torque Components for HST,
            Case III (184 km. x 316 km. Orbital Altitude).
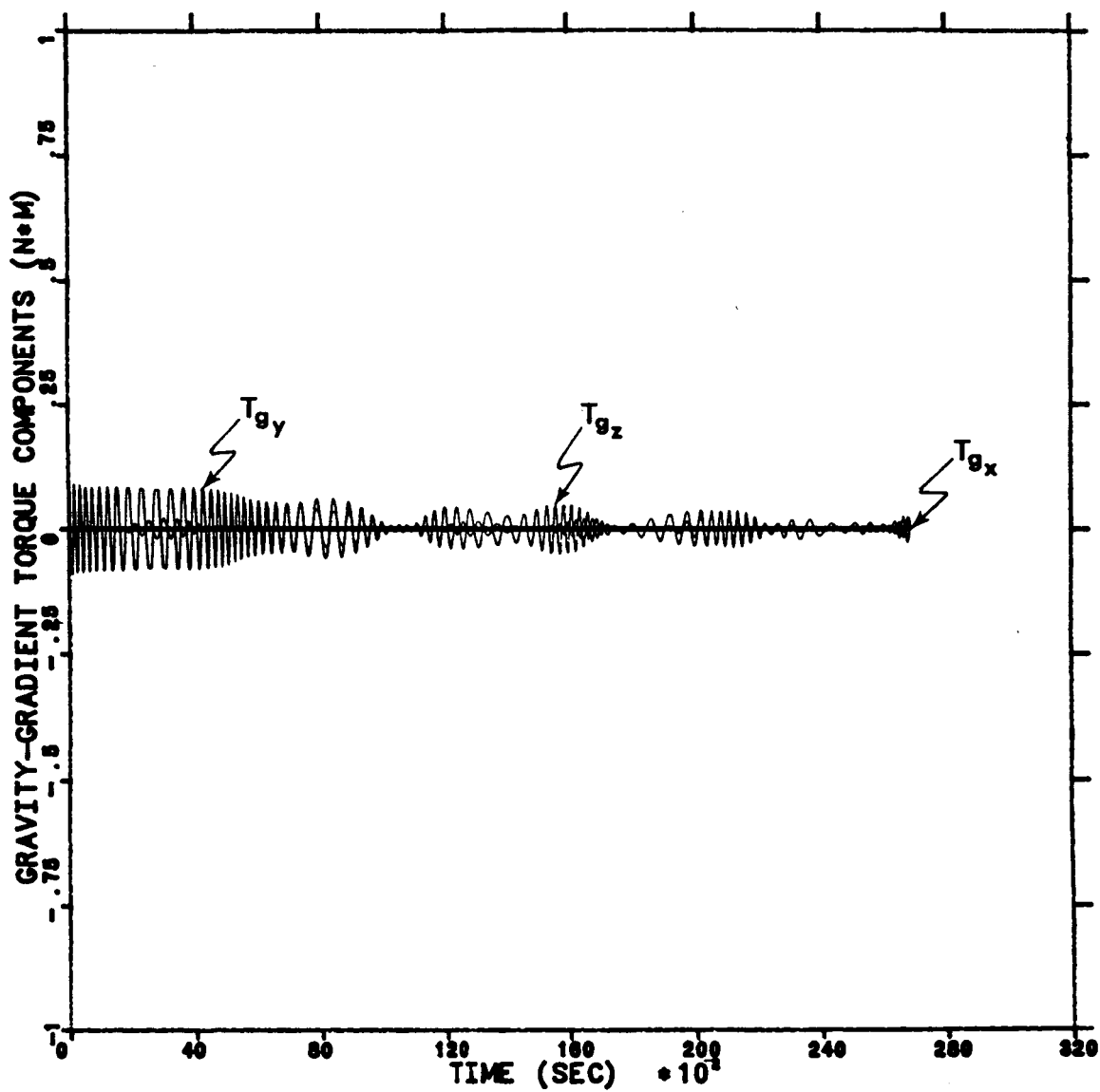
Fig. 20 e. Time-Histories of Gravity-Gradient Torque Components for
HST, Case III (184 km. x 316 km. Orbital Altitude).

lower atmospheric density at the apogee altitude. The yaw angle oscillations have approximately the same frequency as the oscillation in pitch. However, the yaw angle oscillations begin with zero amplitude and then increase. Initially, the yaw amplitude pulses coincide with the pitch amplitude pulses in frequency. As time progresses and the amplitude of the yaw angle pulses grows larger than the diminishing pitch angle pulses, it also becomes out of phase. The y_b- and z_b-components of angular momentum in Fig. 20 c behave very similarly to the pitch and yaw angles, respectively, of the attitude plot. The x_b-component of angular momentum remains nearly constant due to the internal angular momentum of the satellite and the fact that there is no aerodynamic torque (Fig. 20 e) about the x_b-axis. The y_b-component of aerodynamic torque decreases in amplitude with periodic pulses which coincide with perigee passage. The z_b-component of aerodynamic torque remains at a relatively low amplitude with pulses also coincident with the perigee y_b-component pulses. The amplitude of the y_b-and z_b-components of the gravity-gradient torque pulse not so much as a result of the changing orbital altitude as with the changing of orientation due to the rolling motion of the satellite. That is, when the y_b-axis is pointed more towards the center of the earth, the z_b-component of gravity-gradient torque increases in magnitude. The converse is also true.

HST Case IV

This case has the same initial conditions as Case III. However, in this simulation the environmental torque subroutines were "disconnected" so that the motion is torque-free. The Beta plots (Fig. 21 a) show only
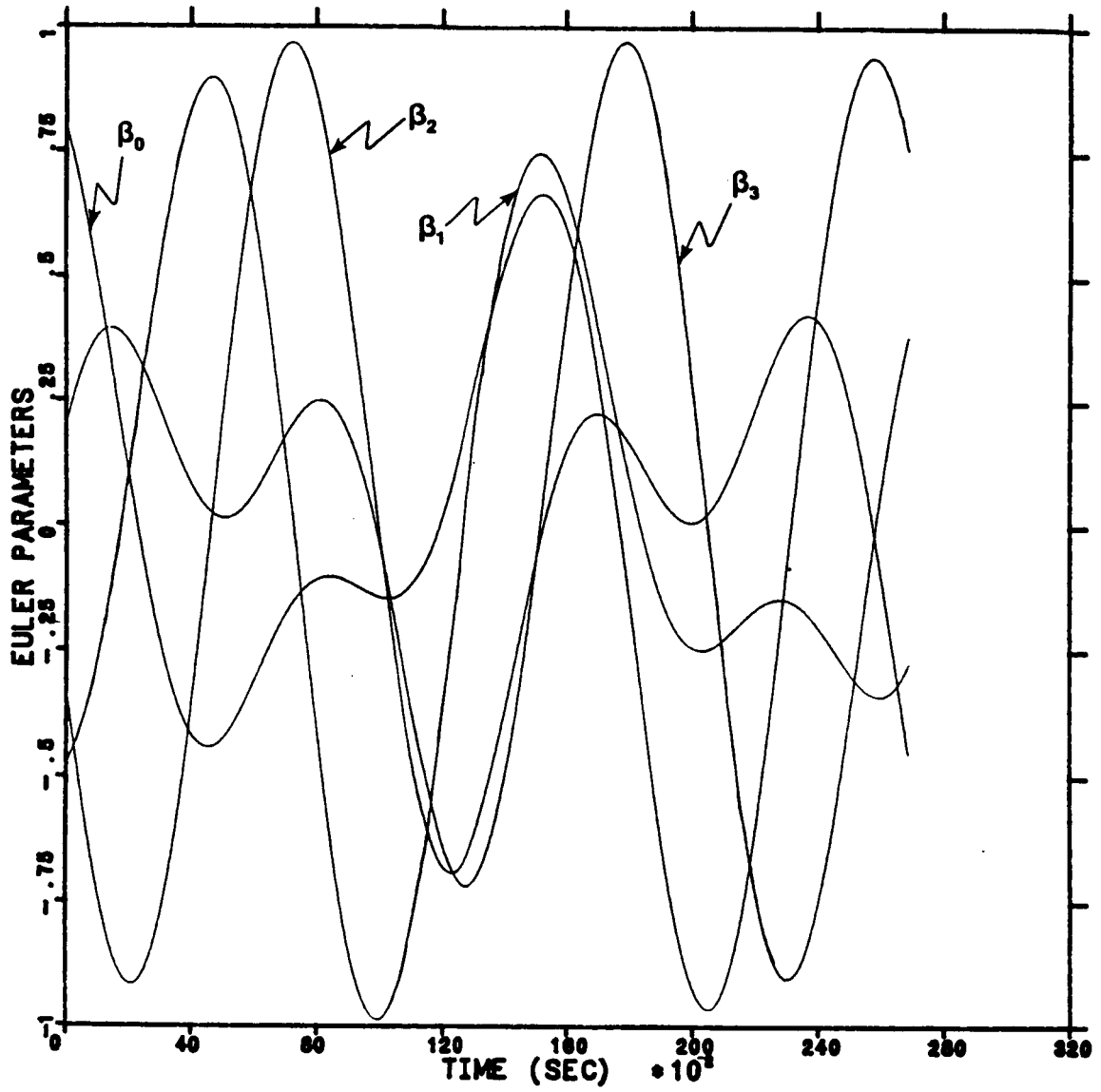
Fig. 21 a. Time-Histories of Euler-Parameters for HST,
            Case IV (184 km. x 316 km. Orbital Altitude without
            Environmental Torques).
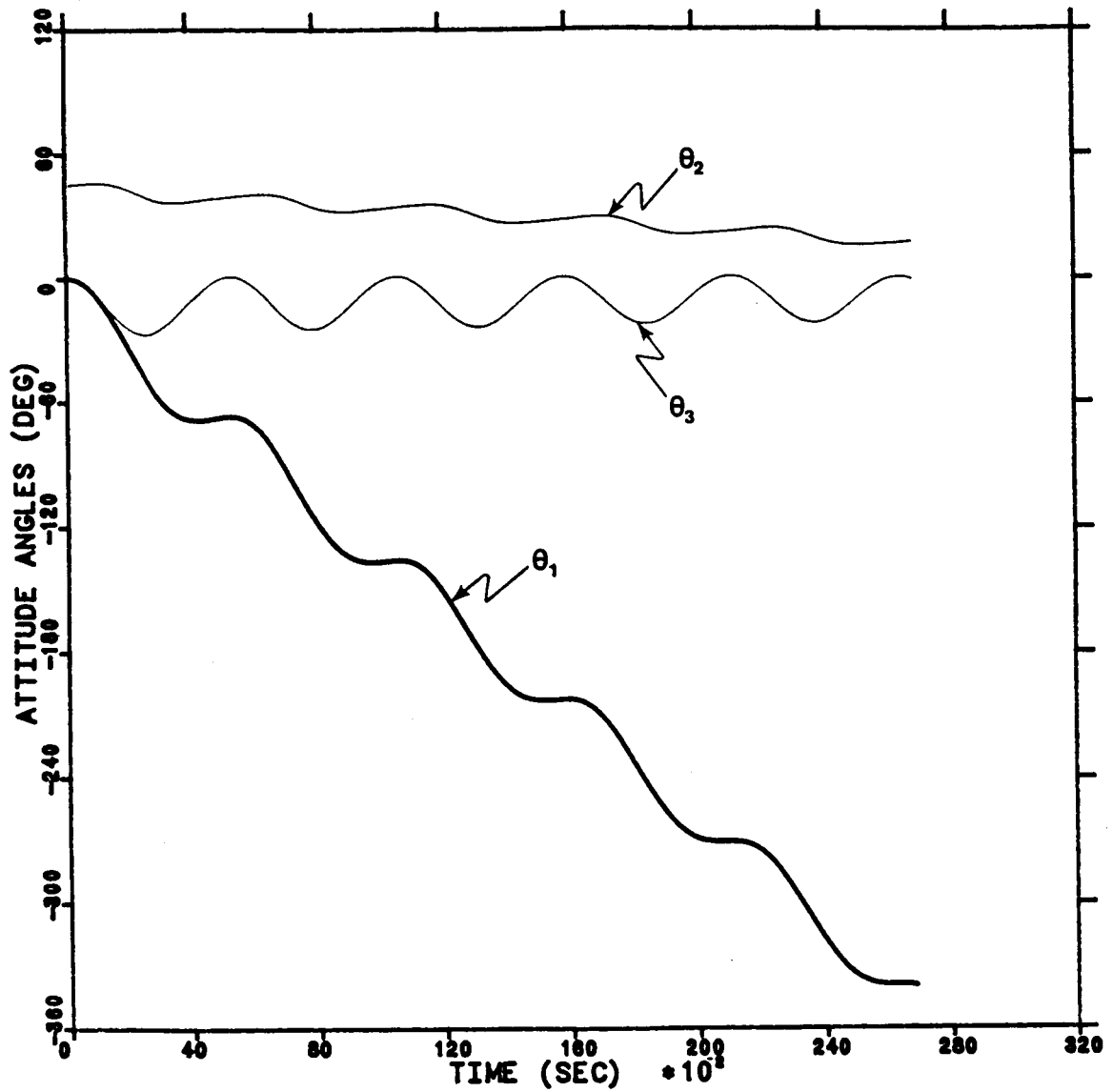
Fig. 21 b. Time-Histories of Roll, Pitch, and Yaw Angles for HST, Case IV (184 km. x 316 km. Orbital Altitude without Environmental Torques).
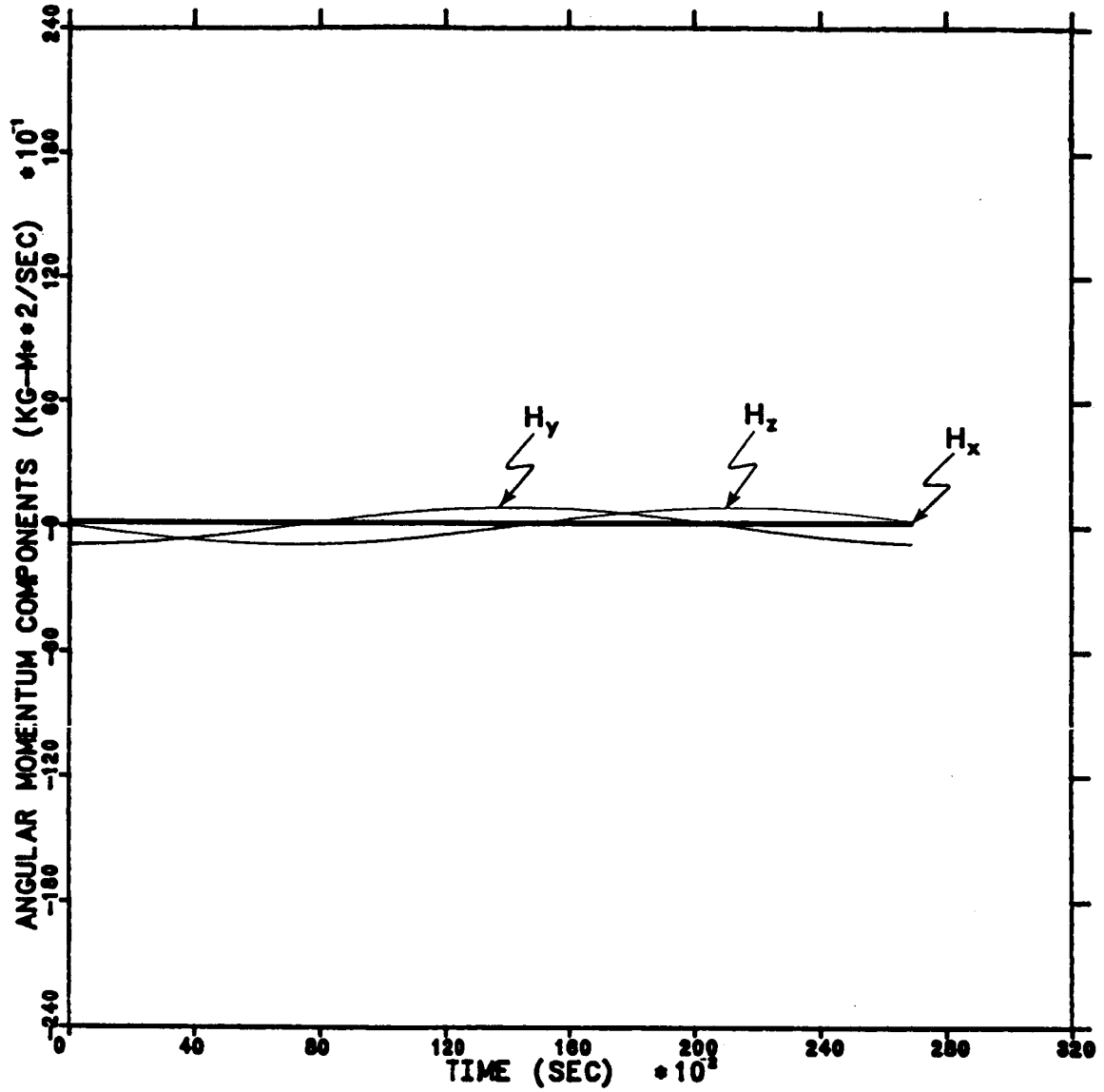
Fig. 21 c. Time-Histories of Angular Momentum Components for HST,
Case IV (184 km. x 316 km. Orbital Altitude without
Environmental Torques).

the expected low frequency/high amplitude oscillations. The attitude angles (Fig. 21 b) show the same secular variation in roll angle and almost the same for low frequency oscillation as in Case III, but the high frequency oscillation has disappeared. The pitch angle has a low frequency/low amplitude oscillation and slight secular departure in the negative direction. The yaw angle shows a slightly higher amplitude and a frequency similar to that of pitch angle. The yaw angle does not appear to change secularly. The angular momentum (Fig. 21 c) has a constant x_b-component, and the y_b-and z_b-components exhibit single-frequency, low-amplitude oscillations, but are out of phase with each other. The low amplitude is due to the low angular rates which are unexcited by environmental torques.

6.2.2 LANDSAT Simulations

The LANDSAT attitude motion simulations differ from the HST simulations in a few respects. First, the satellite physical data indicates that the satellite's moments of inertia are an order of magnitude smaller than the HST. Second, the LANDSAT model possesses no internal angular momentum as did the HST. Third, the initial orientation of LANDSAT model with respect to the local vertical differs from that of the HST. The HST simulations began with an initial pitch angle of 45°, but the LANDSAT simulations begin with a 10° pitch angle and a -80° yaw angle. Fourth, the initial angular rate of the HST was a negative pitch about the y_b-axis at orbital rate, while the initial angular rate of the LANDSAT is ncos10° about the x_b-axis and nsin10° about the z_b-axis, where n is the orbital mean motion for a given orbital radius. Fifth,

the orbits which are used for the LANDSAT simulations are both inclined at 98.2° as compared to the 28.5° inclination used for the HST cases.

The first LANDSAT case is for a circular orbit with an orbital altitude of 352 km. The second LANDSAT case is also for a circular orbit, but the orbital altitude is 705 km. In both of the LANDSAT cases, only gravity-gradient torques were simulated.

Case I

In the 352 km orbital altitude case, the Beta plots (Fig. 22 a) are irregular oscillations which show strong orbital coupling. These oscillations are most similar to the HST Case IV Beta plot (Fig. 21 a), but are somewhat more irregular. The attitude angle plots (Fig. 22 b) shows that roll angle increases secularly with some irregular "oscillations." The pitch angle time-history also shows similar irregular "oscillations," but no secular departure. The yaw angle time-history contains higher amplitude irregularities and is also not changing secularly. The angular momentum plot (Fig. 22 c) indicates that this case is a much lower angular momentum case than the HST cases. Note that the scale used in the plots is two orders of magnitude smaller than that for the previous HST angular momentum component plots. The x_b-component remains nearly constant and the y_b-and z_b-components have low frequency/low amplitude oscillations and no apparent secular change. The gravity-gradient torque component plot (Fig. 22 c) shows that the gravity-gradient torque is an order of magnitude less than it was for the HST cases. This is due to the fact that the LANDSAT satellite is much smaller than the HST.
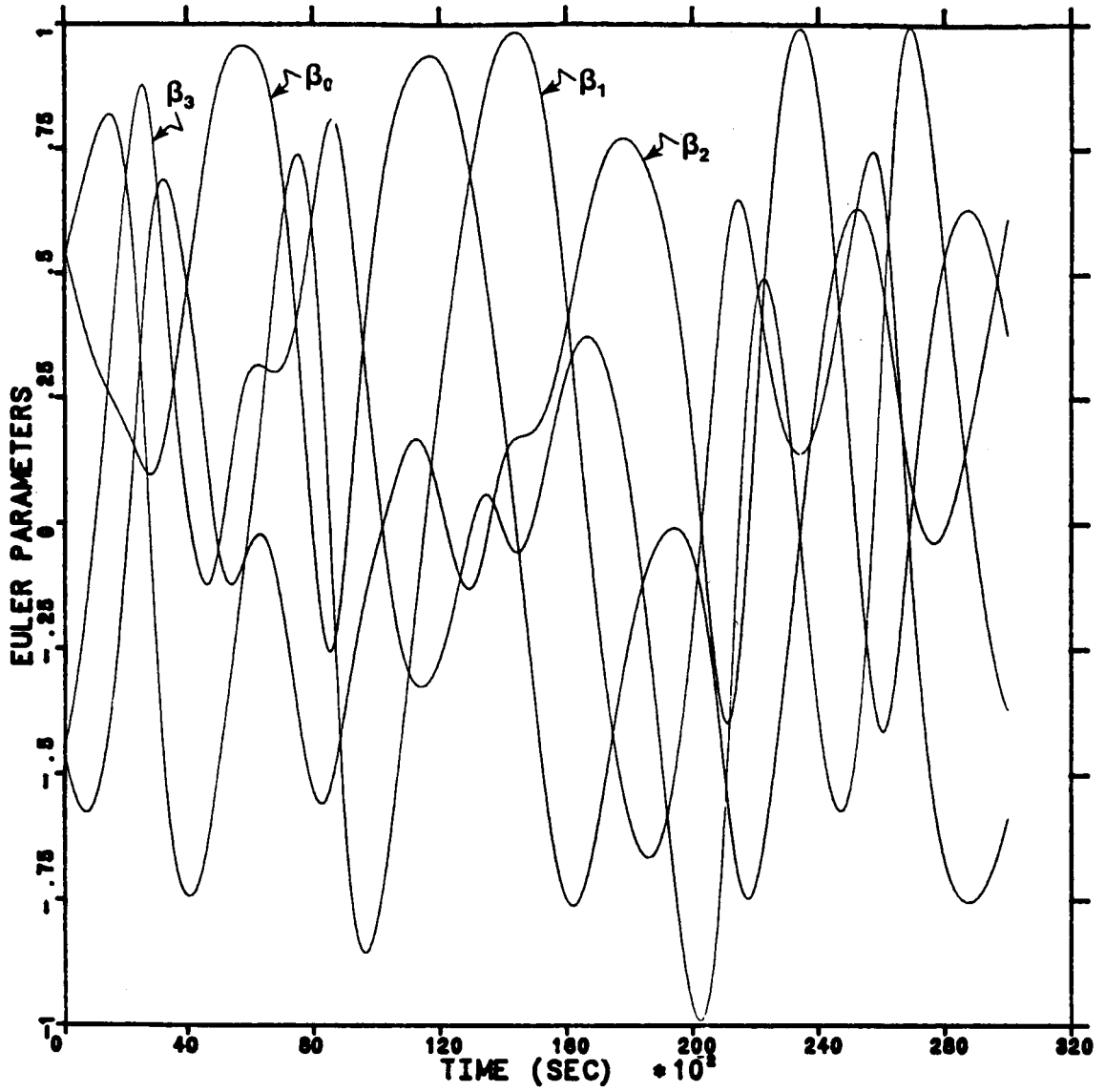
Fig. 22 a. Time-Histories of Euler-Parameters for LANDSAT,
            Case I (352 km. Orbital Altitude, Gravity-Gradient Torque
            Only).
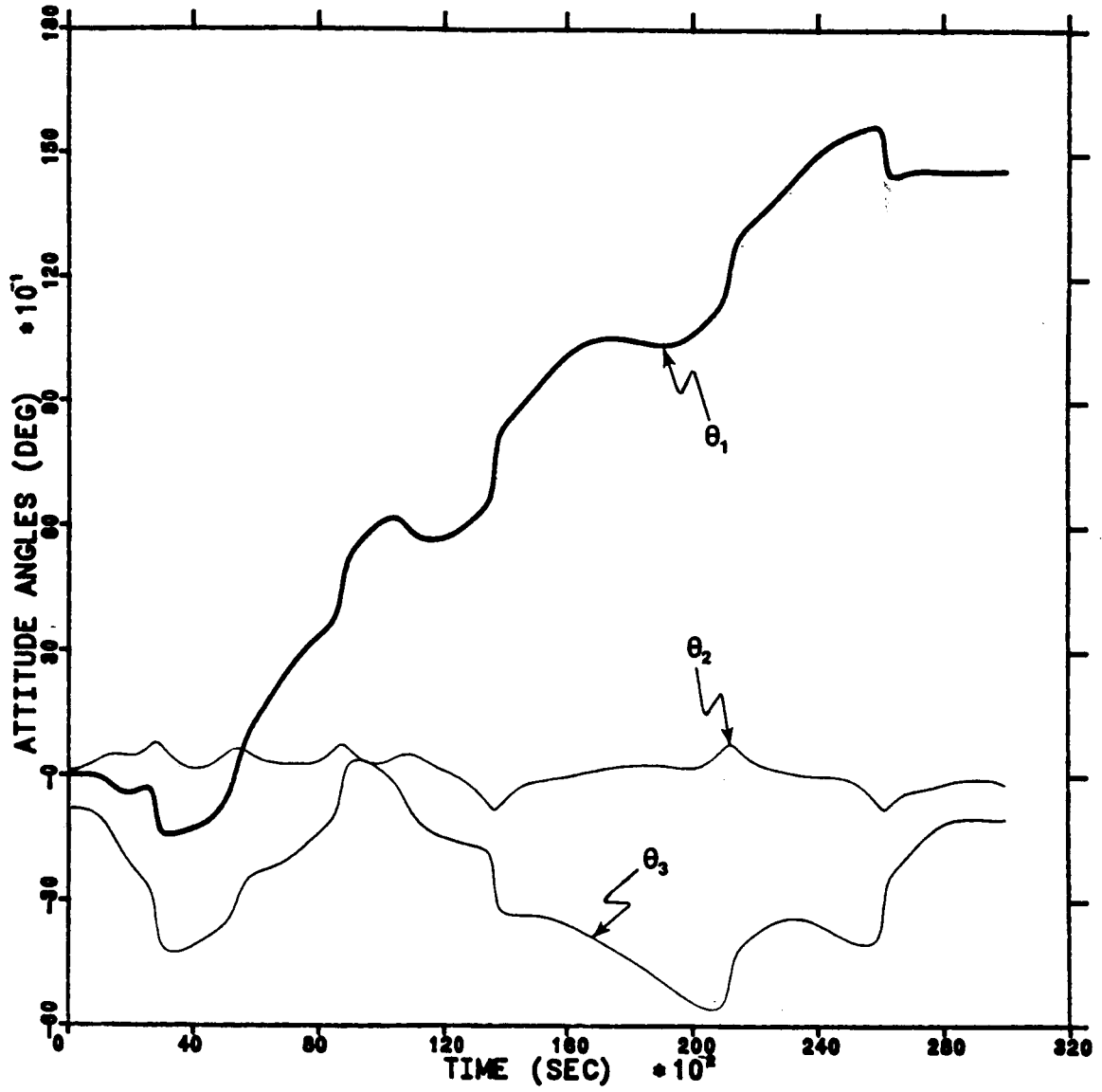
Fig. 22 b. Time-Histories of Roll, Pitch, and Yaw Angles for LANDSAT,
Case I (352 km. Orbital Altitude, Gravity-Gradient
Torque Only).
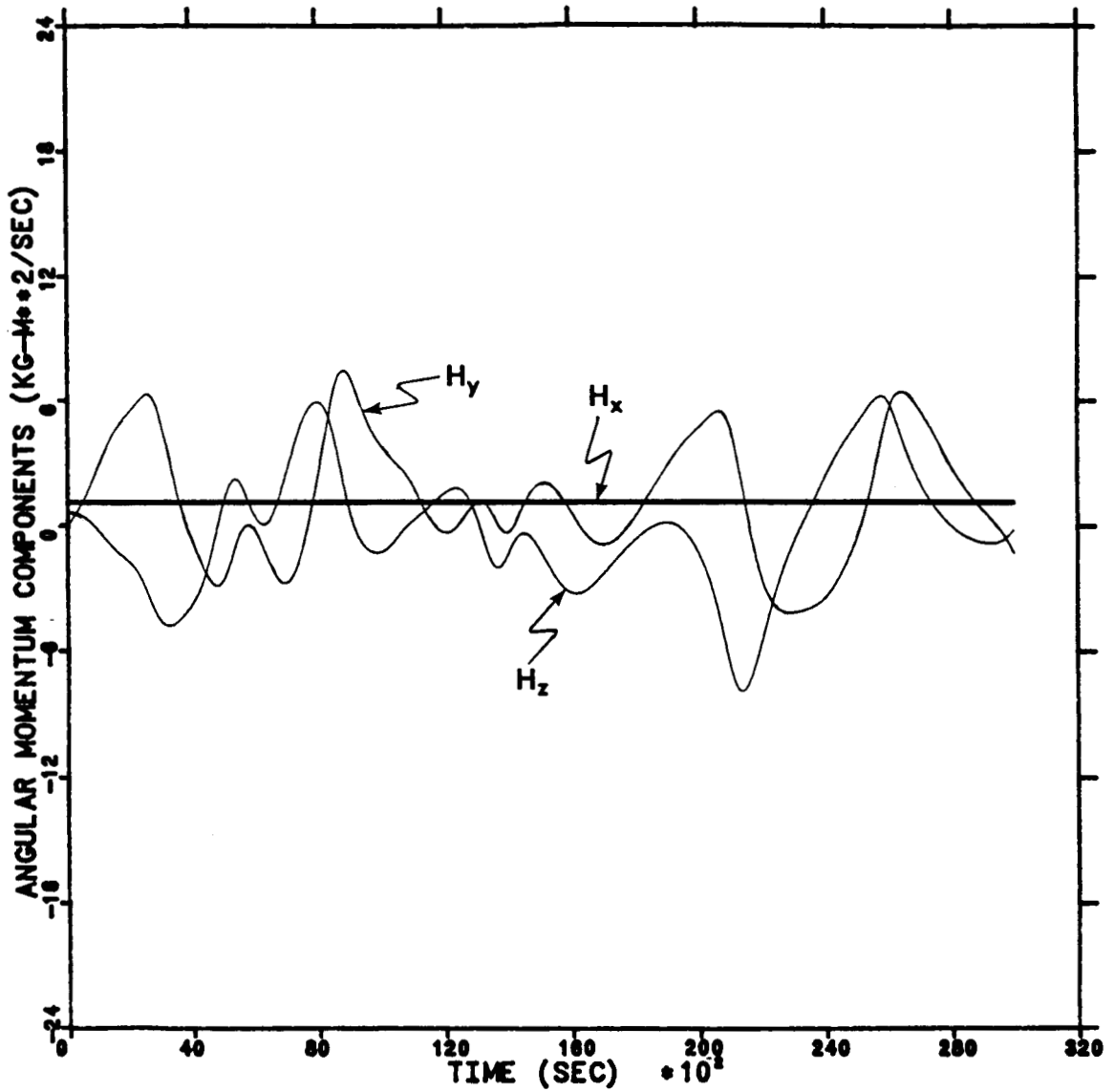
Fig. 22 c. Time-Histories of Angular Momentum Components for LANDSAT,
Case I (352 km. Orbital Altitude, Gravity-Gradient
Torque Only).
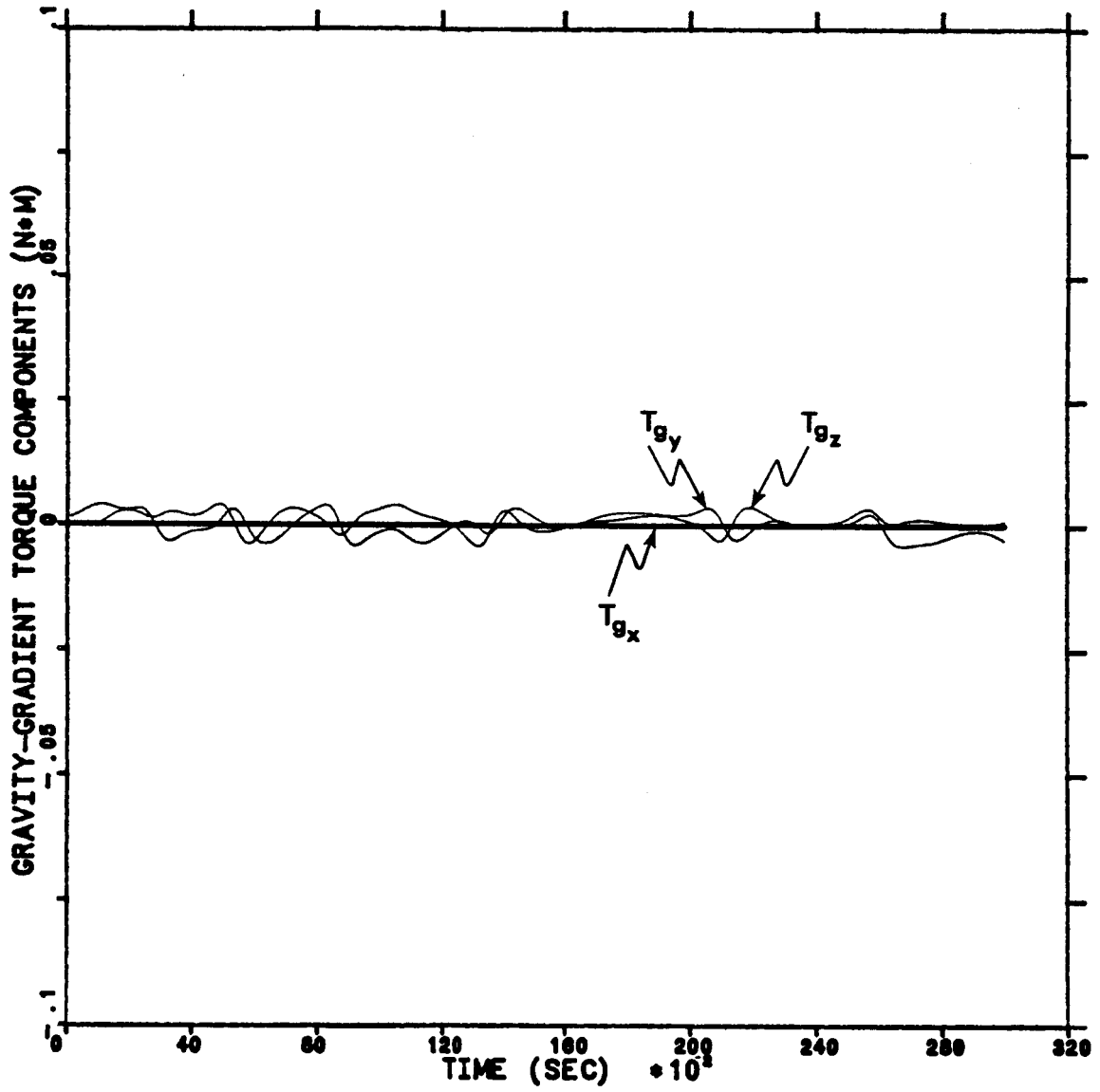
Fig. 22 d.   Time-Histories of Gravity-Gradient Torque Components for
LANDSAT, Case I (352 km. Orbital Altitude, Gravity-
Gradient Torque Only).
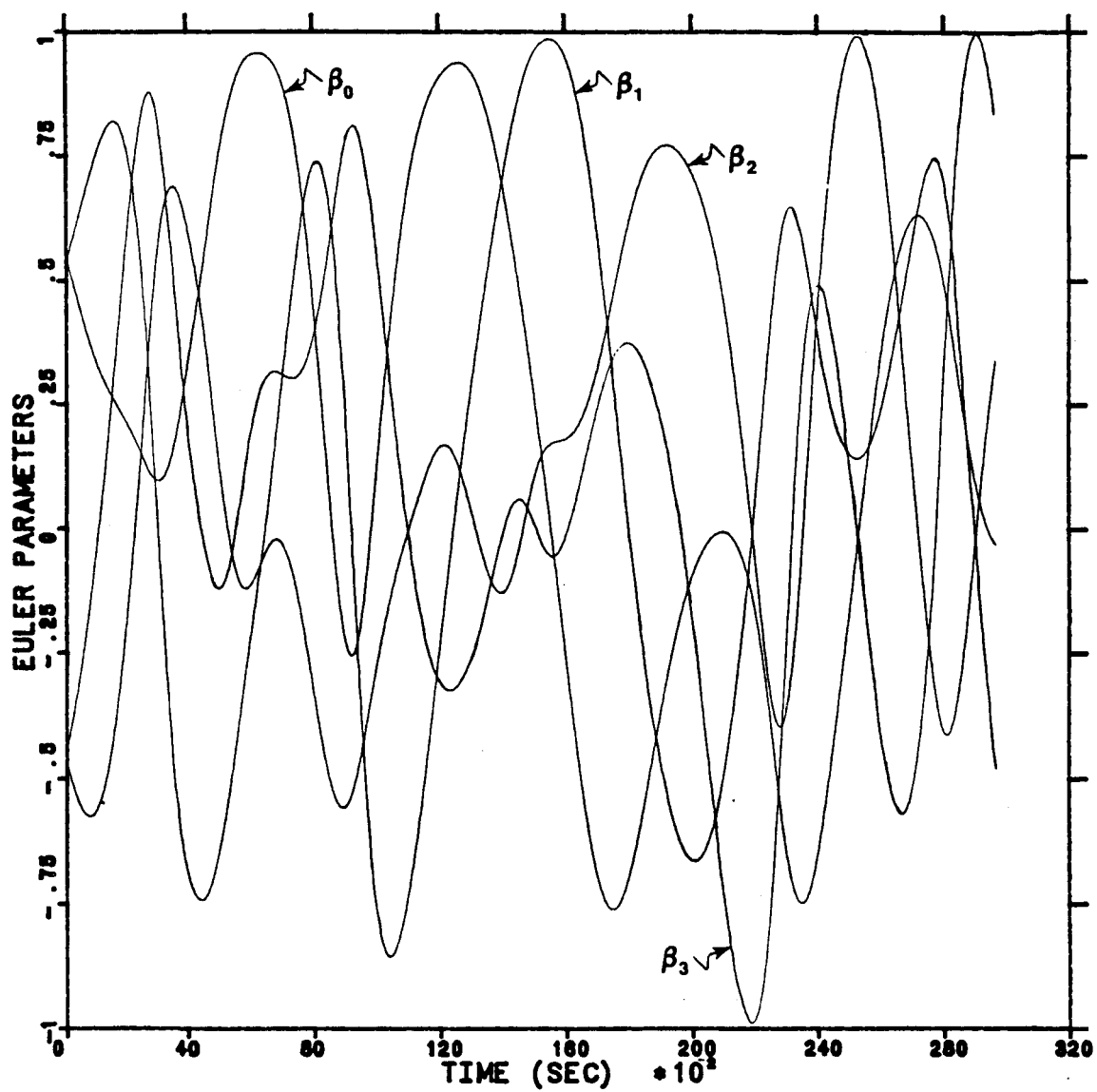
Fig. 23 a. Time-Histories of Euler Parameters for LANDSAT,
Case II (705 km. Orbital Altitude, Gravity-Gradient
Torque Only).
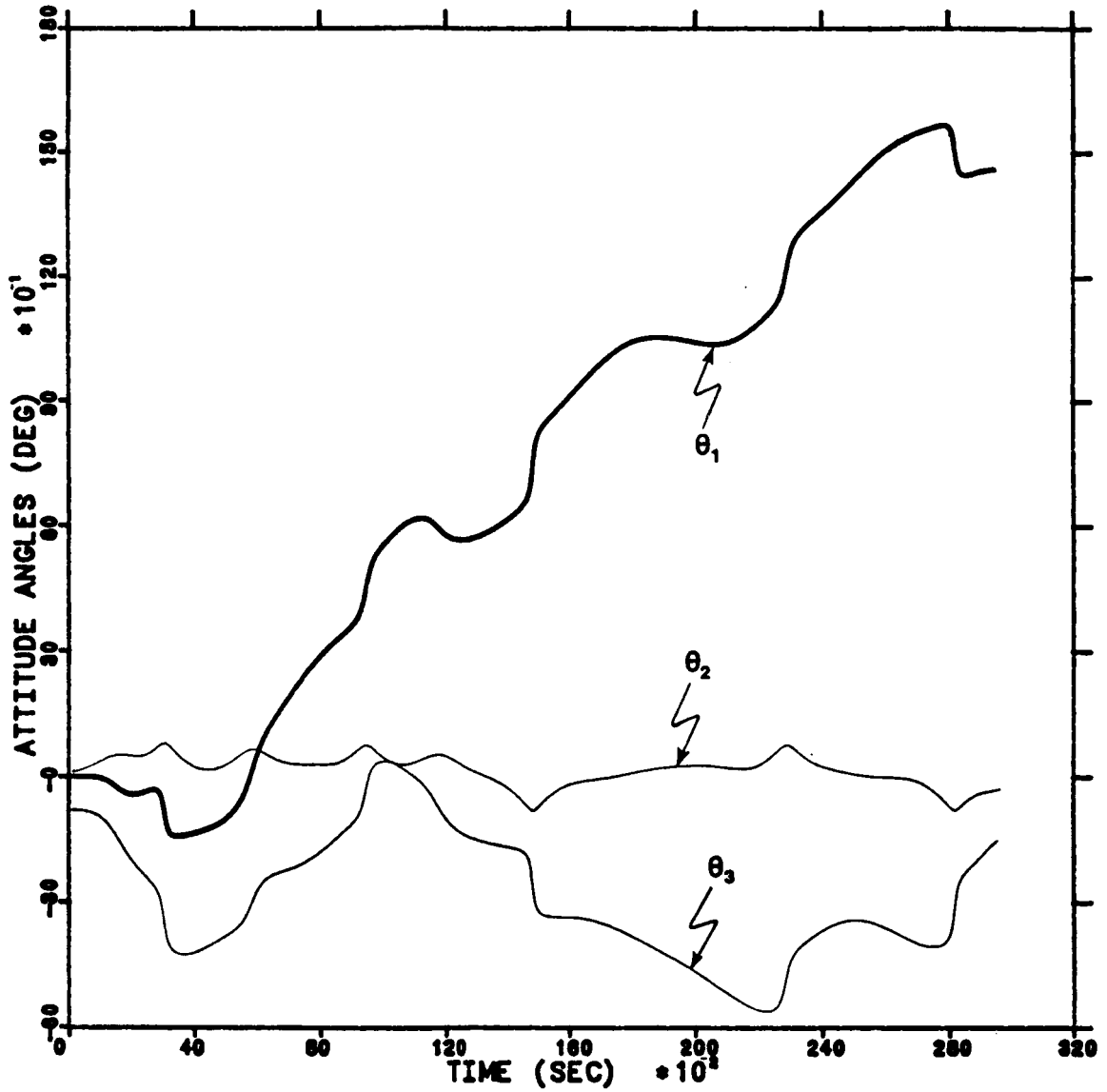
Fig. 23 b. Time-Histories of Roll, Pitch, and Yaw Angles for LANDSAT,
Case II (705 km. Orbital altitude, Gravity-Gradient
Torque Only).
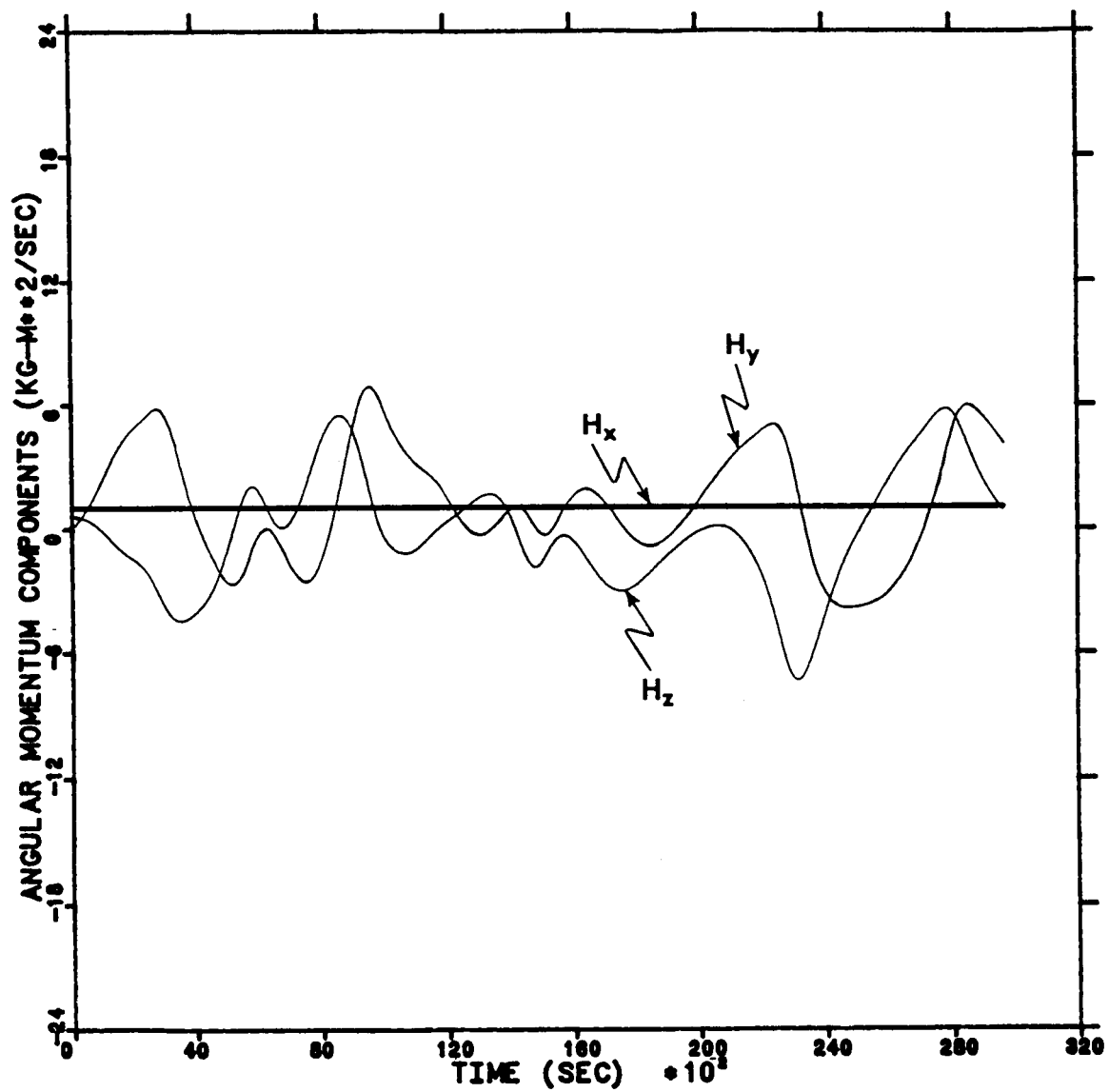
Fig. 23 c. Time-Histories of Angular Momentum Components for LANDSAT,
Case II (705 km. Orbital Altitude, Gravity-Gradient
Torque Only).
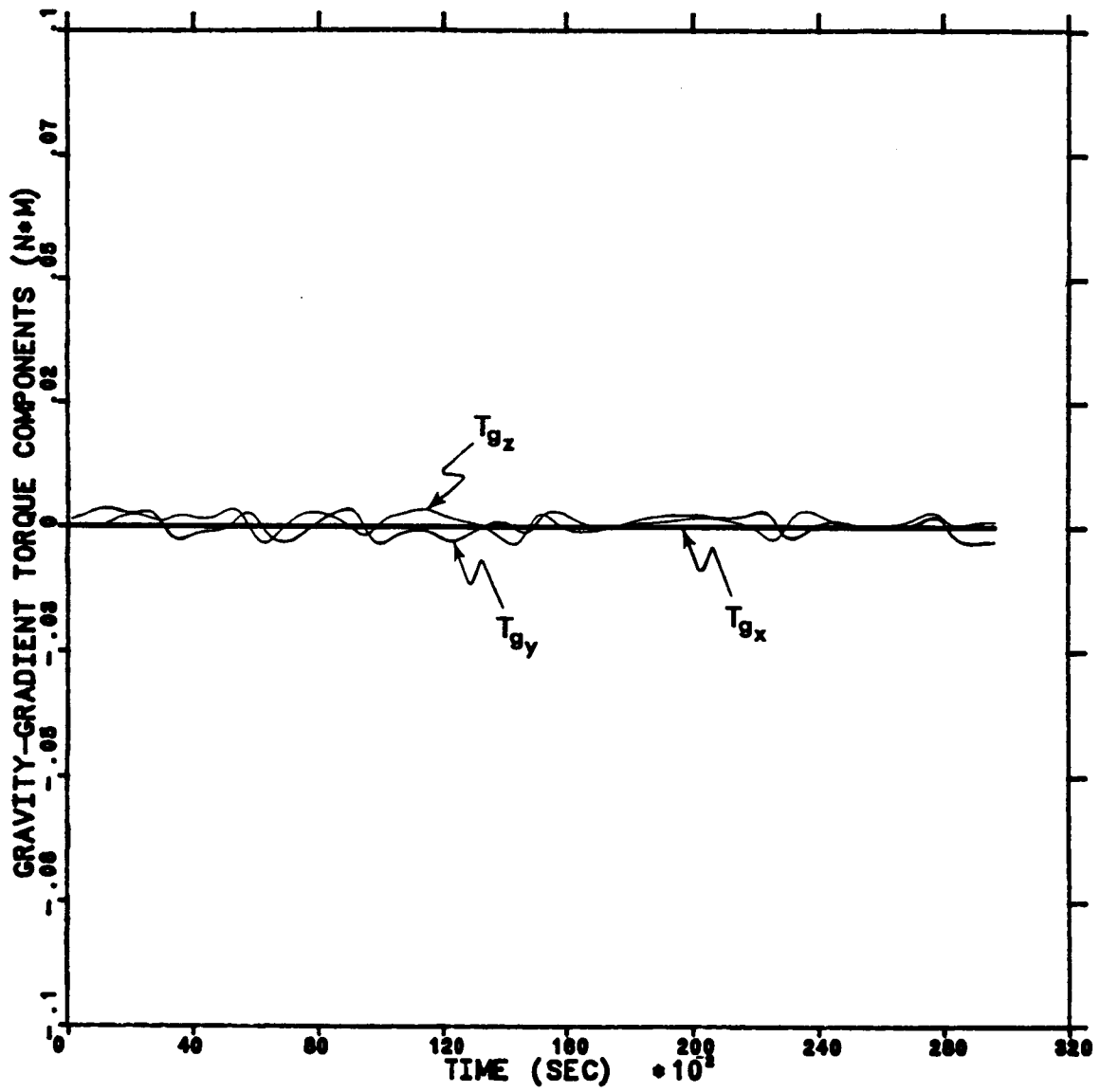
Fig. 23 d. Time-Histories of Gravity-Gradient Torque Components for
LANDSAT, Case II (705 km. Orbital Altitude, Gravity-
Gradient Torque Only).

Case II

The results of the second case are nearly identical to that of the first case. The Beta plot (Fig. 23 a) are almost identical to that for the first case. The attitude angles for both cases (Figs. 22 b and 23 b) are also almost identical. The angular momentum component plots (Figs. 22 c and 23 c) are slightly different. The orbital mean motion in this case is very slightly lower due to the fact that the orbital altitude is 705 km. As a result of the slightly lower angular velocity magnitude, the angular momentum components have slightly lower amplitudes. Again in the gravity-gradient torque plot (Fig. 23 d), the amplitudes are slightly smaller due to the higher orbital altitude.

6.2.3 AXAF Simulations

This is the final satellite considered in the numerical simulations. The AXAF satellite is more similar to the HST than the LANDSAT. Geometrically, the sizes of the AXAF and the HST are nearly identical. However, the moments of inertia of the AXAF are slightly more than twice as large as those of the HST. The AXAF model includes no internal angular momentum. The initial orientation of the satellite model has a 45° pitch angle with respect to the local horizontal as does the HST. Also, the AXAF model has a 45° yaw in the negative sense. The initial angular rates of the AXAF satellite model are 1.0×10^{-3} rad/sec about the x_b-axis and 1.0×10^{-4} rad/sec about the y_b-axis. The orbital inclination is the same as for the HST simulations, 28.5°. Both of the AXAF simulations assume a circular orbit with an altitude of 400 km. In the first case, both of the environmental torques were simulated. In the second case, no environmental torques were included.
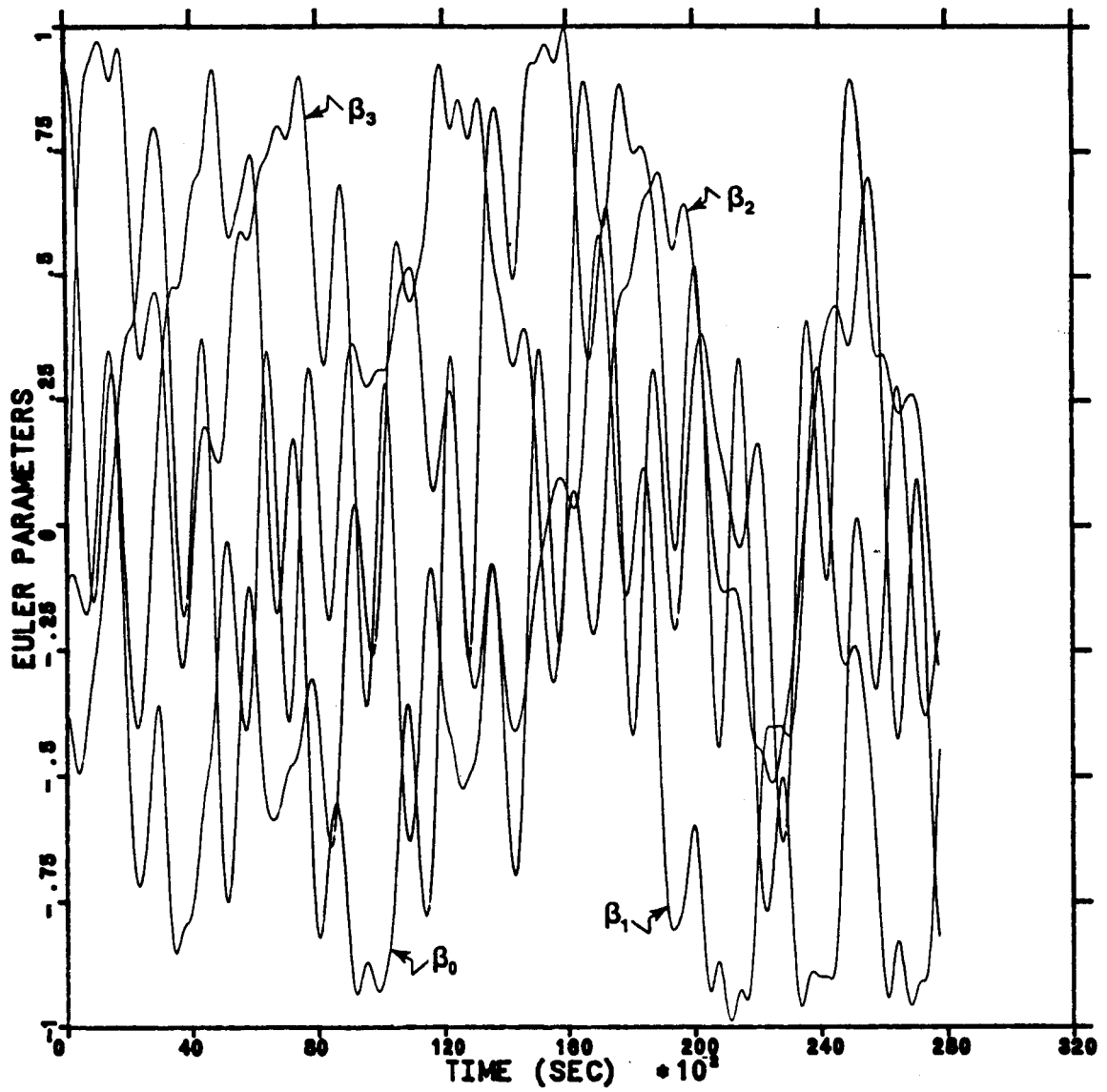
Fig. 24 a. Time-Histories of Euler-Parameters for AXAF,
Case I (400 km. Orbital Altitude).
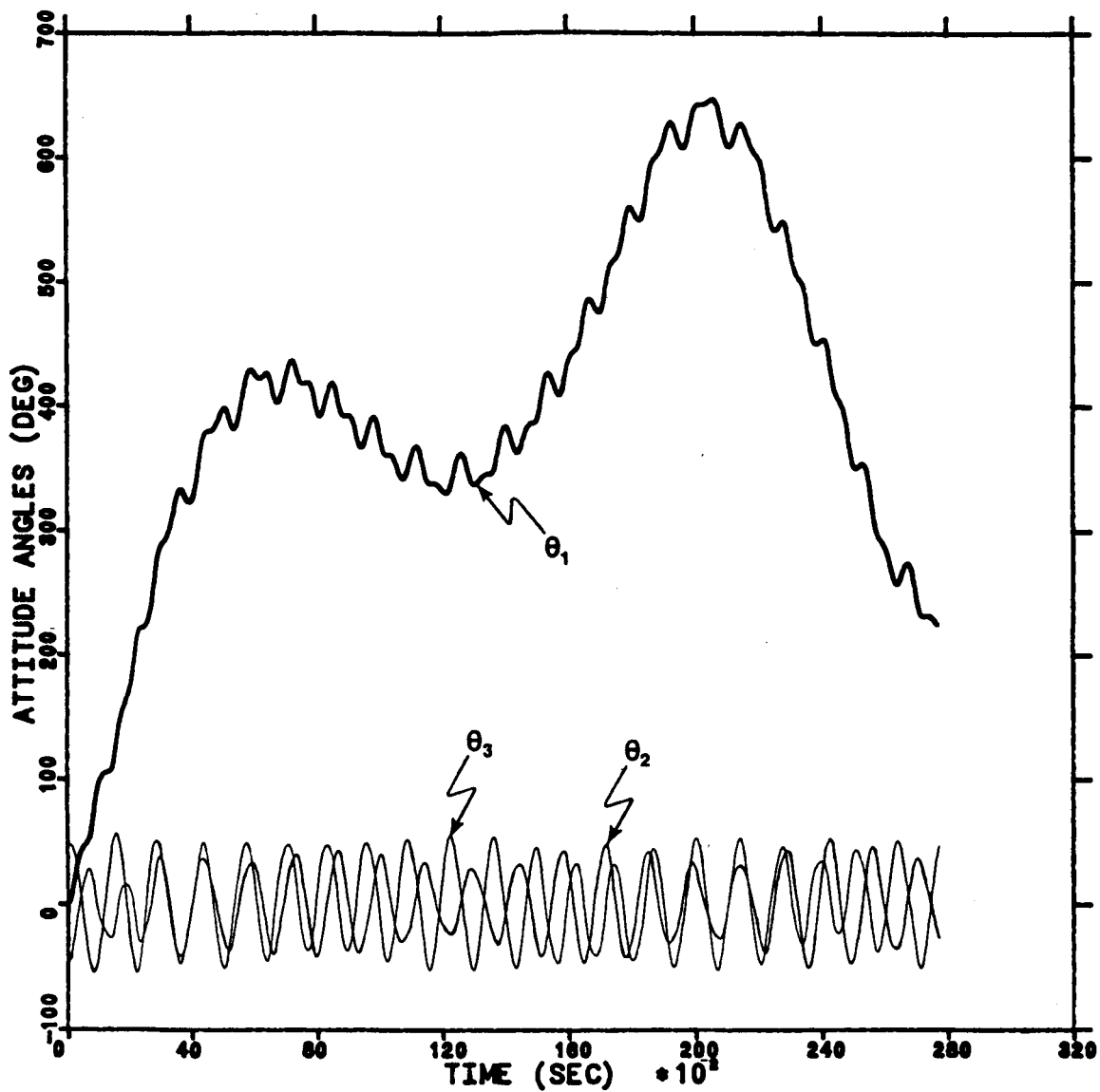
Fig. 24 b. Time-Histories of Roll, Pitch, and Yaw Angles for AXAF,
Case I (400 km. Orbital Altitude).
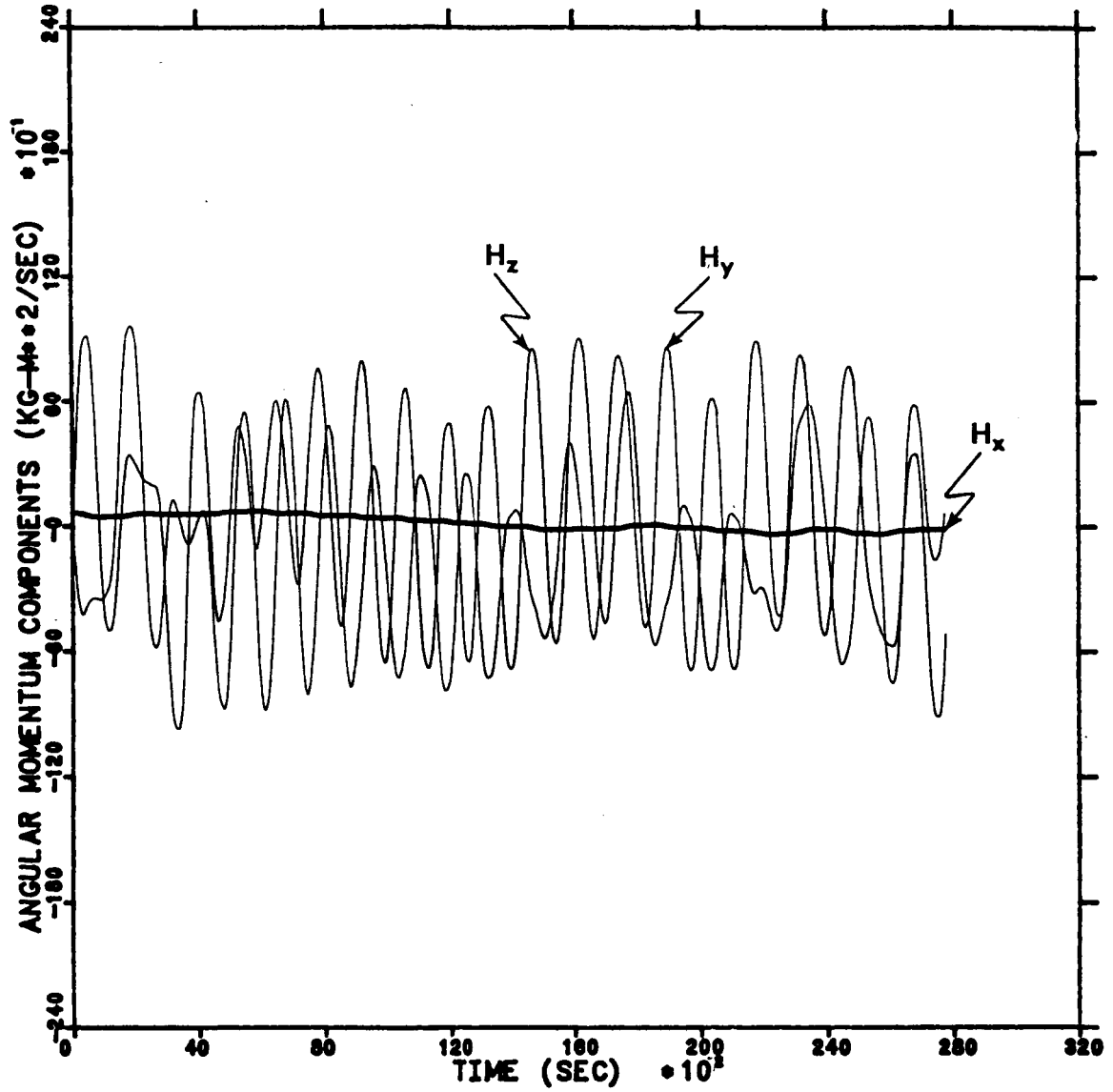
Fig. 24 c.   Time-Histories of Angular Momentum Components for AXAF,
Case I (400 km. Orbital Altitude).
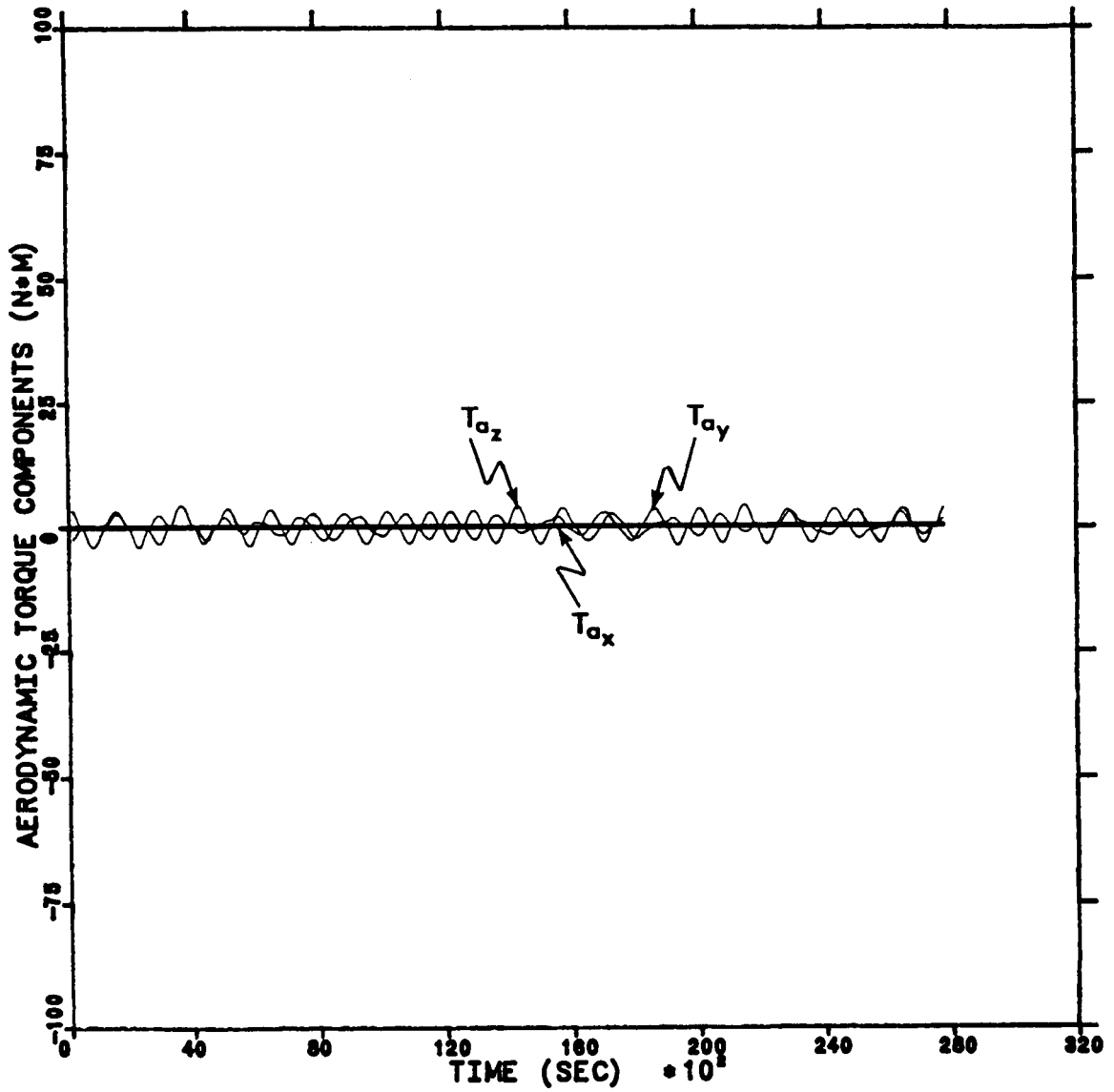
Fig. 24 d. Time-Histories of Aerodynamic Torque Components for AXAF,
Case I (400 km. Orbital Altitude).
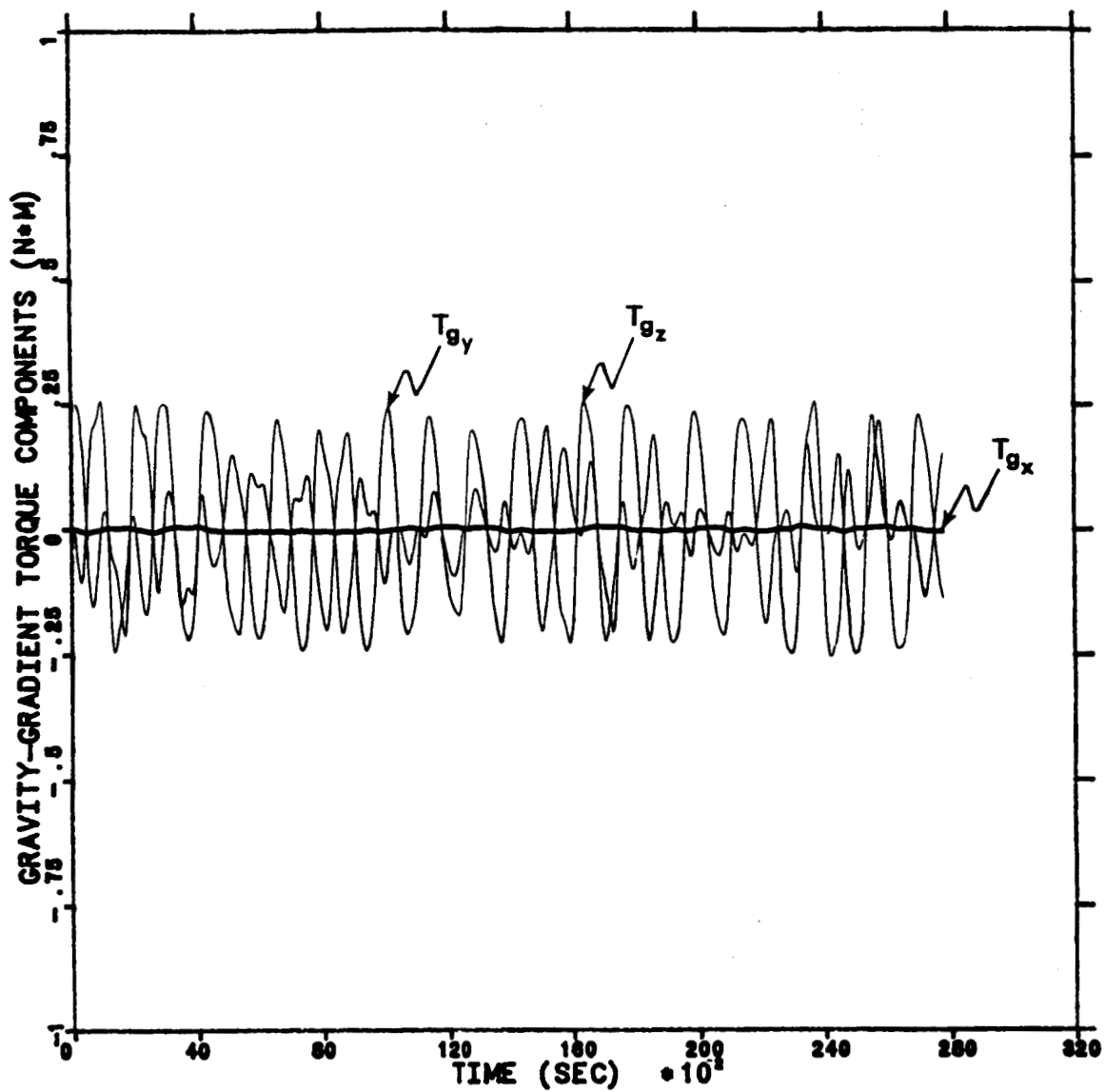
Fig. 24 e.   Time-Histories of Gravity-Gradient Torque Components for
AXAF, Case I (400 km. Orbital Altitude).

Case I

The Beta plots (Fig. 24 a) show the reappearance of the two

frequency mode oscillations seen in the first HST (LEO) case. Here, the

high frequency/low amplitude oscillations have a lower frequency and are

more irregular than those in the first HST case. This is due to the

high frequency/low amplitude oscillations have a lower frequency and are

more irregular than those in the first HST case. This is due to the

intermediate altitude of this case (400 km), which is between the first

HST case (250 km) and the second HST case (800 km) where the high

frequency oscillations have disappeared. The roll angle in Fig. 24 b

behaves much differently than in previous cases. The roll angle

increases to approximately 650°, then decreases to around 200°. The

pitch and yaw angles appear to be almost periodic with no secular

variations. They behave much like the pitch angle in the second HST

case (see Fig. 19 b). The components of angular momentum (Fig. 24 c)

also behave in a manner which suggests that this case represents a

"transition" between the first and second HST cases. Note that the

maximum amplitude of the angular momentum is an order of magnitude

greater in this case. There is no apparent damping effect due to

aerodynamic torque on any of the components. Note that the x_b-component

is not constant as it has been in previous cases. The reason for this

can be seen in the gravity-gradient torque component plot (Fig. 24 e).

The x_b-component of gravity-gradient torque is not constant because

there is a large difference between the moments of inertia I_{yy} and I_{zz}.

The aerodynamic torque components (Fig. 24 d) are essentially

proportional to the angular momentum components. Note that the maximum

amplitude of aerodynamic torque lies somewhere between those for the

first and second HST cases. Also, note that the maximum amplitude of the gravity-gradient torques is approximately twice that of the first HST case. This is due, as we stated previously, to the fact that there are greater differences in the values of the three principal moments of inertia.

Case II

This final numerical simulation case has the AXAF model with initial conditions identical to the first AXAF case. The differences between the two are a result of the absence of environmental torques in the second case.

The Beta plots (Fig. 25a) show only the single low frequency/high amplitude oscillations. The attitude angle plots (Fig. 25 b) show that all three angles "oscillate" at a relatively low frequencies with significant irregularities. The final plot of this section, the angular momentum plots (Fig. 25 c), are similar to the corresponding plots for the second HST case. That is, the x_b-component remains constant, while the other two exhibit smooth oscillations of the same frequency and amplitude and are slightly out of phase.

6.2.4 Summary of Low Angular Momentum Examples

The results of the eight cases given in this section indicate that the time-histories of some of the variables used to describe the attitude motion do not exhibit well-defined patterns. In some cases, aerodynamic and gravity-gradient torques perturb the attitude motion of low angular momentum satellites to such an extent that existing torque-free analytical solutions are not valid for any significant period of time.
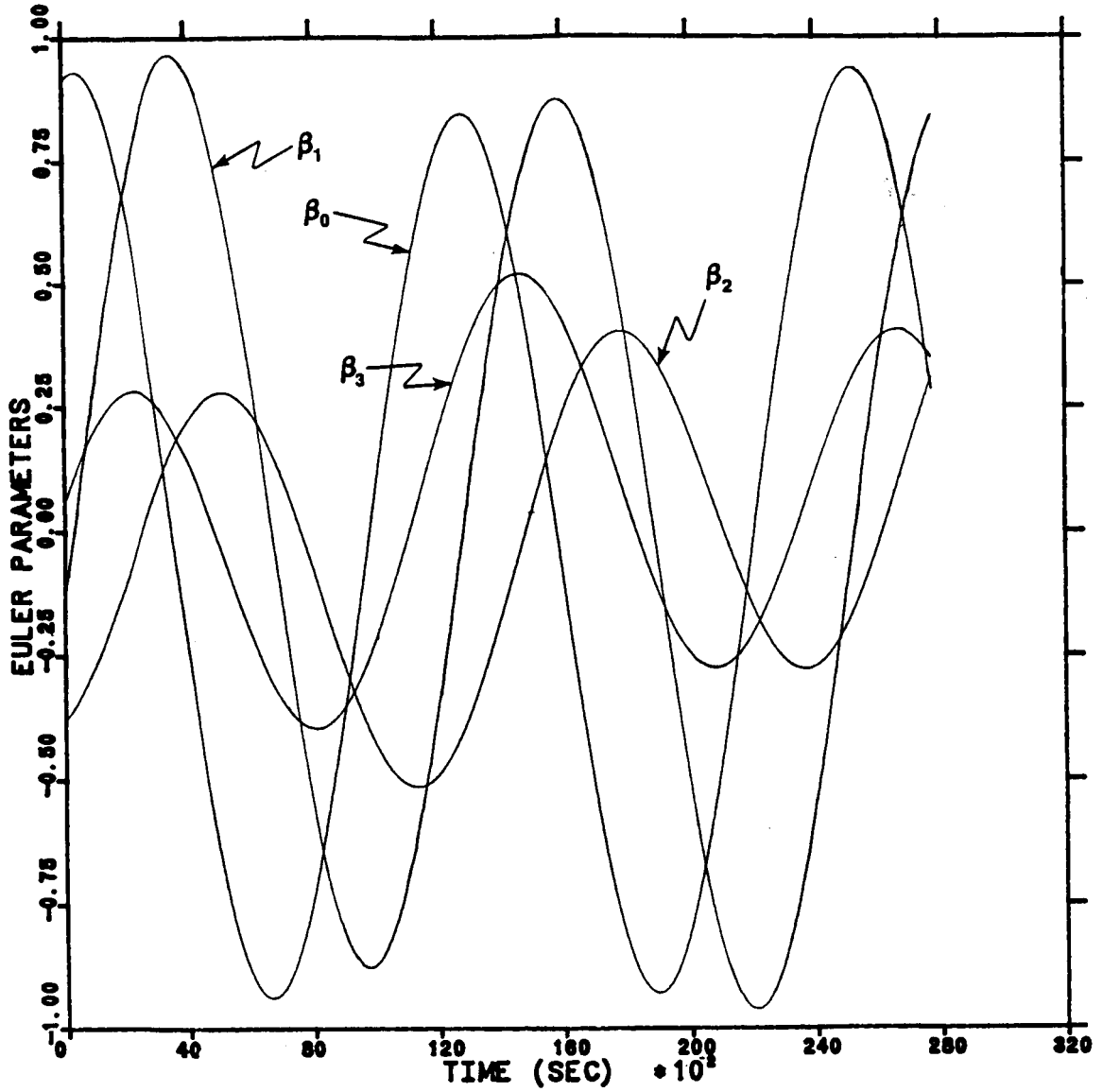
Fig. 25 a. Time-Histories of Euler-Parameters for AXAF,
Case II (400 km. Orbital Altitude, No Environmental
Torques).
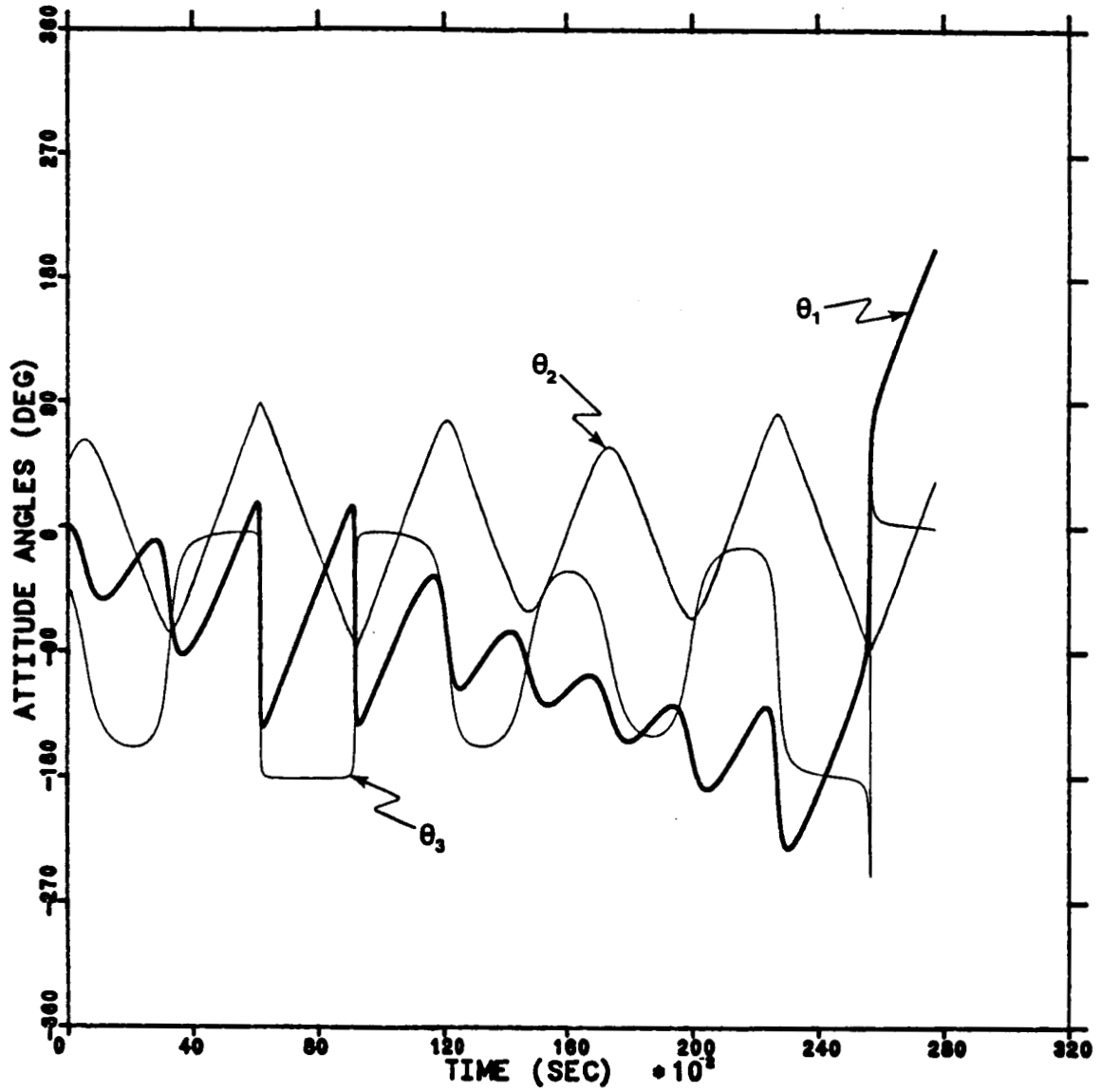
Fig. 25 b. Time-Histories of Roll, Pitch, and Yaw Angles for AXAF,
            Case II (400 km. Orbital Altitude, No Environmental
            Torques).
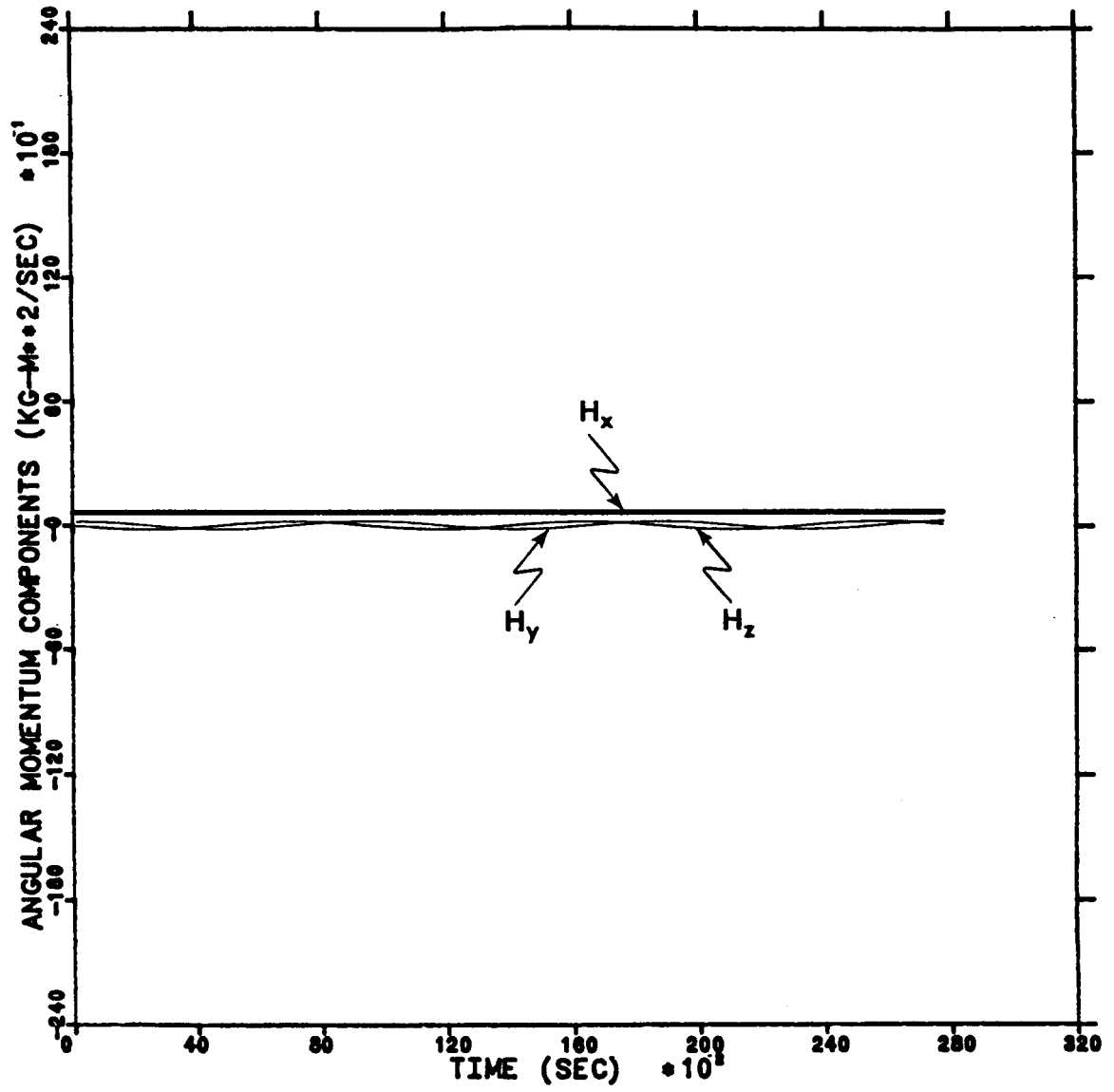
Fig. 25 c. Time-Histories of Angular Momentum Components for AXAF, Case II (400 km. Orbital Altitude, No Environmental Torques).

VII. PREDICTION OF LONG-TERM MOTION

7.0 Rationale

As was stated previously, there will likely be a time lapse of several months between a satellite's "failure" and a recovery attempt. Therefore, a need exists for an accurate long-term attitude motion simulation for mission feasibility studies and planning. This chapter focuses on this need. As with the short-term attitude motion simulations, there are two approaches to the problem of perturbed long-term attitude motion. These are the General Perturbation Methods (GPM), and the Special Perturbation Methods (SPM). To apply the usual GPM, one needs an analytical solution to the unperturbed problem. Examples of unperturbed solutions include two-body orbital motion and "free-Eulerian" rotational motion. Tractable analytical expressions for perturbations are also required. The SPM most commonly applied are that of numerical methods. Examples of numerical perturbation methods applied to orbital motion include the work of Cowell and Encke.[24] Applications to attitude motion include the work of Kraige and Junkins.[25] The short-term motion simulation, described in Chapter IV, also uses numerical perturbation methods.

Both GPM and SPM have shortcomings which hamper their application to attitude dynamics problems. The application of the GPM is difficult or perhaps impossible if the satellite is dynamically complex. On the other hand, the numerical approach, although generally applicable,

often requires large amounts of computer time, especially when higher angular rates necessitate the use of very small integration step sizes. For these reasons, a "hybrid" method was developed and labeled the "Semi-Analytic method." This method incorporates the use of analytical averaging concepts from GPM, and numerical integration techniques from SPM to obtain "averaged equations of motion" which govern the long-term attitude motion of certain classes of satellites.

7.1 Averaging Method

In order to apply the General Method of Averaging to the equations of motion to obtain the "averaged equations of motion," new variables must be introduced. These variables are elements of $\underline{x}$ and $\underline{y}$, where

$$\underline{x} = (H\ H\cos\Theta_H\ \Psi_H), \tag{7.1.1}$$

and

$$\underline{y} = (\phi\ \psi\ M)\ , \tag{7.1.2}$$

where M is the mean anomaly. The elements of $\underline{x}$ are the "slow" variables and the elements of $\underline{y}$ are the "fast" variables. The time derivatives of $\underline{x}$ and $\underline{y}$ take the forms,

$$\dot{\underline{x}} = \epsilon\ \underline{f}_1(\underline{x},\ \underline{y}) \tag{7.1.3}$$

and

$$\dot{\underline{y}} = \underline{g}_0(\underline{x},\ \underline{y}) + \epsilon\underline{g}_1(\underline{x},\ \underline{y})\ , \tag{7.1.4}$$

where $\underline{g}_0(\underline{x},\ \underline{y})$ is the "unperturbed" time derivative of $\underline{y}$, $\epsilon\ \underline{f}_1(\underline{x},\ \underline{y})$ and $\epsilon\ \underline{g}_1(\underline{x},\ \underline{y})$ are the "perturbations" due to external torques on the satellite, and ϵ is the usual small parameter introduced for perturbation analyses.

Here, it will be assumed that the functions of $\underline{f}_1(\underline{x}, \underline{y})$ and $g_j(\underline{x}, \underline{y})$, $j = 0,1$, are periodic with period 2π in the elements of $\underline{y}$. Since the elements of $\underline{y}$ are Euler angles, this will be the case for a variety of torques.

A new set of variables $(\underline{\bar{x}}, \underline{\bar{y}})$ is defined by

$$\underline{x} = \underline{\bar{x}} + \varepsilon \, \underline{u}_1 \, (\underline{\bar{x}}, \underline{\bar{y}}) + \varepsilon^2 \, \underline{u}_2(\underline{\bar{x}}, \underline{\bar{y}}) + \cdots \qquad (7.1.5)$$

and

$$\underline{y} = \underline{\bar{y}} + \varepsilon \, \underline{v}_1 \, (\underline{\bar{x}}, \underline{\bar{y}}) + \varepsilon^2 \, \underline{v}_2(\underline{\bar{x}}, \underline{\bar{y}}) + \cdots \qquad (7.1.6)$$

where the functions $\underline{u}_j$ and $\underline{v}_j$, $j = 1,2$, are to be chosen to make the differential equations for $\underline{\bar{x}}$ and $\underline{\bar{y}}$ simpler than those for $\underline{x}$ and $\underline{y}$. Equations (7.1.5) and (7.1.6) may be differentiated with respect to time to get

$$\underline{\dot{x}} = \underline{\dot{\bar{x}}} + \varepsilon \, \underline{\dot{u}}_1 + \varepsilon^2 \, \underline{\dot{u}}_2 + \cdots \qquad (7.1.7)$$

and

$$\underline{\dot{y}} = \underline{\dot{\bar{y}}} + \varepsilon \, \underline{\dot{v}}_1 + \varepsilon^2 \, \underline{\dot{v}}_2 + \cdots \qquad (7.1.8)$$

The respective right-hand sides of Equations (7.1.3) and (7.1.7), and (7.1.4) with (7.1.8) may be equated to provide

$$\underline{\dot{\bar{x}}} + \varepsilon \, \underline{\dot{u}}_1 + \varepsilon^2 \, \underline{\dot{v}}_2 + \cdots = \varepsilon \, \underline{f}_1(\underline{x}, \underline{y}) \qquad (7.1.9)$$

and

$$\underline{\dot{\bar{y}}} + \varepsilon \, \underline{\dot{v}}_1 + \varepsilon^2 \, \underline{\dot{v}}_2 + \cdots = \underline{g}_0(\underline{x}, \underline{y}) + \varepsilon \, \underline{g}_1(\underline{x}, \underline{y}) \qquad (7.1.10)$$

where the arguments of $\underline{u}_j$ and $\underline{v}_j$ have been dropped for brevity.

The aim of the averaging method is to obtain averaged equations of motion which do not contain the "fast variables." It is assumed that

the $\dot{\underline{u}}_j$ and $\dot{\underline{v}}_j$ are $\mathcal{O}(1)$ (or smaller), and the coefficients of equal

powers of ε in Eqs. (7.1.5) and (7.1.6) are grouped, then the

averaged equations of motion may be obtained in the forms,

$$\dot{\bar{\underline{x}}} = \varepsilon \; \underline{f}_1(\bar{\underline{x}}, \; \bar{\underline{y}}) + \varepsilon \; \overline{\underline{f}_1(\bar{\underline{x}}, \; \bar{\underline{y}})} \qquad (7.1.11)$$

and

$$\dot{\bar{\underline{y}}} = g_0(\bar{\underline{x}}, \; \bar{\underline{y}}) + \varepsilon \; \overline{g_1(\bar{\underline{x}}, \; \bar{\underline{y}})} \qquad , \qquad (7.1.12)$$

where an overbar over a function indicates its "average" value. This

requires that the "periodic perturbations" be chosen such that

$$\dot{\underline{u}}_1 = \underline{f}_1(\bar{\underline{x}}, \; \bar{\underline{y}}) - \overline{\underline{f}_1(\bar{\underline{x}}, \; \bar{\underline{y}})} \qquad (7.1.13)$$

and

$$\dot{\underline{v}}_1 = g_1(\bar{\underline{x}}, \; \bar{\underline{y}}) - \overline{g_1(\bar{\underline{x}}, \; \bar{\underline{y}})} + (\partial g_0 / \partial \underline{x})_0 \; \underline{u}_1$$

$$+ (\partial g_0 / \partial \underline{y})_0 \; \underline{v}_1 \; , \qquad (7.1.14)$$

where $(\;\;)_0$ indicates evaluation of the function $(\;\;)$ at $\varepsilon = 0$. The

function $\underline{u}_1$ can be found by putting the zeroth-order solutions for

$\bar{\underline{x}}$ and $\bar{\underline{y}}$ into $\underline{f}_1$ and integrating with respect to time. Then, $\underline{v}_1$ may be

found by solving Equation (7.1.14), which is a linear differential

equation if the zeroth-order solutions for $\bar{\underline{x}}$ and $\bar{\underline{y}}$ are used. Here,

"average" is defined using the zeroth-order solutions for $\bar{\underline{x}}$ and $\bar{\underline{y}}$. For

a free, single-body satellite, the angles $\bar{\phi}$ and $\bar{\psi}$ are ordinarily

monotonic, while terms like $\sin\theta_H \sin\phi$ have zero averages. Other terms,

for example, $\cos\theta$, usually have non-zero torque-free average values.

In torque-free motion, when the satellite contains spinning rotors ϕ may be bounded. A further explanation of this behavior is given in Ref. 15.

7.2 Equations of Motion

The equations of motion for this semi-analytic method were derived from expressions for the angles Ψ_H, Θ_H, ϕ, ψ, θ and $|\underline{H}|$, the magnitude of the total angular momentum vector. The angles were described in Section 4. The angles Ψ_H and Θ_H describe the long-term motion of the angular momentum coordinate system with respect to the orbital plane coordinate system (see Fig. 7). The angles ψ, θ, and ϕ describe the short-term motion of the satellite's body-fixed coordinate system with respect to the angular momentum coordinate system (see Fig. 8). In vector notation, the total rotational angular momentum vector can be written as

$$\underline{H} = \underline{\underline{I}} \cdot \underline{\omega} + \underline{h} , \tag{7.2.1}$$

where $\underline{\underline{I}}$ is the principal, centroidal inertia dyadic, matrix, $\underline{\omega}$ is the angular velocity vector, and $\underline{h}$ is the internal angular momentum vector. In matrix notation, this expression may be written as

$$(H_x \ H_y \ H_z)^T = \underline{\underline{I}} \ \underline{\omega} + (h_x \ h_y \ h_z)^T \tag{7.2.2}$$

An expression for the angular velocity vector can be derived from Eq. (7.2.2). It is found that

$$\underline{\omega} = \underline{\underline{I}}^{-1} (\underline{H} - \underline{h}) . \tag{7.2.3}$$

The time rate of change of the angular momentum vector, $\underline{H}$, written in vector form is

$$\underline{\dot{H}} = \underline{\overset{\circ}{H}} + \underline{\omega} \times \underline{H} , \tag{7.2.4}$$

where

$$\overset{\circ}{\underline{H}} = (\overset{\bullet}{H}_x \; \overset{\bullet}{H}_y \; \overset{\bullet}{H}_z) \; (\hat{\underline{a}}_1 \; \hat{\underline{a}}_2 \; \hat{\underline{a}}_3)^T \tag{7.2.5}$$

In matrix notation, the external torque expression is

$$\underline{T} = \overset{\bullet}{\underline{H}} - \overset{\sim}{\underline{H}} \, \underline{\omega} \, , \tag{7.2.6}$$

where

$$\overset{\sim}{\underline{H}} = \begin{bmatrix} 0 & -H_z & H_y \\ H_z & 0 & -H_x \\ -H_y & H_x & 0 \end{bmatrix} \tag{7.2.7}$$

and

$$\overset{\bullet}{\underline{H}} = (\overset{\bullet}{H}_x \; \overset{\bullet}{H}_y \; \overset{\bullet}{H}_z)^T \, .$$

$\underline{H}$ can be written in the satellite's body-fixed system, or in the angular momentum system. In the satellite system, it is written

$$\overset{\bullet}{\underline{H}} = \overset{\sim}{\underline{H}} \, \underline{\omega} + \underline{T} \, . \tag{7.2.8}$$

Alternatively, by substituting in Equation (7.2.3), one finds

$$\overset{\bullet}{\underline{H}} = \overset{\sim}{\underline{H}} \, \underline{\underline{I}}^{-1} \, (\underline{H} - \underline{h}) + \underline{T} \, . \tag{7.2.9}$$

In the angular momentum system,

$$\overset{\bullet}{\underline{H}}_H = \overset{\sim}{\underline{H}}_H \, \underline{\omega}_H + \underline{T}_H \, , \tag{7.2.10}$$

where $\underline{H}_H = (0 \; 0 \; H)^T$, $H = |\underline{H}|$ and $\underline{T}_H = (T_{x_H} \; T_{y_H} \; T_{z_H})^T$. The angular velocity of the angular momentum system, $\underline{\omega}_H$, includes the secular effects of the regression of the line of nodes of the satellite's orbit. Explicitly,

$$\underline{\omega}_H = \begin{bmatrix} \dot{\Omega} \text{ si } s\Psi_H \\ \dot{\Omega}[\text{si } c\Theta_H c\Psi_H + \text{ci } s\Theta_H] \\ \dot{\Omega}[\text{ci } c\Theta_H - \text{si } s\Theta_H c\Psi_H] \end{bmatrix}$$

$$+ \begin{bmatrix} \dot{\theta}_H \\ \dot{\Psi}_H \sin\Theta_H \\ \dot{\Psi}_H \cos\Theta_H \end{bmatrix} = \begin{bmatrix} \omega_{x_H} \\ \omega_{y_H} \\ \omega_{z_H} \end{bmatrix}. \qquad (7.2.11)$$

The relationship between $\underline{\omega}$ and $\underline{\omega}_H$ is $\underline{\omega} = \underline{\omega}_H + \underline{\lambda}$, where

$$\underline{\lambda} = \begin{bmatrix} c\phi & s\theta s\phi & 0 \\ -s\phi & s\theta c\phi & 0 \\ 0 & c\theta & 1 \end{bmatrix} \begin{bmatrix} \dot{\theta} \\ \dot{\Psi} \\ \dot{\phi} \end{bmatrix} \qquad (7.2.12)$$

is the angular velocity of the satellite with respect to the angular momentum system.

The equations of motion for the short-term variables include expressions for $\dot{a}$, $\dot{b}$, $\dot{\phi}$ and $\dot{\psi}$. The parameters a and b are used to define θ, the nutation angle, where a and b are defined as

$$a \equiv H \sin\theta \qquad (7.2\ 13a)$$

and

$$b \equiv H \cos\theta . \qquad (7.2.13b)$$

The components of the angular momentum vector can then be found from the relations

$$H_x = a \sin\phi, \qquad (7.2.14a)$$

$$H_y = a \cos\phi, \qquad (7.2.14b)$$

and

$$H_z = b. \qquad (7.2.14c)$$

The time derivatives of a and b, which may be integrated to find the time-history of the nutation angle, are

$$\dot{a} = b\{[(a \sin\phi - h_x) \cos\phi]/A - [(a \cos\phi - h_y) \sin\phi]/B\}$$

$$+ T_x \sin\phi + T_y \cos \qquad (7.2.15)$$

$$\dot{b} = [(B-A)/AB] a \sin\phi \cos\phi + (h_x/A)a \cos\phi$$

$$- (h_y/B) a \sin\phi + T_z, \qquad (7.2.16)$$

where A, B, and C are the principal centroidal moments of inertia, and where T_z is the z_b-component of external torque. From Eqs. (7.2.14), (7.2.15) and (7.2.16), one may obtain the following equations for ϕ and ψ:

$$\dot{\phi} = (b-h_z)/C - b[B \sin^2\phi + A \cos^2\phi]/AB$$

$$+ (b/a)(A h_y \cos\phi + B h_x \sin\phi)/AB$$

$$+ (T_x/a) \cos\phi - (T_y/a)\sin\phi \qquad (7.2.17)$$

and

$$\dot{\psi} = H[B \sin^2\phi + A \cos^2\phi]/AB - \{[Ah_y \cos\phi + Bh_x \sin\phi]/AB$$

$$+ [(T_{x_H}/H) \cos\psi + (T_{y_H}/H) \sin\psi] \cos\theta\}/\sin\theta$$

$$- (T_{x_H}/H) \cot\theta_H - \dot{\Omega} \sin i \cos\Psi_H/\sin\theta_H . \qquad (7.2.18)$$

The time derivatives of the long-term variables Ψ_H, Θ_H, and H are

$$\dot{\Psi}_H = - \dot{\Omega} \sin i \cos\Psi_H \cot\theta_H - \dot{\Omega} \cos i + (T_{x_H}/H)\sin\theta_H , \qquad (7.2.19)$$

$$\dot{\theta}_H = - \dot{\Omega} \sin i \sin\Psi_H - T_{y_H}/H \qquad (7.2.20)$$

and

$$\dot{H} = T_{z_H} \; , \tag{7.2.21}$$

where T_{x_H}, T_{y_H}, and T_{z_H} are the components of external torque in the angular momentum system.

7.3 Results

To demonstrate the capability of the semi-analytic simulation method, two examples are given. The first example[15] involves an axisymmetric satellite which contains two axisymmetric rotors on the satellite's x_b-and y_b-axes, respectively. The second example concerns the Combined Release and Radiation Effects Satellite (CRRES).[26] In this section, a brief description of the computer code designed to use the semi-analytic method is first given. Next, the results of the two examples are presented and finally, a summary of these results is made.

For descriptive purposes the semi-analytic computer code is broken down into four parts: the initialization process; the short-term stage, or Stage 1; the intermediate stage, or Stage 2; and the long-term stage, or Stage 3.

In the initialization process, $\underline{\underline{I}}$, the principal centroidal inertia matrix; $\underline{\omega}_o$, the initial angular velocity vector; $\underline{h}$, the internal angular momentum vector; and the initial values for the angles ψ, Ψ_H, and Θ_H, are entered. From $\underline{\underline{I}}$, $\underline{\omega}_o$, and $\underline{h}$, the total angular momentum vector, $\underline{H}$, are then used to find the initial values of the angles θ and ϕ. The initial gravity-gradient torque is also calculated to find the initial values for Stage 1.

The six equations of motion for the Stage 1 integration are those

for: ϕ; ψ; Ψ_H; P_ψ, the momentum conjugate to ψ, where $P_\psi = H$; P_ϕ, the

momentum conjugate to ϕ, where $P_\phi = b$; and P_{Ψ_H}, the momentum conjugate

to Ψ_H, where $P_{\Psi_H} = H \cos\Theta_H$. The expressions for $\dot{\phi}$, $\dot{\psi}$, $\dot{\Psi}_H$, $\dot{H}$, $\dot{b}$, and

$\dot{\Theta}_H$ can be found in the previous section. The nutation period is

determined either by using an analytical solution, as in the first

example, or numerically, as in the second example. The six equations of

motion are then integrated over one nutation period to find average

values of P_ϕ, P_ϕ, P_{ψ_H}, and ψ, which are to be used as initial conditions

for the "averaged equations of motion" for Stage 2. This completes the

short-term stage, or Stage 1.

The intermediate stage, or Stage 2, uses these "averaged equations

of motion." These four averaged equations of motion are integrated

numerically, over an orbital period. The integration step size is much

larger (two orders of magnitude) than the step size used in Stage 1.

The results are doubly averaged values of P_{ψ_H} and ψ_H which are used then

averaged again over the orbital period to obtain as the initial values

for the "doubley averaged equations of motion" for $\dot{\bar{\bar{P}}}_{\psi_H}$ and $\dot{\bar{\bar{\Psi}}}_H$.

In the final stage, or Stage 3, the two doubly averaged equations

of motion are integrated over a specified "long" period of time using

integration step sizes on the order of one-half day.

Ex{mple 1

Data for the first example is given in Table 7. Using the

analytical solution, a nutation period of 4.6 seconds was obtained and

the mean time rates of change of ϕ and ψ were found to be approximately

1.367 rad/sec and 2.132 rad/sec, respectively. Plots of ϕ, θ, and ψ are

shown in Figure 26 for the Stage 1 portion of the semi-analytical solution process. The mean value of θ during the short-term motion is approximately 6.267 deg. For Stage 2, the numerically determined motion in $\bar{\psi}$, $\bar{P}_{\psi_H}$, and $\bar{\Psi}_H$ is shown in Figure 27. Results for Stage 3, or long-term motion is shown in Fig. 28 in the form of a $\bar{\bar{\Theta}}_H$ vs. $\bar{\bar{\Psi}}_H$ plot. The analytical solution to the averaged equations yields the same information.

<u>Table 7. Data for Semi-Analytic Example 1</u>

$A = B = 400$ kg-m^2	$\psi(0) = 0$
$C = 200$ kg-m^2	$\Psi_H(0) = 0$
$h_x = 20$ kg-m^2/s	$\Theta_H(0) = 80$ deg
$h_y = 0$	$R = 6778.27$ km
$h_z = 150$ kg-m^2/s	$e = 0$
$\omega_x(0) = 0.1$ rad/s	$i = 28.5$ deg
$\omega_y(0) = 0.001$ rad/s	$\dot{\Omega} = -6$ deg/day
$\omega_z(0) = 3.5$ rad/s	$n = 3.998$ deg/min

As a partial check on the accuracy of the semi-analytical theory, the full equations of motion were integrated numerically using a step size of 0.2 seconds. Results using a fourth-order Runge-Kutta algorithm on a Harris 800 minicomputer over 29,164 seconds of CPU time are compared with the semi-analytical results in Fig. 29. The small initial difference in Ψ_H and $\bar{\bar{\Psi}}_H$ is due to using the average value from Stage 2 of the semi-analytical approach. The CPU time for the application of the semi-analytic theory is around 12 seconds. Clearly, good accuracy
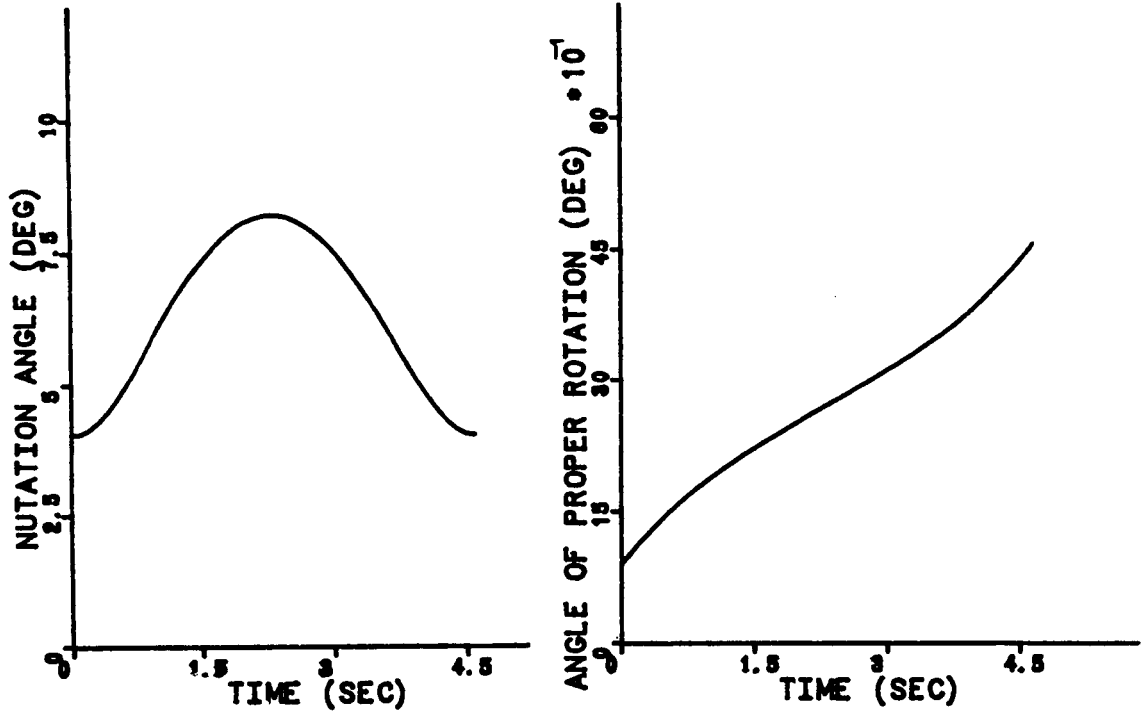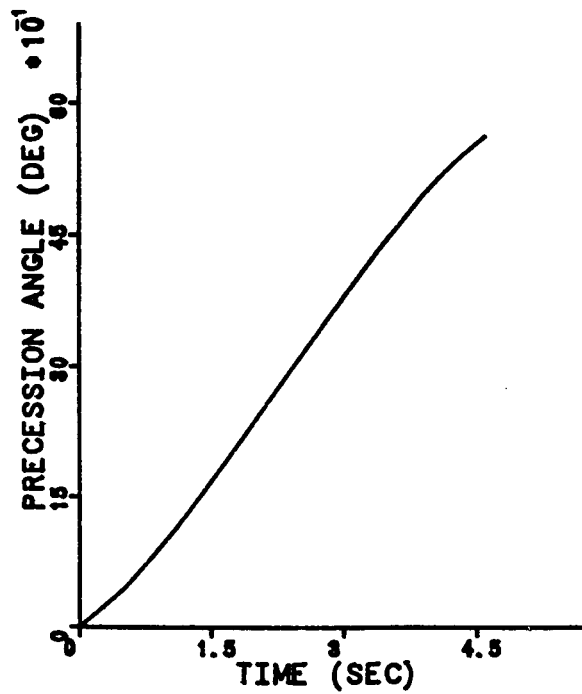
Fig. 26.   Semi-Analytic Example 1, Short-Term Motion, Stage 1.
Time-Histories (a) Nutation Angle; (b) Angle of Proper
Rotation; (c) Precession Angle.
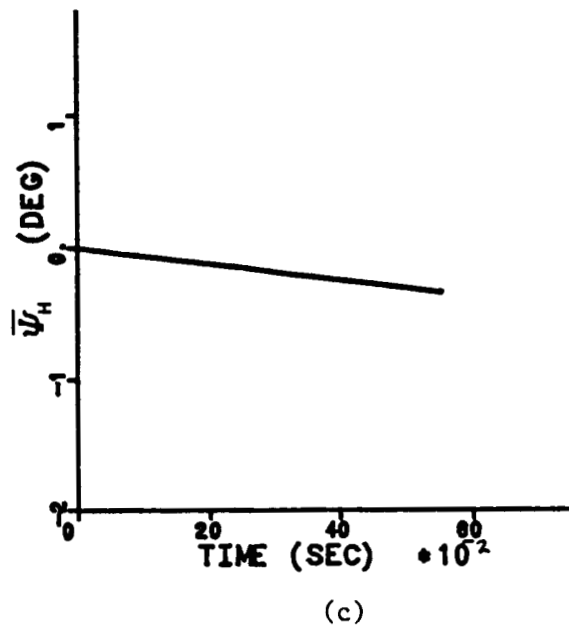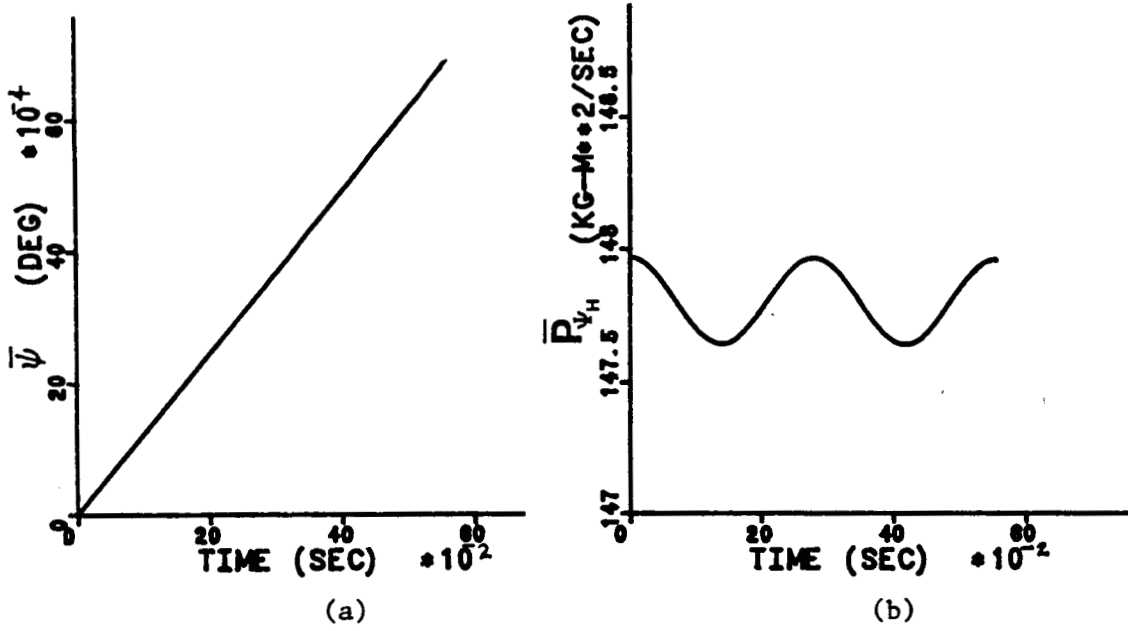
Fig. 27.   Semi-Analytic Example 1, Intermediate Motion, Stage 2.
(a) $\bar{\psi}$; (b) $\bar{P}_{\psi_H}$; (c) $\bar{\psi}_H$
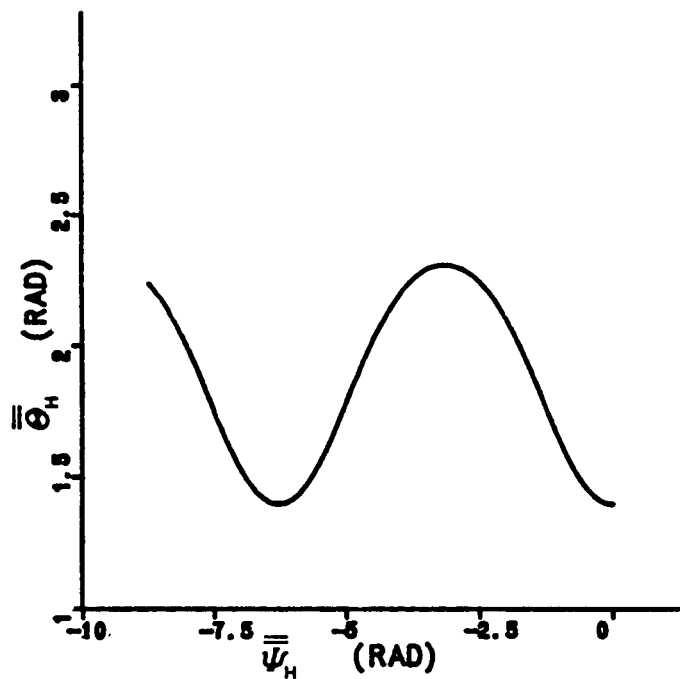
Fig. 28.   Semi-Analytic Example 1, Long-Term Motion, Stage 3.
$\bar{\bar{\Theta}}_H$ vs. $\bar{\bar{\Psi}}_H$
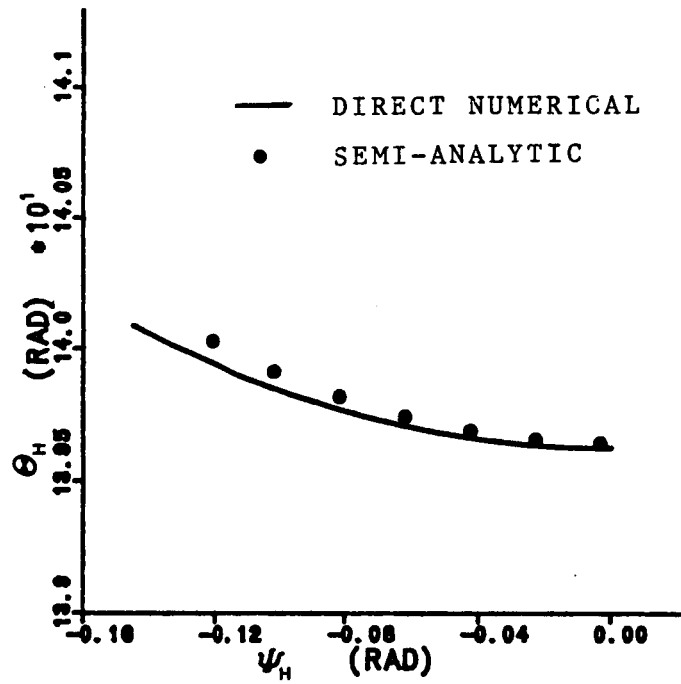
Fig. 29.   Comparison of Direct Integration Results and Semi-
            Analytic Results for Semi-Analytic Example 1.

can be maintained with tremendous savings of computer time using the
semi-analytic theory.

As a second example, long-term attitude motion of the CRRES
satellite was simulated using the semi-analytic method. The data for
this simulation is presented in Table 8. Using a numerical solution, a
nutation period of 3.9 seconds was determined. Plots of ϕ, θ, and ψ are
shown in Fig. 30 for the Stage 1 portion of the semi-analytic process.
The mean value of θ during the short-term motion is approximately 4.58
degrees. For Stage 2, the numerically determined motion in $\bar{\psi}$, $\bar{P}_{\psi_H}$, and
and $\bar{\psi}_H$ is shown in Fig. 31. Results from Stage 3, for long-term motion,
are shown in Fig. 32 in the form of a $\bar{\bar{\Theta}}_H$ vs $\bar{\bar{\psi}}_H$ plot.

Table 8. Data for Semi-Analytic Example 2 (CRRES)

$A = 2263.13$ kg-m^2	$\psi(0) = 0$
$B = 1917.5$ kg-m^2	$\psi_H(0) = 0$
$C = 3719.65$ kg-m^2	$\Theta_H(0) = 5$ deg
$h_x = 0.$	$R = 7378.27$ km
$h_y = 0.$	$e = 0$
$h_z = 0.$	$i = 28.5$ deg
$\omega_x(0) = 0.15$ rad/s	$\dot{\Omega} = -6$ deg/day
$\omega_y(0) = 0.$	$n = 3.4246$ deg/min
$\omega_z(0) = 1.0472$ rad/s	
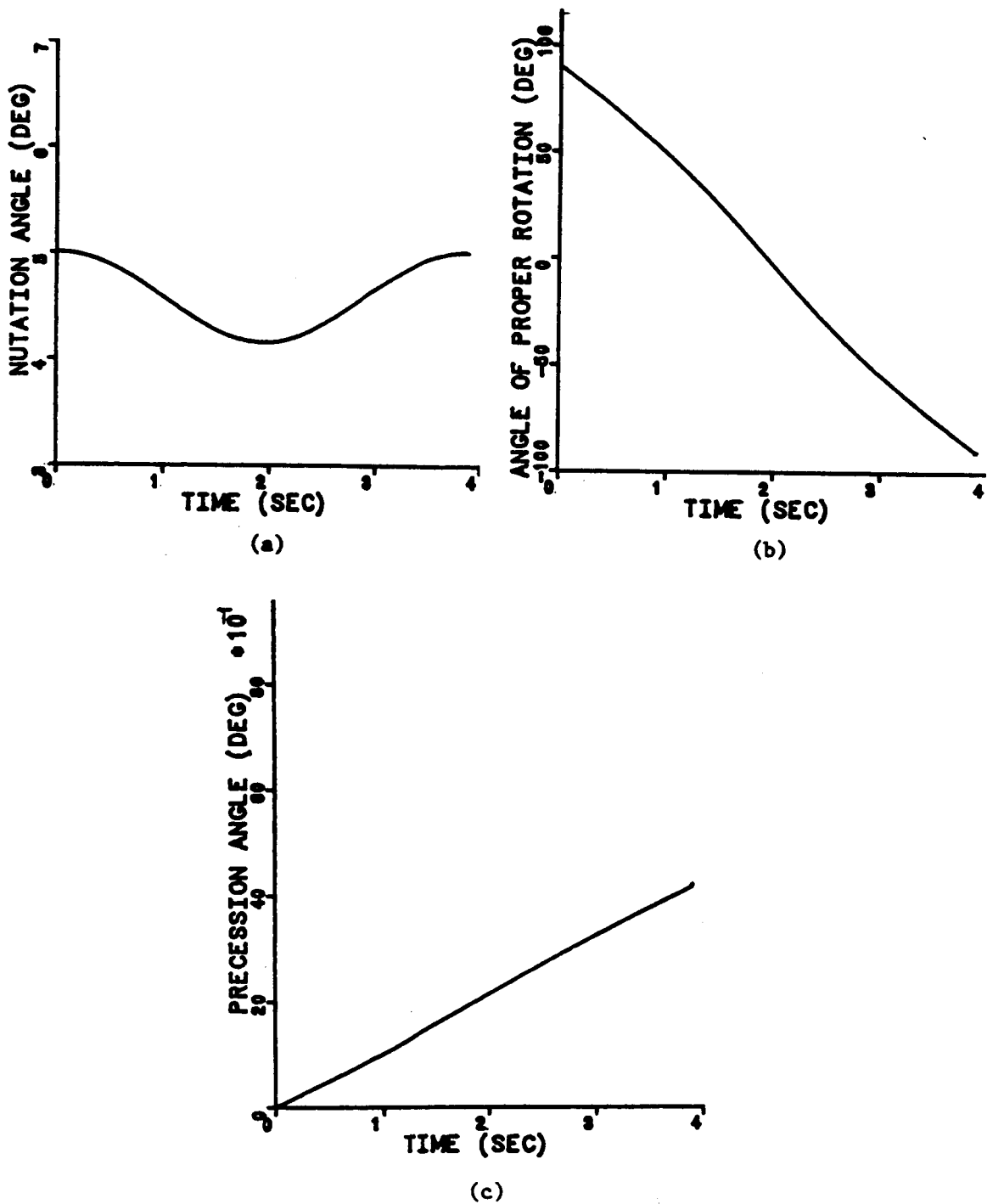
Fig. 30. Semi-Analytic Example 2 (CRRES), Short-Term Motion,
Time-Histories, Stage 1. (a) Nutation Angle;
(b) Angle of Proper Rotation; (c) Precession Angle.
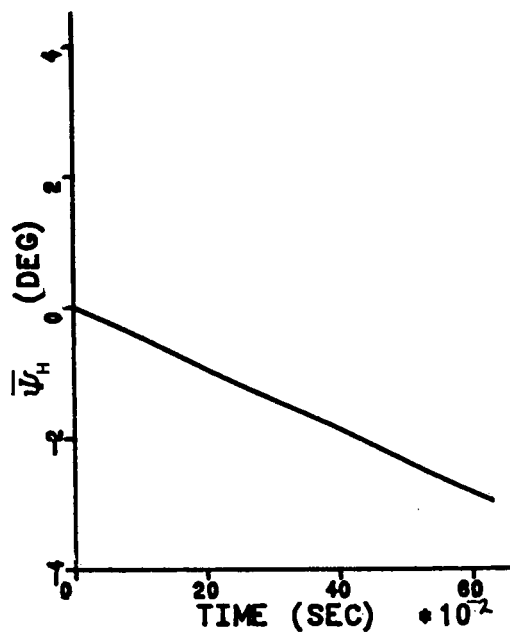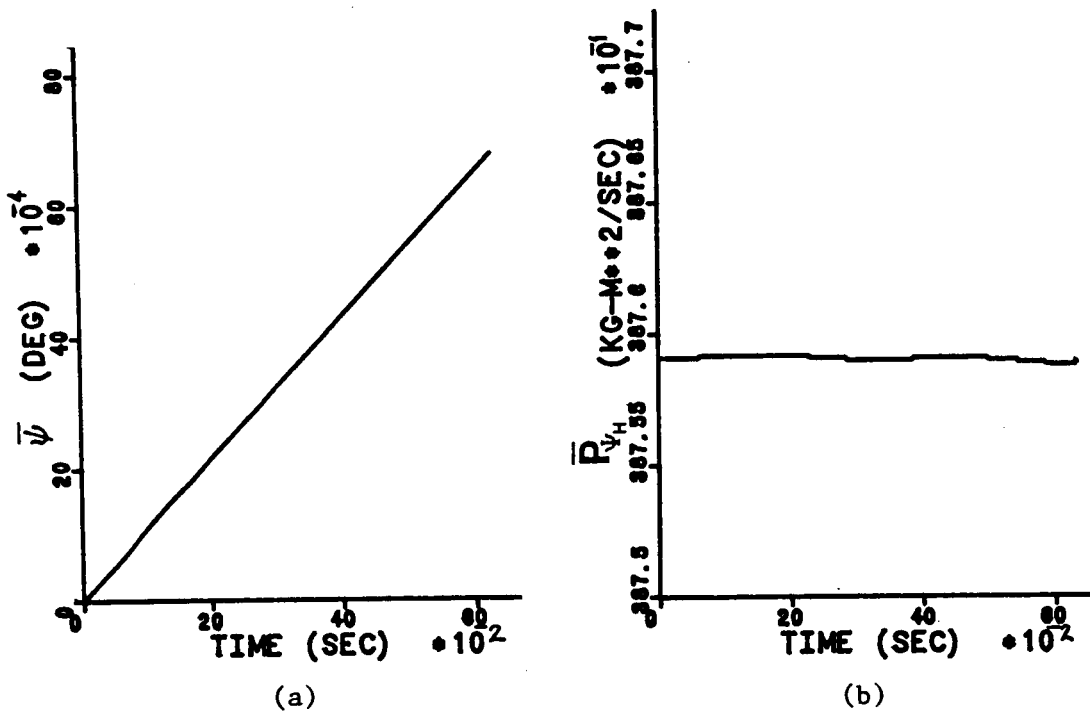
Fig. 31. Semi-Analytic Example 2 (CRRES), Intermediate Motion,
Stage 2. Time Histories (a) $\bar{\psi}$; (b) $\bar{P}_{\psi_H}$; (c) $\bar{\Psi}_H$.
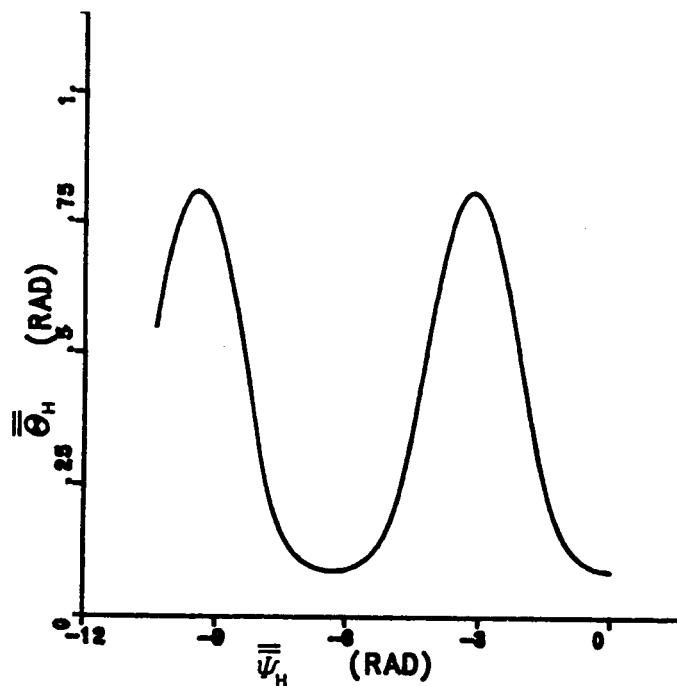
Fig. 32. Semi-Analytic Example 2 (CRRES), Long-Term Motion, Stage 3. $\bar{\bar{\Theta}}_H$ vs. $\bar{\bar{\Psi}}_H$.

The CPU time required for the second example was 9.22 seconds. The integration time step size was 0.1 sec for Stage 1, 20 sec for Stage 2 and 1.2 day for Stage 3.

A semi-analytic method for predicting the long-term attitude motion of uncontrolled satellites has been described. The method can be used effectively when the square of the rotational angular momentum of the satellite under consideration is much larger than the maximum magnitude of the torque multiplied by the largest moment of inertia of the satellite. The method is applicable in both cases in which the unperturbed solution is known and in cases for which it must be determined numerically. The problem of determining the attitude motion of a satellite with constant internal angular momentum and subjected to gravity-gradient torque was used in the first example. The problem of determining the attitude motion of a satellite which has no internal angular momentum, but is spinning quite rapidly and is subjected to gravity-gradient torque was considered in the second example. The speed with which solutions can be obtained using the method, relative to that of straightforward numerical integration is of the order of 2430 to 1. Such time savings are of considerable significance.

VIII. CONCLUSIONS AND RECOMMENDATIONS

8.1 Conclusions

Much of the emphasis of this investigation has been placed on
analytical solutions for the attitude motion of uncontrolled satellites.
Analytical solutions to the torque-free equations of rotational motion
for three satellite models were verified using numerical integration.
The majority of this verification was done using a digital simulation
code which contains a rather general dynamic model of a two-body
satellite. The applicability of one of the torque-free analytical
solutions for the attitude motion of satellites with asymmetric internal
angular momentum was tested using a model for the gravity-gradient
torque. It was determined that for high angular momentum cases the
fidelity of the torque-free analytical solution was very good. However,
for cases in which the satellite is modeled as slowly tumbling in the
presence of environmental torques, the torque-free analytical solution
does not accurately model the motion. Numerical results were obtained
using physical characteristics of actual satellites for cases of low
angular momentum in the presence of environmental torques.

The investigation of long-term attitude motion emphasized the
semi-analytic method. Good results with a substantial savings in CPU
time were obtained using this method. It can be utilized in cases where
the unperturbed analytical solution is known, and also those in which
the unperturbed solution must be determined numerically.

8.2 Recommendations

It is recommended that for short-term modeling of satellite attitude motion, for use in capture and retrieval simulators, the "driver" for dynamically simple, high angular satellites should be a "torque-free," closed-form analytical solution if available. This recommendation is based upon the "computational-speed advantage" of closed-form, analytical solutions. If, on the other hand, the satellite in question has such complex dynamics that an analytical solution is not available and/or is a low angular momentum satellite which is moving in the presence of significant environmental torques, a perturbed analytical solution or a numerical solution is required. Numerical integration of the attitude equations becomes more efficient in the low angular momentum regime because larger integration step sizes may be employed at lower angular rates.

No analytical solutions for short-term prediction of the attitude motion of low angular momentum satellites are included in this report. It is recommended that such solutions be developed. These solutions would be very useful in satellite capture and retrieval operations.

The recommendation for long-term prediction of satellite attitude motion is to use a semi-analytic method. Such a method should provide results which are sufficiently accurate for the purposes of predicting the state of the satellite's attitude motion sufficiently far in advance for capture and retrieval mission planning.

The semi-analytic method presented herein does not address the problem of internal energy dissipation. Therefore, it is recommended

that "energy-sink" models be incorporated in the present semi-analytic method.

Finally, for low earth orbit cases, due account must be taken of the aerodynamic torque. To do this precisely would require that the aerodynamics of each target in low earth orbit be modeled. It is therefore recommended that methods be developed to produce quickly attitude time histories of fairly general satellites perturbed by aerodynamic torques.

REFERENCES

1. Covault, C., "Shift Urged in Shuttle Landing Site," <u>Aviation Week &</u> <u>Space Technology</u>, April 23, 1984, pp. 18-23.

2. Marsh, A. K., "Satellite Retrieval Succeeds Despite Equipment Problem," <u>Aviation Week & Space Technology</u>, November 19, 1984, pp. 16-19.

3. Covault, C., "Orbiter Crew Restores Solar Max," <u>Aviation Week &</u> <u>Space Technology</u>, April 16, 1984, pp. 18-28.

4. Lennox, H., et al., "Teleoperator Maneuvering System," Preliminary Definition Study, George C. Marshall Space flight Center, Alabama, June 1983.

5. Cochran, John E., Jr., and Lahr, B. S., "Satellite Recovery-- Attitude Dynamics of the Targets," AAS/AIAA Astrodynamics Specialists Conference, Vail, Colorado, August 12-15, 1985, Paper AAS 85-324.

6. Crenshaw, J. W., and Fitzpatrick, P. M., "Gravity Effects on the Rotational Motion of a Uniaxial Artificial Satellite," <u>AIAA</u> <u>Journal</u>, Vol. 6, No. 11, pp. 2140-2145.

7. Cochran, J. E., Jr., "On the Effects of Gravity-Gradient Torque on the Rotational Motion of a Triaxial Artificial Satellite in a Precessing Elliptic Orbit," <u>Celestial Mechanics</u>, Vol. 6, No. 4, 1972, pp. 127-150.

8. Liu, J. J. F., "General Study of the Rotational Motion of an Orbiting Rigid Body About Its Center of Mass Under the Influence of Conservative and Nonconservative Torques," Dissertation, Auburn University, Alabama, December 1971.

9. Beletskii, V. V., "Motion of an Artificial Satellite About Its Center of Mass," NASA TT F-429, U.S. Department of Commerce, Springfield, Virginia, 1966.

10. Liu, J. J. F., and Fitzpatrick, P. M., "Poisson Equations of Rotational Motion for a Rigid Triaxial Body with Applications to a tumbling Artificial Satellite, <u>Celestial Mechanics</u>, Vol. 12, No. 4, December 1975, pp. 463-487.

11. Jacobi, C. G. J., <u>Journal für Mathematiks</u>, XXXIX, 1944, pp. 293f.

12. Leimanis, E., *The General Problem of Motion of Coupled Rigid Bodies about a Fixed Point*, Springer-Verlag, New York, Inc., New York, 1965, pp. 12f.

13. Cochran, J. E., Jr., Shu, P. H., and Rew, S. D., "Attitude Motion of Asymmetric Dual-Spin Spacecraft," *Journal of Guidance and Control*, Vol. 5, No. 1, January-February 1982, pp. 37-42.

14. Cochran, J. E., and Shu, P. H., "Attitude Motion of Spacecraft with Skewed Internal Angular Momenta," *The Journal of the Astronautical Sciences*, Vol. XXXI, No. 2, April-June, 1983, pp. 203-215.

15. Lahr, B. S., Cochran, J. E., Jr., and Kumar, K., "Semi-Analytical Theory for Long-Term Rotational Motion of Uncontrolled Satellites," AIAA Paper No. 86-2272, AIAA/AAS Astrodynamics Conference, Williamsburg, Virginia, August 18-20, 1986.

16. Shrivasta, S. K., and Modi, V. J., "Satellite Attitude Dynamics and Control in the Presence of Environmental Torques--A Brief Survey," *Journal of Guidance and Control*, Vol. 6, No. 6, November-December 1983, pp. 461-471.

17. Hughes, P. C., *Spacecraft Attitude Dynamics*, John Wiley & Sons, New York, 1986, pp. 232-272.

18. NASA: "Spacecraft Gravitational Torques," NASA SP-8024, May 1969.

19. Cochran, J. E., Jr., "On the Effects of Gravity-Gradient Torque on the Rotational Motion of a Triaxial Artificial Satellite in a Precessing Elliptic Orbit," Dissertation, University of Texas, Austin, Texas, 1970.

20. Etkin, B., *Dynamics of Atmospheric Flight*, Wiley, New York, 1972, pp. 89.

21. Evans, W. J., "Aerodynamics and Radiation Disturbance Torques on Satellites Having Complex Geometry," *The Journal of Astronautical Sciences*, Vol. IX, No. 4, 1962, pp. 93-99.

22. Stanley, M. G., "Satellite Data for Uncontrolled Motion Study," Memorandum, George C. Marshall Space Flight Center, Marshall Space Flight Center, Alabama, April 9, 1985.

23. Doughorty, H., et al., "Space Telescope, Observatory in Space," AIAA Paper No. 80-1784, Presented at the AIAA Guidance and Control Conference, Danvers, Massachusetts, August 11-13, 1980.

24. Danby, J. M. A., *Fundamentals of Celestial Mechanics*, The Macmillan Company, New York, 1962, pp. 234-238.

133

25. Kraige, L. G., and Junkins, J. L., "Perturbation Formulations for Satellite Attitude Dynamics," Celestial Mechanics, 13, 1976, pp. 39-64.

26. Henrickson, C., et al., "NASA/MSFC Combined Release and Radiation Effects Satellites (CRRES), Delta Critical Design Review," Ball Aerospace Systems Division under Contract NAS8-34025, April 2-5, 1985.

27. Cochran, J. E., Jr., and Speakman, N. O., "Rotational Motion of a Free Body Induced by Mass Redistribution," Journal of Spacecraft and Rockets, Vol. 12, No. 2, February 1975, pp. 89-95.

28. Byrd, P. F., and Friedman, M. D., Handbook of Elliptic Integrals for Engineers and Scientists, Springer-Verlag, New York, 1971.

APPENDICES

APPENDIX A

SINGLE-RIGID-BODY MATHEMATICAL MODEL

A.1 Introduction

Many satellites may be considered to be "single bodies" which are fairly rigid. The simplest physical model for such a satellite which takes into account the possibility of mass asymmetries is an asymmetric, or "tri-inertial," rigid body. Although the solution for the torque-free rotational motion of such a body is well known[11] because it forms the basis for perturbed motion analyses and, principally, because it does provide a good approximation to the motion of many satellites over short time periods, a summary of the solution is included in this report. This summary closely follows that given in Ref. 27.

A.2 Mathematical Model

Let the principal, centroidal moments of inertia of the body be A, B and C where either $A \geq B > C$ or $C > B \geq A$. Let the motion of principal axes x_b, y_b and z_b, be measured with respect to a (fixed) rotational angular momentum coordinate system which has its z_H-axis collinear with $\underline{H}$, the angular momentum of the body about its center of mass C. Let the principal axes components of $\underline{\omega}$, the angular velocity of the body, be ω_y, ω_x, and ω_z. Also, let ψ, θ and ϕ denote Euler angles such that

$$\omega_x = \dot{\phi} - \dot{\psi} \sin\theta$$

$$\omega_y = \dot{\psi} \cos\theta \sin\phi + \dot{\theta} \cos\phi \qquad\qquad (A.2.1)$$

$$\omega_z = \dot{\psi} \cos\theta \cos\phi - \dot{\theta} \sin\phi$$

Note that the Euler angle sequence used here is a 3-2-1 sequence.

The equations of rotational motion for the body are

$$A\dot{\omega}_x + (C-B)\omega_y\,\omega_z = 0$$

$$B\dot{\omega}_y + (A-C)\omega_z\,\omega_x = 0 \qquad\qquad (A.2.2)$$

$$C\dot{\omega}_z + (B-A)\omega_x\,\omega_y = 0$$

Also, the angular momentum can be expressed as either

$$\underline{H} = A\omega_x\,\hat{\underline{b}}_1 + B\omega_y\,\hat{\underline{b}}_2 + C\omega_z\,\hat{\underline{b}}_3 \;, \qquad\qquad (A.2.3a)$$

or

$$\underline{H} = H(-\sin\theta\,\hat{\underline{b}}_1 + \cos\theta\,\sin\phi\,\hat{\underline{b}}_2 + \cos\theta\,\cos\phi\,\hat{\underline{b}}_3), \qquad (A.2.3b)$$

where $\hat{\underline{b}}_j$, j=1,2,3, are unit vectors attached to the $Cx_b y_b z_b$ system.

Equations (A.2.1) have two immediate integrals,

$$A\omega_x^2 + B\omega_y^2 + C\omega_z^2 = 2\,\mathcal{T} \qquad\qquad (A.2.4b)$$

and

$$A^2\omega_x^2 + B^2\omega_y^2 + C^2\omega_z^2 = H^2 \;, \qquad\qquad (A.2.4b)$$

where $\mathcal{T}$ is the rotational kinetic energy. These integrals may be used in Eqs. (A.2.1) to obtain[2/] the equation,

$$\dot{\xi}^2 = \lambda^2(1 - k^2\,\sin^2\xi), \qquad\qquad (A.2.5)$$

where the new variable $\xi \equiv \sin^{-1}(\omega_y/Q)$, $Q = (d/e)^{1/2}$, $d = 2\,C\mathcal{T} - H^2$, $e = B(C-B)$, $\lambda^2 = [(C-B)(H^2 - 2A\mathcal{T})]/(ABC)$ and $k^2 = [(B-A)(2C\mathcal{T} - H^2)]/[(C-B)(H^2 - 2A\mathcal{T})]$.

It follows from Eq. (A.2.5) that

$$\sin\xi = \text{sn } u \qquad\qquad (A.2.6)$$

where sn u is one of the Jacobian elliptic functions, $u = \lambda t - \nu$, and

ν is the value of u at t=0. Hence,

$$\omega_y = Q \text{ sn } u \ . \tag{A.2.7}$$

For C>B>A, the integrals (A.2.4) amd (A.2.5) and Eq. (A.2.7)

may be used to get

$$\omega_x = P \text{ cn } u \tag{A.2.8}$$

and

$$\omega_z = R \text{ dn } u \ , \tag{A.2.9}$$

where $P^2 = (2C\mathcal{J} - H^2)/[A(C-A)]$, $R^2 = (H^2 - 2A\mathcal{J})/[C(C-A)]$ and cn u and

dn u are Jacobian elliptic functions.

By using Eqs. (A.2.3) and defining p = AP/H, q = BQ/H and

r = CR/H, the following relationships may be obtained from Eqs. (A.2.7)

through (A.2.9):

$$-\sin\theta = p \text{ cn } u \ ,$$

$$\cos\theta \sin\phi = q \text{ sn } u \tag{A.2.10}$$

and

$$\cos\theta \cos\phi = r \text{ dn } u \ .$$

The angle of precession can be obtained from

$$\dot{\psi} = H\{1 + [(C-B)/B] \sin^2\phi\}/C \ , \tag{A.2.11}$$

which is derivable from Eqs. (A.2.1) and (A.2.2). By using

$\tan\phi = (B/C)(q/r)(\text{sn } u/\text{dn } u)$ in Eq. (A.2.11), it is found that

$$\psi = \psi_0 + \int_{t_o}^{t} (H/C)[1 + g^2 \text{ sn}^2 u/(1 + \sigma^2 \text{ sn}^2 u)]dt \ , \tag{A.2.12}$$

where

$$g^2 = \sigma^2 (C-A)/A$$

and

$$\sigma^2 = [A(C-B)]/[C(B-A)] \ k^2 \ .$$

The integral in (A.2.12) is a form of elliptic integrals of the third kind and may be evaluated using methods described in Ref. 28.

APPENDIX B

DUAL-SPIN SATELLITE MATHEMATICAL MODEL

B.1   Introduction

A "dual-spin" satellite is usually a satellite which is composed of a nonrotating, or "despun," "platform" and a rapidly rotating "rotor." More generally, a dual-spin satellite is one which has two parts which spin at different rates. The latter description is used for the purposes of this appendix. Additional requirements on the model of a dual-spin satellite adopted here are explained in the following.

A solution to the equations of torque-free attitude motion of a particular dual-spin satellite physical model is given in this appendix. It is taken from Ref. 13. The physical model consists of a rigid, axisymmetric body and a rigid asymmetric body (see Fig. 3). Either can represent the platform (rotor). The axisymmetric body rotates with respect to the asymmetric body about its axis of symmetry which is parallel to one of the axes of extremal moment of inertia of the asymmetric body. For the solution given, the torque between the rotor and platform is assumed to be zero. However, the form of the solution is the same if the relative spin rate of the rotor is constant.

B.2   Equations of Motion

Let A^*, B and C represent the principal, centroidal moments of inertia of the satellite about the x_b-, y_b- and z_b-axes, respectively, which are fixed in the asymmetric body. Also, let B_1 denote the moment of inertia of the axisymmetric body about its symmetry axis, which is assumed to be parallel to the x_b-axis. Furthermore, let $A = A^* - B_1$.

The components of the rotational angular momentum are

$$H_x = A\omega_x + P_\alpha \tag{B.2.1a}$$

$$H_y = B\omega_y \tag{B.2.1b}$$

and

$$H_z = C\omega_z \, , \qquad (B.2.1c)$$

where ω_x, ω_y and ω_z are the components of angular velocity of the asymmetric body and

$$P_\alpha = B_1(\omega_x + \Omega) \qquad (B.2.2)$$

is the angular momentum of the axisymmetric body about its symmetry axis.

In Eq. (B.2.2), Ω is the x-axis component of the angular velocity of the axisymmetric body with respect to the other body.

Because the motion is torque-free, the angular momentum system $Cx_H y_H z_H$ (see Fig. B.1) is fixed and the Euler angles ψ, θ and ϕ are defined so that

$$H_x = H \cos\theta \, , \qquad (B.2.3a)$$

$$H_y = H \sin\theta \sin\phi \qquad (B.2.3b)$$

and

$$H_z = H \sin\theta \cos\phi \, , \qquad (B.2.3c)$$

where $H = (H_x^2 + H_y^2 + H_z^2)^{1/2}$. Note that in _this_ _appendix_ and Appendix C, the x_H-axis is aligned with $\underline{\underline{H}}$ and the Euler angle sequence is 1-2-1.

The equations of motion and the kinematic equations for ψ and α, the angle of relative rotation of the axisymmetric body, are

$$\dot{H}_x = [(B-C)/(BC)]H_y H_z \, , \qquad (B.2.4a)$$

$$\dot{H}_y = - \{[(A-C)/(AC)]H_x + P_\alpha/A\}H_z \, , \qquad (B.2.4b)$$

$$\dot{H}_z = \{[(A-B)/(AB)]H_x + P_\alpha/A\}H_y \, , \qquad (B.2.4c)$$

Fig. B.1   Angular Momentum and Body-Fixed Coordinate Systems for
Appendices B and C.

$$\dot{P}_\alpha = 0 \qquad\qquad\qquad (B.2.4d)$$

and

$$\dot{\psi} = H(H_y^2/B + H_z^2/C)(H^2 - H_x^2) \qquad\qquad (B.2.4e)$$

$$\dot{\alpha} = P_\alpha(A+B_1)/(AB_1) - H_x/A \ . \qquad\qquad (B.2.4f)$$

B.3 Solutions for ψ, θ, ϕ and α

Equations (B.2.4) have the "immediate" integrals[13]

$$H^2 = H_x^2 + H_y^2 + H_z^2, \text{ constant }, \qquad\qquad (B.3.1)$$

$$P_\alpha = \text{constant} \qquad\qquad\qquad (B.3.2)$$

and

$$2T = (H_x - P_\alpha)^2/A + H_y^2/B + H_z^2/C, \text{ constant.} \qquad (B.3.3)$$

These three integrals may be used to write

$$f_2(H_x) = H_y^2/\{(B(A-C))/[A(B-C)]\} = [H_{x_o} + C\,P_\alpha/(A-C)]^2$$

$$+ H_{y_o}^2\,[A(B-C)]/[B(A-C)] - [H_x + C\,P_\alpha/(A-C)]^2 \qquad (B.3.4a)$$

and

$$f_3(H_x) = H_z^2/\{[C(A-B)]/[A(B-C)]\} = [H_x + B\,P_\alpha/(A-B)]^2$$

$$+ H_{z_o}^2\,[A(B-C)[/[C(A-B)] - [H_{x_o} + B\,P_\alpha/(A-B)]^2, \qquad (B.3.4b)$$

where a subscript o denotes an _initial_ value.

Hence, H_y and H_z are functions of H_x, and $\dot{H}_x^2$ may be written in the form,

$$\dot{H}_x^2 = [(A-C)(A-B)/(ABC)]f_2(H_x)f_3(H_x) \ . \qquad\qquad (B.3.5)$$

The solution to Eq. (B.3.5) depends upon whether the roots of the equations $f_2 = 0$ and $f_3 = 0$ are real or complex. For physically realizable motion, the roots of $f_2 = 0$ must be real. The roots of $f_3 = 0$ may, however, be either real or complex. Hence, two cases are possible.

Case 1. Four Real Roots, $a > b > c > d$

In this case,

$$H_x = (D_1 + D_2 \ sn^2 u)/(D_3 + D_4 \ sn^2 u), \qquad (B.3.6)$$

where sn u is a Jacobian elliptic function of modulus

$$k = \{[(a-b)(c-d)]/[(a-c)(b-d)]\}^{1/2} \qquad (B.3.7)$$

and argument,

$$u = \lambda t - u_o , \qquad (B.3.8)$$

in which

$$\lambda = \{[(A-B)(A-C)/(BC)]^{1/2}[(a-c)(b-d)]^{1/2}\}/2A . \qquad (B.3.9)$$

The forms of the D_j, j=1,2,3,4, depend upon H_{x_o}. It turns out that H_{x_o} is never between b and c for real motion. For $b \le H_{x_o} \le a$, $D_1 = a(b-d)$, $D_2 = d(a-b)$, $D_3 = b-d$ and $D_4 = a-b$. For $d \le H_{x_o} \le c$, $D_1 = d(a-c)$, $D_2 = a(c-d)$, $D_3 = a-c$ and $D_4 = c-d$.

Case 2. Two Real Roots

If only the roots of $f_2 = 0$ are real, the solution for H_x has the form,

$$H_x = (C_1 + C_2 \ cn \ u)/(C_3 + C_4 \ cn \ u). \qquad (B.3.10)$$

Here, cn u is a Jacobian elliptic function of modulus

$$k = \left\{ [(a-b)^2 - (\alpha^* - \beta^*)^2]/(4\,\alpha^*\beta^*) \right\}^{1/2}, \tag{B.3.11}$$

where a and b are the real roots (a>b) and α^* and β^* are the real and imaginary parts, respectively, of the <u>complex</u> root c. In the argument, $u = \lambda t + u_0$,

$$\lambda = [(A-C)(A-B)/(A^2 BC)]^{1/2}(\alpha^*\beta^*)^{1/2}. \tag{B.3.12}$$

The constants C_j, j=1,2,3,4, are defined as $C_1 = a\beta^* + b\alpha^*$, $C_2 = b\alpha^* - a\beta^*$, $C_3 = \alpha^* + \beta^*$ and $C_4 = \alpha^* - \beta^*$.

Solutions to the equations for ψ, ϕ, and α may be obtained for each of the two cases above. For Case 1, the solution for ψ is

$$\psi = \sum_{j=0}^{2} b_j \int_{u_0}^{u} du/(1-\alpha_j^2 \, sn^2 u) + \psi_0, \tag{B.3.13}$$

where

$$b_0 = (c_1 + c_2 c_4 + c_3 c_6)/\lambda$$

$$b_1 = -c_3 c_7/\lambda \tag{B.3.14}$$

$$b_2 = c_2 c_5/\lambda$$

$$c_1 = H/A \quad ; \quad c_2 = [2AT-(H+P_\alpha)^2]/(2A)$$

$$c_3 = [2AT-(H-P_\alpha)^2]/(2A) \quad ; \quad c_{4,6} = D_4/(D_4 H \pm D_2) \tag{B.3.15}$$

$$c_{5,7} = (D_3 D_2 - D_1 D_4)/[(D_3 H \pm D_1)(D_4 H \pm D_2)]$$

$$\alpha_0 = 0$$

$$\alpha_1^2 = -(D_4 H - D_2)/(D_3 H - D_1) \tag{B.3.16}$$

$$\alpha_2^2 = -(D_4 H + D_2)/(D_3 H + D_1)$$

The integrals which appear in the solution for ψ are elliptic integrals of the third kind (see Ref. 28, pp. 232-237),

For Case 2, the solution for ψ is

$$\psi = \sum_{j=0}^{2} d_j \int_{u_o}^{u} du/(1 - \beta_j^2 \, cn \, u) + \psi_o \, , \qquad (B.3.17)$$

where the d_j and β_j have the same _forms_ as b_j and α_j but C_k replaces D_k in the definitions. Also, the modulus and parameter λ have the required forms. The integrals in Eq. (B.3.17) are also elliptic integrals of the third kind (see Ref. 28, pp. 215 and 232-237).

The solution for ϕ has the form,

$$\phi = \sum_{j=0}^{2} p_j \int_{u_o}^{u} du/(1 - \alpha_j^2 \, sn^2 u) + d_o \, , \qquad (B.3.18)$$

for case 1. The constants p_j are defined as

$$p_o = [P_\alpha/A - c_3 c_6 + c_2 c_4]/\lambda \, ,$$

$$p_1 = c_3 c_7/\lambda \qquad \qquad (B.3.19)$$

and

$$p_2 = c_2 c_5/\lambda \quad .$$

For Case 2, the solution for ϕ is analogous to the solution for ψ in that case.

Solutions for α are similar to those for ψ and ϕ, but are simpler because only one elliptic integral is involved. For Case 1,

$$\alpha = a_o (u - u_o) + a_1 \int du/(1 - \alpha_3^2 \, sn^2 u) \, , \qquad (B.3.20)$$

where

$$a_o = [P_\alpha(A+B_1)/B_1 - D_2/D_4]/(A\lambda),$$

$$a_1 = (D_2 D_3 - D_1 D_4)/(A\ D_3 D_4\ \lambda) \qquad\qquad (B.3.21)$$

and

$$\alpha_3{}^2 = -\ D_4/D_3\ .$$

The solution for α for Case 2 can be obtained in the manner described above for ψ and ϕ.

APPENDIX C

MULTI-ROTOR SATELLITE MATHEMATICAL MODEL

C.1 Introduction

The model presented in Appendix B cannot be used to represent a satellite which contains a part (or parts) which is rotating about an axis which is not parallel to a principal axis of the carrier body. A model which can be used to represent such a satellite, if the system is axisymmetric, is presented in this appendix. In fact, the satellite model can be used to represent a satellite which contains several constant-speed, rigid "rotors." Hence, the label, "Multi-Rotor Satellite."

The physical model is depicted in Fig. 4. It consists of a torque-free carrier body and one, or more, constant-speed, axisymmetric, rigid rotors. These rotors are arranged so that their resultant angular momentum due to rotation relative to the carrier body (internal angular momentum) is not parallel to any axis, except possibly the y_b-axis of the system $Cx_by_bz_b$ fixed in the carrier body. The x_b-axis of the system is an axis of symmetry. Hence, the y_b-axis can always be chosen such that the z_b-component of the internal angular momentum is zero. The angular momentum system $Cx_Hy_Hz_H$ is fixed because there are no external torques.

Equations of Motion

The mathematical model presented here is based, for the most part, on Ref. 14. Let H_x, H_y and H_z denote the x_b-, y_b-and z_b-components, respectively, of the total angular momentum about C. Also, let h_x and h_y denote the x_b-and y_b-components, respectively, of the internal angular momentum and let A and C be the principal centroidal moments of

inertia of the <u>system</u> of carrier body and rotors, with A about the x_b-axis. Then, the equations of rotational motion may be put into the forms,[14]

$$\dot{H}_x = H_z h_y / C , \qquad \text{(C.2.1a)}$$

$$\dot{H}_y = -\{[(A-C)/(AC)]H_x + h_x/A\}H_z \qquad \text{(C.2.1b)}$$

and

$$\dot{H}_z = \{[(A-C)/(AC)]H_x + h_x/A\}H_y - H_x h_y / C . \qquad \text{(C.2.1c)}$$

The corresponding kinematic equations are

$$\dot{\phi} = (H_x - h_x)/A - (H_x/C)[1 - h_y H_y/(H^2 - H_x^2)] \qquad \text{(C.2.2a)}$$

and

$$\dot{\psi} = (H/C)[1 - h_y H_y/(H^2 - H_x^2)] . \qquad \text{(C.2.2b)}$$

Here, ϕ and ψ are the angle of proper rotation and the precession angle of the body, respectively (see Fig. B.1 in previous appendix).

The nutation angle θ is given by

$$\theta = \cos^{-1}(H_x/H) , \qquad \text{(C.2.3)}$$

where $H = (H_x^2 + H_y^2 + H_z^2)^{1/2}$.

The following expressions for the angular velocity components ω_x, ω_y, and ω_z may also be required at times:

$$\omega_x = (H_x - h_x)/A \qquad \text{(C.2.4a)}$$

$$\omega_y = (H_y - h_y)/C \qquad \text{(C.2.4b)}$$

$$\omega_z = H_z/C \qquad \text{(C.2.4c)}$$

Furthermore, the angles θ, ϕ and ψ can be used to write

$$H_x = H \cos\theta \qquad \text{(C.2.5a)}$$

$$H_y = H \sin\theta \sin\phi \qquad \text{(C.2.5b)}$$

and

$$H_z = H \sin\theta \cos\phi . \qquad (C.2.5c)$$

Equations (C.2.1) admit from "first" and "second" integrals

H = constant and

$$(H_x - h_x)^2/A + (H_y - h_y)^2/C + H_z^2/C = 2T, \text{ constant} \qquad (C.2.6)$$

Equation (C.2.6) may be rewritten (by using $\underline{H} \cdot \underline{H}$ = constant) in the form,

$$H_y = aH_x^2 + 2bH_x + c , \qquad (C.2.7)$$

where

$$a = (C-A)/(2Ah_y) , \qquad (C.2.8a)$$

$$b = - h_x C/(2Ah_y) \qquad (C.2.8b)$$

and

$$c = [(C/A)h_x^2 + h_y^2 + H^2 - 2CT]/(2h_y). \qquad (C.2.8c)$$

Equation (C.2.7) represents a family of parabolic cylinders in angular

momentum space. The terminus of the vector $\underline{H}$ describes, on the sphere

$H^2 = H_x^2 + H_y^2 + H_z^2$, a curve which is an intersection of a parabolic

cylinder with the sphere.

These integrals may be used in Eq. (C.2.1a) to get the equation

$$\dot{H}_x^2 = (h_y/C)^2 H_z^2(H_x) , \qquad (C.2.9)$$

where

$$H_z^2(H_x) = a^2[-H_x^4 + c_3 H_x^3 + c_2 H_x^2 + c_1 H_x c_0] \qquad (C.2.10)$$

$$c_3 = - 4 h_x C/(A-C) \qquad (C.2.11a)$$

$$c_2 = - 4(A^2 h_y^2 + C^2 h_x^2)/(A-C)^2$$

$$\qquad\qquad + 2[Ch_x^2 + Ah_y^2 + A(H^2 - 2CT)]/(A-C) \qquad (C.2.11b)$$

$$c_1 = 4[C^2 h_x{}^3 + ACh_x h_y{}^2 + ACh_x(H^2 - 2CT)]/(A-C)^2 \qquad \text{(C.2.11c)}$$

$$c_o = A^2\{4h_y{}^2 H^2 - [(C/A)h_x{}^2 + h_y{}^2 + H^2 - 2CT]^2\}/(A-C)^2. \qquad \text{(C.2.11d)}$$

C.3 Solutions for θ, ϕ and ψ

The general solution to Eq. (C.2.9) can be expressed in terms of elliptic functions of the time. The form of the solution depends on the number of real roots of the quartic equation, $H_z{}^2(H_x) = 0$.

Case 1. Four Real Roots

In this case, if the roots are H_{x_j}, j=1,2,3,4, and $H_{x_j} < H_{x_k}$ for k>j, then

$$H_x = (D_1 + D_2\, sn^2 u)/(D_3 + D_4\, sn^2 u) \ , \qquad \text{(C.3.1)}$$

where sn u is Jacobi's sine amplitude function and the D_j are determined by H_{x_o}, the initial value of H_x.

If $H_{x_1} \geq H_{x_o} > H_{x_2}$, then

$$D_1 = H_{x_1}(H_{x_2} - H_{x_4}); \ D_3 = H_{x_2} - H_{x_4} \qquad \text{(C.3.2)}$$

$$D_2 = H_{x_4}(H_{x_1} - H_{x_2}); \ D_4 = H_{x_1} - H_{x_2}$$

If $H_{x_2} \geq H_{x_o} > H_{x_3}$, then

$$D_1 = H_{x_2}(H_{x_1} - H_{x_3}); \ D_3 = H_{x_1} - H_{x_3} \qquad \text{(C.3.3)}$$

$$D_2 = H_{x_1}(H_{x_2} - H_{x_3}); \ D_4 = H_{x_2} - H_{x_3}$$

Finally, if $H_{x_3} \geq H_{x_o} > H_{x_4}$, then

$$D_1 = H_{x_4}(H_{x_1} - H_{x_3}); \quad D_3 = H_{x_1} - H_{x_3}$$

$$D_2 = H_{x_1}(H_{x_3} - H_{x_4}); \quad D_4 = H_{x_3} - H_{x_4} \quad . \tag{C.3.4}$$

The argument of the elliptic functions is

$$u = \lambda t + u_o \quad , \tag{C.3.5}$$

where

$$\lambda^2 = [ah_y/(2C)][(H_{x_2} - H_{x_4})(H_{x_1} - H_{x_3})] \tag{C.3.6}$$

$$k^2 = \left\{[(H_{x_1} - H_{x_2})(H_{x_3} - H_{x_4})]/[(H_{x_1} - H_{x_3})(H_{x_2} - H_{x_4})]\right\} \quad . \tag{C.3.7}$$

By using the solution for H_x in Eq. (C.2.2a), and considerable algebraic manipulation, one may put the equation for ϕ into the form,

$$\phi = \sum_{j=0}^{3} P_j \int_{u_o}^{u} du/(1 - \alpha_j \, sn^2 u) \quad , \tag{C.3.8}$$

where $\alpha_o = 0$,

$$\alpha_1 = -(D_4/D_3)d_9/d_7$$

$$\alpha_2 = -(D_4/D_3)d_8/d_6$$

$$\alpha_3{}^2 = -D_4/D_3$$

$$P_o = [(d_{12} + d_4 d_8)d_1 - d_5 d_9 d_2 + d_{13}D_2/D_4]/\lambda \tag{C.3.9}$$

$$P_1 = d_5 d_{11}/\lambda$$

$$P_2 = d_4 d_{10}/\lambda$$

$$P_3 = [d_{13}(D_1 D_4 - D_2 D_3)/(D_3 D_4)]/\lambda \quad .$$

In writing Eqs. (C.3.7), use was made of the defined constants,

$$d_1 = D_4(D_3H + D_1)/[D_3(D_4H + D_2)]$$

$$d_2 = D_4(D_3H - D_1)/[D_3(D_4H - D_2)]$$

$$d_3 = H(1 + ah_y)/C$$

$$d_4 = -h_y(aH^2 - 2bH + c)/(2C)$$

$$d_5 = -h_y(aH^2 + 2bH + c)/(2C)$$

$$d_6 = D_4/(D_4H + D_2)$$

$$d_7 = D_6/(D_4H - D_2) \tag{C.3.10}$$

$$d_8 = D_3/(D_3H + D_1)$$

$$d_9 = D_3/(D_3H - D_1)$$

$$d_{10} = (D_3D_2 - D_4D_1)/[(D_4H + D_2)(D_3H + D_1)]$$

$$d_{11} = (D_3D_2 - D_4D_1)/[(D_4H - D_2)(D_3H - D_1)]$$

$$d_{12} = -(h_x/A + 2bh_y/C)$$

$$d_{13} = 1/A - (1 + ah_y)/C .$$

The integrals in Eq. (C.3.18) are elliptic integrals of the third kind. A set of subroutines has been developed to evaluate these.

By using a similar procedure, it may be shown that

$$\psi = \sum_{j=0}^{3} Q_j \int_{u_o}^{u} \frac{du}{1 - \alpha_1 \, sn^2u} + \psi_o , \tag{C.3.11}$$

where

$$Q_o = (d_3 + d_4d_6 + d_5d_7)/\lambda$$

$$Q_1 = -P_1 \tag{C.3.12}$$

and

$$Q_2 = P_2$$

Case 2. Two Real Roots

When the quartic equation has two real roots, $H_{x_1} > H_{x_2}$, and two complex roots, $\gamma \pm \delta i$, the solution for H_x has the form,

$$H_x = (C_1 + C_2 \text{ cn } u)/(C_3 + C_4 \text{ cn } u), \qquad (C.3.13)$$

where, if,

$$r = [(H_{x_1} - \gamma)^2 + \delta^2]^{1/2} \qquad (C.3.14a)$$

and

$$s = [(H_{x_2} - \gamma)^2 + \delta^2]^{1/2}, \qquad (C.3.14b)$$

then

$$C_1 = H_{x_1} s + H_{x_2} r \quad , \qquad (C.3.15a)$$

$$C_2 = H_x r - H_{x_1} s \quad , \qquad (C.3.15b)$$

$$C_3 = r + s \qquad (C.3.15c)$$

and

$$C_4 = r - s \ . \qquad (C.3.15d)$$

The modulus of cn u is given by

$$k = \left\{ [(H_{x_1} - H_{x_2})^2 - (r - s)^2]/(4rs) \right\}^{1/2} \qquad (C.3.16)$$

As in Case 1, u has the form,

$$u = \lambda t + u_o \ . \qquad (C.3.17)$$

But, for this case,

$$\lambda = a h_y [rs]^{1/2}/C. \qquad (C.3.18)$$

Regarding the _forms_ of the solutions for ϕ and ψ, the only way in which this case differs from Case 1 is that the C_j are used in place of the D_j and the elliptic function cn u replaces $sn^2 u$. The elliptic integrals are still of the third kind (see Ref. 28, pp. 215, 232–237).

APPENDIX D

GRAVITY-GRADIENT AND AERODYNAMIC TORQUE MATHEMATICAL MODELS

D.1 Gravity-Gradient Torque Mathematical Models

Two mathematical models were derived during this investigation to model the gravity-gradient torque experienced by a satellite orbiting the earth. The first model was used for the short-term numerical simulation program. The second was used for the long-term semi-analytic simulation program.

Short-Term Mathematical Model

The unit vector $\hat{\underline{e}}_g$ describes the attitude relationship between the satellite's body-fixed axes and the z_v-axis of the local vertical system. Recall that the z_v-axis always points toward the center of the earth. Thus, the third column of the $\underline{\underline{L}}_{bv}$ transformation matrix provides the unit vector of interest in the __matrix__ form,

$$\underline{e}_g = -\underline{\underline{L}}_{bv} \begin{bmatrix} 0 \\ 0 \\ 1 \end{bmatrix} . \qquad\qquad (D.1.1)$$

This expression for $\underline{e}_g$ may then be used to complete the expression,

$$\underline{T}_g = \frac{3\mu_E}{R^3} \tilde{\underline{e}}_g \underline{\underline{I}} \, \underline{e}_g , \qquad\qquad (D.1.2)$$

where μ_E is the gravitational constant of the earth, R is the distance from the center of the earth to the center of mass of the satellite and $\underline{\underline{I}}$ is the matrix of the satellite.

Long-Term Mathematical Model

The model of the perturbing effects of gravity-gradient torque on the satellite attitude motion used in the semi-analytic simulation is based on a rigid axisymmetric body with centroidal moments of inertia A=B≠C. The components of the gravity-gradient torque can be derived by

taking partial derivatives of the expression for gravity-gradient potential,

$$V_g = [3\mu_E/(2R^3)](C-A) \cos^2\chi, \qquad\qquad (D.1.3)$$

where the angle χ is the angle between the position vector of the satellite's center of mass and the body-fixed z_b-axis (the axis of symmetry). In terms of the angles θ, Θ_H, ψ, and $\mu = \Psi_H - u$, which are defined in the body of the report, the $\cos^2\chi$ may be expressed as follows:

$$\cos^2\chi = \frac{1}{4} [1 + c^2\theta_H + c^2\theta - 3c^2\theta_H \, c^2\theta]$$

$$+ \frac{1}{4} [1 - c^2\theta_H - 3c^2\theta_H \, c^2\theta] \cos 2\mu$$

$$+ \frac{1}{4} [-1 + c^2\theta_H + c^2\theta - c^2\theta_H \, c^2\theta] \cos 2\psi$$

$$- \frac{1}{8} [(1 + 2c\theta_H + c^2\theta_H) \, s^2\theta] \cos 2(\psi-\mu)$$

$$+ \frac{1}{8} [(1 + 2c\theta_H) \, s^2\theta] \cos 2(\psi+\mu)$$

$$+ [s\theta_H c\theta_H \, s\theta \, c\theta] \cos \psi$$

$$+ \frac{1}{2} [(1 - c\theta_H)s\theta_H \, c\theta \, s\theta] \cos (\psi-2\mu)$$

$$- \frac{1}{2} [(1 + c\theta_H)s\theta_H \, c\theta \, s\theta] \cos (\psi+2\mu). \qquad (D.1.4)$$

D.2 Aerodynamic Torque Mathematical Model

The results of the derivation of the aerodynamic torques on the right-circular cylinder are as follows. The total aerodynamic torque acting on the right circular cylinder is a sum of the torques

$\underline{T}_{a_1}$, $\underline{T}_{a_2}$, and $\underline{T}_{a_3}$ contributed by the surfaces S_1, S_2, and S_3, respectively (as shown in Fig. 11). That is

$$\underline{T}_a = \underline{T}_{a_1} + \underline{T}_{a_2} + \underline{T}_{a_3} \tag{D.2.1}$$

The torque contributed by the front endcap, S_1, is

$$\underline{T}_{a_1} = (T_{a_{1_x}} \quad T_{a_{1_y}} \quad T_{a_{1_z}})^T \tag{D.2.2}$$

where

$$T_{a_{1_x}} = \frac{\pi}{8}\, \rho\, c_d\, r_c^4\, [2Up - Wr - Vq],$$

$$T_{a_{1_y}} = -\frac{\pi}{4}\, \rho\, c_d\, r_c^4\, U[(r_c^2 + 2x_1^2)q - 2Wx_1],$$

and

$$T_{a_{1_z}} = -\frac{\pi}{4}\, \rho\, c_d\, r_c^4\, U[(r_c^2 + 2x_1^2)\, r + 2Vx_1] \tag{D.2.3}$$

where r_c is the radius of the right circular cylinder, U, V, W are the x_b-, y_b-, and z_b-components of the "relative wind," where $U = |\underline{V}_c|\cos\alpha_a\cos\beta_a$, $V = |\underline{V}_c|\sin\beta_a$, and $W = |\underline{V}_c|\sin\alpha_a\cos\beta_a$, and p, q, and r are the components of angular velocity about x_b-, y_b-, and z_b-axes, respectively, and x_1 is the distance from the centroid of the cylinder to center of the front end cap along the x_b-axis. The aerodynamic torque contributed by the sides of the cylinder, surface S_2, is

$$\underline{T}_{a_2} = (T_{a_{2_x}} \quad T_{a_{2_y}} \quad T_{a_{2_z}})^T \tag{D.2.4}$$

where

$$T_{a_{2_x}} = - \rho \, c_d \, r_c^3 \, L \, \sqrt{(V^2 + W^2)} \; ,$$

$$T_{a_{2_y}} = - \frac{1}{2} \rho \, c_d \, r_c \{ W[\frac{\pi}{2} U \, r_c \, L - \sqrt{(V^2 + W^2)} \, (d_1^2 - d_2^2)]$$

$$- p[\frac{\pi}{4} V \, r_c (d_1^2 - d_2^2)] + q[\frac{2}{3}(\sqrt{(V^2 + W^2)}$$

$$+ \frac{W^2}{\sqrt{(V^2 + W^2)}})(r_c^2 \, L + d_1^3 + d_2^3)$$

$$- \frac{\pi}{4} U \, r_c (d_1^2 - d_2^2)] - r[\frac{2}{3} \frac{VW}{\sqrt{(V^2 + W^2)}} (r_c^2 \, L$$

$$+ d_1^3 + d_2^3)] \} ,$$

and

$$T_{a_{2_z}} = - \frac{1}{2} \rho \, c_d \, r_c \{ V[\sqrt{(V^2 + W^2)} (d_1^2 - d_2^2) - \frac{\pi}{2} U \, r_c \, L]$$

$$- p[\frac{\pi}{4} W \, r_c (d_1^2 - d_2^2)] - q[\frac{2}{3} \frac{VW}{\sqrt{(V^2 + W^2)}} (r_c^2 \, L + d_1^3 + d_2^3)]$$

$$+ r[\frac{2}{3}(\sqrt{(V^2 + W^2)} + \frac{V^2}{\sqrt{(V^2 + W^2)}})(r_c^2 \, L + d_1^3 + d_2^3)$$

$$- \frac{\pi}{4} U \, r_c \, (d_1^2 - d_2^2))] \} \; . \tag{D.2.5}$$

Here, L is the length of the cylinder, d_1 is the distance along the x_b-axis between the front endcap and the center of gravity, and d_2 is the distance from the rear endcap to the center of gravity. Finally, the aerodynamic torque contributed by the rear endcap, S_3, is

$$\underline{T}_{a_3} = (T_{a_{3_x}} \quad T_{a_{3_y}} \quad T_{a_{3_z}})^T \tag{D.2.6}$$

where

$$T_{a_{3_x}} = \frac{\pi}{8} \rho \, c_d \, r_c^4 \, [2Up - Vq - Wr],$$

$$T_{a_{3_y}} = \frac{\pi}{4} \rho \, c_d \, r_c^2 \, U[2Wx_2 + (r_c^2 + 2x_2^2)q],$$

and

$$T_{a_{3_z}} = -\frac{\pi}{4} \rho \, c_d \, r_c^2 \, U[2Vx_2 - (r_c^2 + 2x_2^2)r] \; . \tag{D.2.7}$$

Here, x_2 is the distance from the center of the rear endcap to the centroid of the cylinder.